CO_2 removal from air for alkaline fuel cells operating with liquid hydrogen

A thesis
submitted for the degree
of

Doctor of Philosophy

by

Vikas Ahuja BE(Hons)

Department of Mechanical Engineering
University of Canterbury
Christchurch
New Zealand
April 1996

Abstract

The aim of this project was to explore the synergistic use of alkaline fuel cells and liquid hydrogen.

For electrochemical power generation, alkaline fuel cells offer the highest efficiency, as well as the possibility of using electrocatalysts that do not include platinum. However, since they operate at low temperatures they do not support hydrogen production by reformation of carbonaceous fuels. Further, they are rendered inoperative by the CO_2 content of the (reformed) fuel and/or air. Their use has been limited due to this inability to use hydrogen or air which contains CO_2, and the added complexity of CO_2 removal.

For storing hydrogen the most suitable system in terms of low mass and volume, is cryogenic storage of liquid hydrogen. The large temperature difference between the stored liquid and its surroundings means that a substantial thermomechanical exergy component, in addition to the chemical exergy, is available from the fuel. Thermomechanical exergy recovery has the potential to make the use of liquid hydrogen more efficient.

The basis of this thesis is the conceptual design, development and testing of a new process for CO_2 removal from air for use in alkaline fuel cells operating with hydrogen stored as a liquid, addressing simultaneously:

- CO_2 removal from atmospheric air, and
- thermomechanical exergy recovery from liquid hydrogen.

This project was an attempt to address these issues by using the cooling available from vaporisation of liquid hydrogen and/or boil-off vapour, to remove CO_2 from the alkaline fuel cell feed air by refrigeration purification, ie. by freezing the CO_2 out of the air.

A schematic description of the process and an energy balance for refrigeration purification for the CO_2 removal are presented, showing that the process relies on high effectiveness heat exchangers and water re-vaporisation. The high effectiveness heat transfer is achieved using perforated plate matrix heat exchangers. Experimental results of heat exchanger effectiveness tests and CO_2 removal tests indicate that heat exchangers of the requisite effectiveness were designed and manufactured, and that the proposed process was successful in CO_2 removal to the required level.

Implicit in this work was:

- The development of a new sizing procedure for matrix heat exchangers based on a recently developed approximate analytical solution for their performance.
- Experimental testing of matrix heat exchanger performance and correlation with a recently published numerical solution for their performance prediction.
- The development of a new method for construction of perforated plate matrix heat

exchangers.

- The development of a fully instrumented apparatus to test matrix heat exchangers at cryogenic temperatures.
- The setting up of a mass spectrometer for gas analysis and continuous process monitoring to monitor the CO_2 removal process.
- Testing of matrix heat exchangers when used as reversing heat exchangers.

Preface

This project was initiated to complement research on transport power generation using hydrogen, being carried out by the Fuels and Combustion Research Group at the University of Canterbury. The premise for this research was that liquid hydrogen offered the best medium of storing hydrogen on-board vehicles.

Early readings, amongst which was the Fuel Cell Handbook by Appleby and Foulkes (*Van Nostrand Reinhold, 1989*); indicated that alkaline fuel cells were best suited to transport power generation applications but for their intolerance of CO_2 in the fuel and/or air. Since this project was concerned with the use of liquid hydrogen, the CO_2 content of the fuel was not a consideration. The initial readings also encompassed work by Furuhama et al. (*Proc 8th WHEC, vol.3, 1990*) and Sussman (*Adv Cryo Eng, vol.25, 1980*) on the use of thermomechanical exergy recovery from cryofuels to run Rankine cycle engines. Liquid hydrogen at a storage pressure of 4 bar (typical) has a boiling point of -247°C. The work that can be derived by using the temperature difference between the stored liquid and its surroundings represents an additional ~10% of the chemical exergy of the fuel.

CO_2 removal from air for alkaline fuel cells, and thermomechanical exergy recovery from liquid hydrogen, seemed to tie in simply, by using the liquid hydrogen and the cold boil-off gaseous hydrogen to run a refrigeration purification process to effect CO_2 removal from alkaline fuel cell feed air. The pertinent issues of alkaline fuel cells and liquid hydrogen use are presented in chapter one.

The calculations for CO_2 removal by refrigeration purification showed that this process was reliant on very high effectiveness heat transfer, and that even the heat released by the natural humidity or water content in the air would be too much for this process to work. High effectiveness heat exchangers, and CO_2 removal from air in breathing atmospheres in space vehicles and air liquefaction systems, were investigated. As a result of this study a design for a feasible CO_2 removal process emerged. The refrigeration purification calculations and the schematic layout of the proposed process are shown in chapter two.

Studying high effectiveness heat exchangers led to an excellent review article on matrix heat exchangers by Venkatarathnam and Sarangi (*Cryogenics, vol.30, 1990*). By design, matrix heat exchangers are very compact, very high effectiveness heat exchangers, and it seemed appropriate to try them in the CO_2 removal application. Venkatarathnam had developed a new method for analysing the thermal performance of matrix heat exchangers. He, kindly, provided a copy of his Ph.D thesis. The numerical solution he had worked out was incorporated into a program included in his thesis. The program was designed to be used to determine the performance of the matrix heat exchanger for given flow and geometric parameters. The program in his thesis did not

run. Correspondence with Venkatarathnam was undertaken to try to correct the program in his thesis or obtain a running version. Furthermore, the program did not lend itself to easy optimisation of matrix heat exchanger geometry, or a better understanding of the effect of matrix heat exchanger geometric and flow variables. Using Venkatarathnam's approximate analytical solution, a sizing equation was derived, which allowed a desired effectiveness to be specified and the required gross geometry to be calculated, to obtain that effectiveness. This allowed simple optimisation of the matrix heat exchanger geometry. Corrections made to Venkatarathnam's matrix heat exchanger performance prediction program and a running version only became available in time to compare the experimental results obtained in this work with those predicted using his program.

Venkatarathnam's analysis for matrix heat exchangers was developed specifically for thermal performance analysis for effectiveness >~90%. For whatever reason, he had been unable to construct matrix heat exchangers of a high enough effectiveness to do any experimental correlation. As part of this project a new method for construction of perforated plate matrix heat exchangers was developed. This allowed some experimental correlation for his analysis. The sizing procedure derivation, construction method and the optimisation of matrix heat exchanger geometry in conjunction with manufacturing limits is discussed in chapter three.

Alongside the conceptual development of this process and designing heat exchangers to perform the required duty, an apparatus was developed for evaluating the CO_2 removal process and the heat exchanger performance. This was based on an apparatus used by Gifford et al. (*Adv Cryo Eng, vol.14, 1969*) for measuring cryogenic regenerator performance. For gas analysis a mass spectrometer, and associated vacuum, baking and batch sampling system was set up. This was done in collaboration with Julian Robinson (*M.E thesis, University of Canterbury, 1995*), who was investigating NO_x formation in heterogeneous hydrogen air mixtures. For this project a variable throughput continuous sampling system was developed for use with the mass spectrometer. The design, development and instrumentation of the apparatus is covered in chapter four.

The experimental work was done in four main parts to establish: single heat exchanger effectiveness; system effectiveness; CO_2 removal from dry air; and reversing heat exchanger operation using moist air. The results of this testing are reported and discussed in chapter five.

The conclusions reached as result of the investigations undertaken are presented in chapter six.

Programs written for matrix heat exchanger sizing and optimisation, and process monitoring and control (data acquisition) are listed in the appendices. Analysis of self-pressurisation in liquid hydrogen tanks is covered briefly in an appendix.

This project touches on the areas of hydrogen and fuel cell use, CO_2 removal for alkaline fuel cells, high effectiveness heat exchangers, mass transfer in heat exchangers, and mass spectrometric trace analysis. For the sake of readability the vast background

and review material for each of these topics has not been included. Key references are given as part of the main text.

Publications arising from this work:

GREEN,R.K. and AHUJA,V.; Carbon dioxide removal from air for alkaline fuel cells operating with liquid hydrogen; *Hydrogen Energy Progress X*, vol.3, 1994, p1695-1704
- encapsulating chapter 1 and 2, giving a project rationale and basic refrigeration purification calculation, and the matrix heat exchanger sizing equation from chapter 3.

AHUJA,V. and GREEN,R.K.; Carbon dioxide removal from air for alkaline fuel cells operating with liquid hydrogen - heat exchanger development; *Int. J. Hydrogen Energy* vol.21, no.5, 1996, p415-421
- results of effectiveness tests on a single heat exchanger (chapter 5) are given along with the basic refrigeration purification calculations (chapter 2) and matrix heat exchanger sizing procedure (chapter 3).

AHUJA,V. and GREEN,R.K.; Carbon dioxide removal from air for alkaline fuel cells operating with liquid hydrogen - experimental results; *Hydrogen Energy Progress XI*, vol.2, 1996, p1945-1950
- CO_2 removal test results, system effectiveness results and single heat exchanger effectiveness results from chapter 5 are presented.

In preparation:

Matrix heat exchanger performance at low Reynolds number flows; for submission to *Cryogenics*.

Carbon dioxide removal from air for alkaline fuel cells operating with liquid hydrogen - a synergistic advantage; for submission to the *Int J Hydrogen Energy*.

A new construction method for perforated plate matrix heat exchangers; for submission to *Cryogenics*.

Acknowledgements

I am grateful to my supervisor, Dr. Roger Green, for his guidance and friendship.

I would also like to thank:

Dr. Neil Glasson for his ever available help with computers, electronics, and programming, and for numerous technical discussions and constructive criticisms.

Dr. Peter Harland, without whom I might still be trying to get sensible readings from the AEI Minimass or AEI MS-10 mass spectrometers, for his help with mass spectrometry.

Geoff Leathwick for his remarkable ability in locating and acquiring the various materials and instruments used in this project.

Ken Brown for advice on design details and his workmanship on the apparatus built in the Mechanical Engineering Workshop.

Russell Gillard for his invaluable help on vacuum systems and all the stainless steel welding.

Neville Foot for his help with the AEI MS-10.

Julian Murphy for help with the data acquisition and associated electronics.

Julian Robinson and Ramon Brown particularly, amongst the post-graduate students in the 'Green-Team', for all the hours of intense technical discussion.

Nomenclature

All abbreviations and symbols used in the text have the following meanings unless otherwise defined. In cases where the same symbol is used to represent different things, the meaning of the symbol for that case, is defined in the accompanying text.

Abbreviations

AFC	alkaline fuel cell
FC	fuel cell
FOM	figure of merit
HCV	higher calorific value
LH2	liquid hydrogen
LN2	liquid nitrogen
LN2-HX	liquid nitrogen heat exchanger
m/e	mass to charge ratio
MHE	matrix heat exchanger
CO2-MHE	CO_2 subliming heat exchanger
H2O-MHE	reversing heat exchanger
PAFC	phosphoric acid fuel cell
PEM	proton exchange membrane
SPFC	solid polymer electrolyte fuel cell
ZEV	zero emission vehicle

Symbols

a	square perforation side,m
A	heat transfer surface area,m^2
A_{cr}	spacer area,m^2
A_{fr}	frontal area,m^2
b	separator width,m
B	thermomechanical exergy,kJ/kg
C	mc_p,J/s-K
C_s	volume concentration of impurity
c_p	specific heat, fluid,J/kg-K
d	perforation diameter,m
D	diameter,m
f	friction factor
G_o	G/p, fluid mass velocity in perforation,kg/s-m^2
h	heat transfer coefficient,W/m^2-K
h_D	mass transfer coefficient,m/s
h,H	enthalpy,kJ/kg
H_f	Fin height,m
h_{fg}	enthalpy of vaporisation,kJ/kg
k	conductivity,W/m-K
k_{ax}	axial conductivity,W/m-K
k_c	contraction loss coefficient
k_e	expansion loss coefficient
k_{plate}	conductivity, plate material,W/m-K
k_s	conductivity, spacer material,W/m-K
L	length,m
Le	Lewis no.
$\dot{m}$	mass flow rate,kg/s
M	mass,kg
M	molar mass,kg/mole
n	number of plates in MHE
n	number of moles
Ntu	Number of transfer units
Nu	Nusselts no.
p	plate porosity
p	partial pressure,Pa
P	pressure,Pa

Pr	Prandtl no.
Q	throughput,bar cm^3/s
$\dot{Q}$	rate of heat transfer,kJ/s
R	Universal gas constant
Re	Reynolds no.
s	separator thickness,m
S	entropy,kJ/kg-K
S	standard error
Sc	Schmidt no.
T	temperature,°C or K
U	overall heat transfer coefficient,W/m^2-K
$\dot{v}$	volume flow rate,m^3/s
w	mixing ratio,kg/kg
W	Plate width,m
W	work,kJ/kg
x_t	transverse pitch, distance between holes/hole diameter
x_l	spacer pitch, $(\delta+s)/s$
X	mean value
y	mole fraction
β	surface area per unit volume,m^2/m^3
δ	plate thickness,m
Δ	denotes difference
μ	viscosity,Pa-s
ε	effectiveness
λ	overall axial conduction parameter, (3.14)
λ_p	plate conduction parameter, (3.13)
ξ	drag coefficient, (3.28)
ρ	density,kg/m^3
σ	standard deviation
ϕ	$Ntu_{p,i}/Ntu_{f,i}$

Subscripts

a	air
c,i	cold side inlet
c,o	cold side outlet
D	design
eff	effective
f	fluid
h,i	hot side inlet
h,o	hot side outlet
i	channel number
I	impurity
i,j	i^{th},j^{th} component
m	mixture
m	molecular
min	minimum
max	maximum
n,m	number of samples
o	overall
p	plate (perforated)
r	regenerator
s	surface
T	tube
v	viscous
0	reference state
1,2	channel number or inlet, outlet or initial, final

Temperature subscripts such as T_{BPin} are defined in Figure 5.5 or Figure 4.1.

Superscripts

H	high pressure
L	low pressure

Table of contents

Chapter 1

Alkaline fuel cells and liquid hydrogen for transport applications

The salient issues regarding alkaline fuel cell use for power generation and the storage of hydrogen as a liquid fuel for transport applications are presented to establish the basis for this project.

'Black smoke hung over the city like bad news. The saddest of cities, a city so ruinously sad that it had forgotten its name'. The city of Kahani from Salman Rushdie's novel for children, Haroun and the Sea of Stories, is made happy in the end by rain. It would seem that the negative effects of air pollution on life are now being recorded even in children's literature.

There is an increasing awareness of pollution, particularly of the pollution caused by vehicles in urban areas. This awareness is being reflected in the debate over new legislation. The California Air Resources Board recently passed the requirement, for California, that all major vehicle manufacturers market zero emission vehicles (ZEV). The number of these ZEV's was to represent at least 2% of their total vehicles offered for sale in California, by 1998, 5% by the year 2001 and 10% by 2003. There has perhaps not been such outcry over vehicle legislation since the Federal Emission Regulations in the US, in 1975. The 2% and 5% limits have consequently been dropped while the 10% 2003 figure has been retained for the time being[1].

This increased awareness of vehicular pollution is, as David Scott discusses, in a series of articles published in the International Journal of Hydrogen Energy[2], part of the evolution of the energy system. Describing quality of service, convenience, economic efficiency, energy efficiency and environmental gentility as the indicators of this evolution, he anticipates the use of hydrogen as an energy carrier. Hydrogen can be produced from any primary energy source, and as with electricity, it is completely de-coupled from that energy source. This means that it can be used to power a large range of service technologies and that it is less limited geographically in where these services may be provided. Scott suggests that hydrogen will play a role in transportation, comparable to that played by electricity in communications.

For power generation for transport applications, fuel cells are being tipped as the emerging technology. Helmut Werner, chairman of Mercedez Benz AG, was recently reported[3] as saying, "I am convinced that by the year 2005 we will have fuel cell driven vehicles...which actually operate without emissions. That will be a huge opportunity for the automobile industry." A number of research and demonstration

programs for fuel cell powered vehicles are being carried out: Ballard[4], Daimler Benz[5], EQHHPP[6], Eureka[7] (current status unknown, following the demise of Elenco nv.), Green car[8], Lasercell[9] and H-Power[10]. Fuel cells made by Ballard Power Systems are being used by Daimler Benz and General Motors[11] in their ZEV development programs.

The subjects of hydrogen utilisation and fuel cells are vast. The role of hydrogen as an energy carrier, it production, utilisation, etc. have been written about at length. Background and technical aspects of hydrogen use, production etc. are available in the book by Winter and Nitsch[12]. For fuel cells too, extensive literature is available. The books by Appleby and Foulkes[13], and Blomen and Mugerwa[14] are comprehensive. The book by Wendt[15] covers electrochemical production and combustion of hydrogen. The rest of this chapter covers only the aspects of fuel cells and hydrogen use in automobiles relevant to this project. The salient issues regarding alkaline fuel cell use and storage of hydrogen as a liquid for transport applications are presented to establish the basis for this project.

1.1 Fuel cells for transport applications

Three types of fuel cells have usually been considered for transport applications[16]: phosphoric acid fuel cells (PAFC), alkaline fuel cells (AFC) and proton exchange membrane fuel cells (PEM - also called solid polymer electrolyte fuel cells - SPFC).

PAFC's have an operating temperature of about 200°C. Waste heat available at this temperature allows reformation of carbonaceous fuels such as methanol, on-board vehicles. This has been seen as simplifying the problems of fuel availability and distribution in the short term, and on-board fuel storage. Their reliance on platinum as an electrocatalyst, and the added weight of an on-board reformer have been seen as shortcomings. It must be pointed out that a vehicle with an on-board reformer does not meet the ZEV criteria.

Several researchers such as Appleby[13-p186] have reiterated that for fuel cell (FC) powered vehicles, hydrogen fuelled alkaline fuel cells are ideal. They have very fast start up times, do not require platinum for an electrocatalyst, have low operating temperatures, low structural corrosion problems, and considerably higher power density; up to a 33% weight saving compared to an acid fuel cell[17]. The electrolyte (KOH) in an AFC is, however, poisoned by the CO_2 in the reformed fuel and air, causing rapid deterioration in performance. To date no CO_2 removal system has been demonstrated that meets the criteria of cost, efficiency, weight, and volume for vehicular applications[13-p187;16].

Proton exchange membranes consist of a polymer matrix with functional groups which allow hydronium ion transfer. They are thus acidic in nature. They are gels and require water for conductivity. In the past few years there have been tremendous improvements in the performance of proton exchange membranes. A large part of this is due the work of Srinivasan and his colleagues at Texas A&M University, and Ballard Power Systems Inc.. In recent years, platinum loadings have been reduced 100 fold while at the same time power density has been tripled[18]. As a result SPFC's have become the current focus of vehicular fuel cell projects.

1.1.1 Comparison of PEM and AFC's for transport use

In a paper based on a study for Canadian National Railways, Scott et al.[19] state that of the various types of fuel cells SPFC's and AFC's are especially suitable for transport power generation. They go on to state that the emergence of SPFC's is probably due to the greater number of manufacturers concentrating on SPFC's rather than any inherent technical advantage over AFC's. In keeping with this trend, Elenco nv., the only commercial manufacturer of alkaline fuel cells, was recently declared bankrupt. At the same time Ballard Power Systems Inc., the developer of the PEM fuel cell bus, has won a US$5.9 million contract to develop a 100kW PEM fuel cell for a transit bus for Georgetown University[20]. On a technical basis there are four main issues for comparison between AFC's and SPFC's: efficiency, use of platinum as an electrocatalyst, other material constraints, and ability to use reformed hydrocarbon fuels.

A comparison of the electrochemical performance shown by Barendrecht[21] shows that the potential at the cathode, for oxygen reduction, is consistently higher in an alkaline medium than for an acidic medium. This results in efficiencies for the alkaline system 10-15% higher than the acidic medium.

Platinum loadings for PEM cells are currently 0.05mg/cm^2[18] at the cathode. State of the art SPFC performance reported by Appleby and Yeager[22] in 1986, gave the Pt loading as 4mg/cm^2. Yet the use of Pt has been of concern due to the uncertainty of its availability[23]. Alkaline fuel cells do not require Pt. They have been operated successfully on non-noble electrocatalysts at low temperatures[13-p262;24-p42]. Aqueous KOH is the least corrosive of commonly used electrolytes[13-p411]. For the same reason, the range of construction materials that can be used in acid media is much less.

The use of reformed hydrocarbon fuels poses difficulties for both these types of fuel cells. AFC's cannot tolerate CO_2. Electrolyte carbonation occurs by the reaction

$$CO_2 + 2OH^- \rightarrow CO_3^{2-} + H_2O \tag{1.1}$$

The presence of carbonate:

- reduces the OH^- ion concentration interfering with electrode kinetics;

- increases the viscosity of the electrolyte, limiting the diffusion rate; and
- alters the surface tension of the electrolyte which can result in electrolyte precipitation in the micropores of the electrode rendering it partly inactive.

AFC's cannot even tolerate the 380ppm or so of CO_2 in air. A calculation for the rate at which carbonation occurs is given by Piperopoulou and Bloomfield[17].

The noble metal electrocatalysts in acid media at low temperature are poisoned by CO. For PEM cells the use of reformed hydrocarbon fuel requires some method of removing CO to less than 20ppm[25]. External selective oxidation was used by Ballard to convert CO to CO_2. The reformate is mixed with a small amount of air and then passed through a column packed with 0.5% Pt on alumina. This method has subsequently been adopted by other PEM researchers[26].

1.2 Vehicular storage of hydrogen

The three usual ways of storing hydrogen on board a vehicle are: as a compressed gas, in metal hydrides, or as a liquid. A comparison of these three methods, and others, has been presented by DeLuchi[27]. Figure 1.1 shows the storage density for an amount of stored hydrogen equivalent in energy to 15l of petrol[28]. Liquid hydrogen (LH2) offers the lowest combined mass and volume.

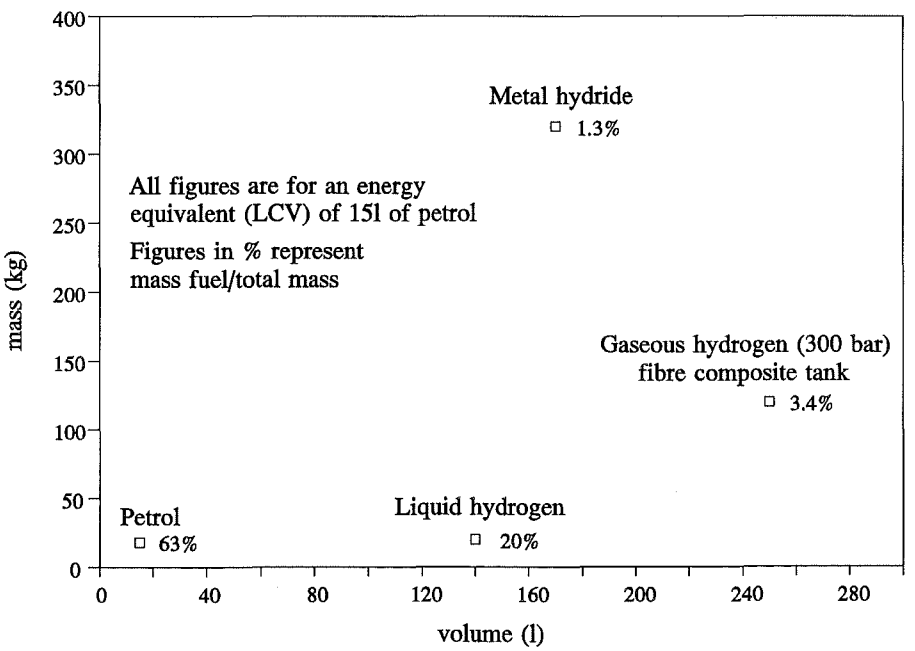

Figure 1.1 Comparison of hydrogen storage options. Source of data: Daimler-Benz AG Publication ÖWU/C 6705•2084-02•0790

1.2.1 Advantage of high energy storage density

High energy storage density means lower mass and volume for the storage system. The low mass particularly, and to some extent the volume, is favourable in terms of vehicle fuel consumption. A comparison of liquid hydrogen storage with hydride storage by Carpetis[29], shows that the fuel consumption in a vehicle carrying hydrides is substantially increased due to the added weight of the hydrides. The calculations are based on the SAE J227a Schedule D driving cycle and a typical family car. For a design range of 200km the fuel consumption for the hydride fuelled vehicle (dual metal hydride, FeTi + MgNi) is 23.6% greater than a liquid hydrogen fuelled vehicle due to the added mass of hydrides alone.

The main drawbacks of liquid hydrogen are considered to be the gaseous boil-off which occurs from all stored liquid hydrogen, and the added energy expended in liquefying hydrogen in the first place.

1.2.2 Boil-off from stored liquid hydrogen

Liquid hydrogen, at typical storage pressures of around 4 bar, has a boiling point of ~-247°C. This creates a large temperature gradient between the stored liquid and its surroundings. As a result there is always some heat leakage into stored liquid hydrogen causing it to vaporize slowly, or boil off, resulting in a rise in pressure inside the storage vessel. To achieve the same density as liquid hydrogen, gaseous hydrogen at ambient temperature requires a pressure of 150 MPa[30], ie. the pressure in a liquid hydrogen container will continue to rise to 150 MPa if the container and its contents are warmed to ambient temperature (provided the container doesn't rupture). Liquid hydrogen containers must therefore necessarily be vented. This venting is wasteful of fuel and potentially hazardous since the vented hydrogen may form a combustible mixture with air.

1.2.2.1 Hydrogen vented from a parked vehicle

Since hydrogen gas is extremely buoyant and disperses rapidly it is difficult to say at what point vented boil-off forms a combustible mixture for what period of time. Safety systems devised and used on vehicles based on liquid hydrogen, use either a catalyst or automatic pilot flame to convert the vented hydrogen to water[31]. Edeskuty and Stewart[30] when discussing disposal of continuously vented hydrogen from liquid hydrogen storage suggest that low flows, up to 1-2g/s, can be vented directly to the atmosphere without flaring. This may not be suitable for small enclosed spaces such as home garages. Swain and Swain[32] have modelled gas cloud motion from a residential gas leak, of methane, propane and hydrogen. They have examined different

leak rates, in four different kitchen geometries. Each kitchen geometry included a simple vent (no fan) above the stove and no stove hood. By mapping the shape and volume of the combustible portion of the fuel cloud as a function of time they found that the dispersion rate of hydrogen was high enough to prevent a combustible mixture from forming in any of the kitchen geometries. Under the same conditions propane and methane leaks were far more dangerous.

A 1W heat leak into an LH2 container corresponds to an amount of hydrogen being vented from which 318W (HCV) may be generated. Blanchard[33] suggests that boil-off losses from vehicles may be minimised by plugging in a refrigerator on occasion of prolonged storage or even perhaps that people may plug their cars in to parking meters for electrical supply to reliquefiers. According to Appleby[34], magnetic refrigeration devices which would be suitable, require engineering breakthroughs. He suggests the use of a hydride container or cold carbon adsorber at the dewar (cryogenic container) outlet.

1.2.2.2 Lock up times

Liquid hydrogen tanks are super insulated to minimise heat transfer into the liquid and the rate at which it boils off. Ewald[35] and Rüdiger[36] give the current minimum boil-off rate as 1.3% per day, corresponding to a total heat leak of 0.6W, for liquid hydrogen tanks built for automobiles. At present vehicular liquid hydrogen tanks have minimum initial lock up times of several days[37], at least exceeding 64 hours (5 pm Friday to 9 am Monday; Stewart[38] gives the lock up time for VLHD-B tank, with a 2W heat leak as 60 hours). Lock up times for a vehicle in use may be longer. This is because due to the movement of the vehicle the tank has been cooled and there is no stratification in the stored liquid, and hence the initial rate of pressure rise is much lower than after prolonged storage.

1.2.2.3 Pressure rise prediction

During the initial evaluation of LH2, theoretical methods of predicting rates of pressure rise (self-pressurisation) in cryogenic tanks were examined. For this work the homogeneous model based on given values of heat leak was used to predict pressure rise, and find an optimum vent pressure. The results for pressure rise match those of Rotenburg[39]. The difference between specific enthalpy and internal energy is maximum for pressures between 2-4 bar. This difference being the flow work, implies that this is theoretically the best venting pressure in terms of cooling achieved due to venting. The equations used for pressure rise and total storage time calculations and a brief review of the other models for self-pressurisation is given in appendix D.

1.2.3 Energy expended in liquefaction

The energy expended in liquefaction of hydrogen has been considered a drawback by some researchers (Appleby[34]). Bracha et al.[40] have reported the performance of the Linde hydrogen plant at Ingolstadt, Germany, which produces 4.4 tons of liquid hydrogen per day. Liquefaction energy is 0.95 kWh/l or 13 kWh/kg. This represents 33% of the total energy available from that hydrogen[34]. Since almost the entire work input is for gas compression, in terms of energy consumption, liquefaction is better than gas compression for high pressure gaseous storage. For example a precooled Linde-Hampson cycle operating between 101.3 kPa and 5.066 MPa gives a liquid yield of about 13%. The work input per kg of liquid hydrogen is equivalent to that for compressing 1 kg of gas to about 385 bar (assuming that the polytropic index is the same). The primary energy input for liquefying hydrogen is thus lower than that for compressing gaseous hydrogen to achieve the same storage energy density. The advantages of utilising a high energy storage density have been discussed previously in section 1.2.1.

In addition to this, thermomechanical exergy recovery from cryofuels can be used to increase the total system efficiency. In the case of LH2, the thermomechanical exergy represents 10.7% of the chemical exergy available from the fuel. Furuhama et al.[41] have developed a Rankine cycle engine which produces enough power to run the LH2 pump which supplies the main I.C. engine. Fyke et al.[42] show that a cryo-engine of 30% thermal efficiency could provide an additional 10kW working with a 120kW fuel cell operating with LH2.

Several projects are under way using liquid hydrogen as the storage medium on board research and demonstration vehicles: DLR-BMW-Messer Griesheim[35], Musashi Institute of Technology[43], Solar Wasserstoff Bayern GmbH[44], Eureka[7], EQHHPP[6], BMW - Linde AG[36], Linde AG-MAN[45] and Greenbus[46].

1.3 Alkaline fuel cells operating with hydrogen stored as liquid

Appleby and Foulkes[13-p187] state that if pure hydrogen were readily available and easily stored on board a vehicle, AFC's would be an obvious choice for vehicular applications. Using LH2 as the storage medium eliminates the complexity, cost, added weight, and emmissions of a reformer. There is no CO_2 contamination from the fuel. The air side CO_2 contamination remains, but is a smaller problem.

The aim of this project was to explore the synergistic possibilities of operating hydrogen-air alkaline fuel cells using hydrogen stored as a liquid, by addressing

simultaneously the issues of;

- the CO_2 removal from air for hydrogen-air alkaline fuel cells, and
- thermomechanical exergy recovery from liquid hydrogen.

This project was an attempt to address these issues by using the cooling available from vaporisation of liquid hydrogen and or boil-off vapour, to remove CO_2 from the fuel cell feed air by refrigeration purification, ie. by freezing the CO_2 out of the air.

As an extension of this process the vented hydrogen boil-off, which occurs while the vehicle is not in use, may be used to generate power, perhaps for trickle charging of batteries while the vehicle is parked. By using the boil-off and recovering the thermomechanical exergy of the cryofuel, it would make the use of liquid hydrogen safer as well as more efficient.

Chapter 2

Evaluation of CO_2 removal using thermomechanical exergy recovery

Viable methods of air side CO_2 removal are discussed. Basic calculations for CO_2 removal from air by refrigeration purification are presented. Exergy calculations are used to show that only 15-17% of the cooling required for refrigeration purification is available. A schematic description of the proposed new process for CO_2 removal is given.

2.1 Methods of air side CO_2 removal for alkaline fuel cells

The CO_2 content of reformed carbonaceous fuel for use in fuel cells, has been the focus of CO_2 removal techniques[47]. CO_2 removal from the air for use in fuel cells (air side) has been variously considered either debilitating, as by Howard and Greenhill[48] or simply written off as by K.Kordesch (in discussion with Bloomfield[17]). Experimental or demonstration hydrogen-air AFC vehicles (Karl Kordesch's Austin A-40[49;13-p193], Elenco's Eureka fuel cell bus[7]) have used soda lime exclusively, to scrub CO_2 from air. Three methods for air side CO_2 removal for an AFC are reviewed here:

- soda lime - because it has been used in this application previously;
- molecular sieve carbon/zeolites - because they are commonly used to remove CO_2 in air separation; and
- in-cell electrochemical removal.

Details of these and several other processes for CO_2 removal from fuel and air side, and their evaluation has been presented previously by Giner and Swette[47], Piperopoulou and Bloomfield[17], and Appleby and Foulkes[13-p266].

2.1.1 Soda lime

Soda lime is a granular solid; a hydrated mixture of calcium hydroxide and sodium hydroxide. Carbon dioxide removal from a gas stream passed through soda lime occurs because of the absorption of CO_2 on the NaOH followed by the reaction of the resulting Na_2CO_3 with $Ca(OH)_2$ to form $CaCO_3$. The overall reaction is

$$Ca(OH)_2 + CO_2 \rightarrow CaCO_3 + H_2O \qquad (2.1)$$

As the soda lime becomes spent a film of $CaCO_3$ is formed around the particles and it is not regenerable. The presence of moisture is essential to the reactions and only moist

gas can be scrubbed of CO_2 in this manner. The water formed in the reaction must be allowed to drain or it may, in combination with small particles, result in blockage of the flow passages. Filters are necessary down stream to contain caustic dust. Soda lime has been used in preference to other expendable absorbers such as lithium hydroxide because it is cheaper and more readily available.

The adsorptive capacity of soda lime increases with decreasing particle size because of increased surface area. Appleby and Foulkes[13-p267] quote a reference saying that one kg of soda lime can clean $1000m^3$ of air, taking the CO_2 concentration from 300ppm to 10ppm. $1000m^3$ of air is required to generate 135 to 250kWh of electricity under normal AFC operating conditions (20-30% oxygen utilisation). Elenco[50], as part of standard peripheral equipment, provided a soda lime CO_2 scrubber with their BCB-1 AFC module rated at a soda lime consumption of 1 kg per 9.6kWh. Piperopoulou and Bloomfield[17] give a figure of 28 lb/h for a 5kW power plant, which equates to 1 kg per 0.4kWh. The Eureka Fuel Cell Bus[7] with an alkaline fuel cell of 78kW nominal power carried 500kg of soda lime[51]. It has not been stated how frequently this had to be changed, but from their soda lime consumption figures, 500 kg would last about 60 hours at nominal load.

It would seem from the above figures that the use of soda lime in automotive applications is not suitable for other than low power applications, or for prolonged use, because it requires large amounts to be carried or frequent replacement. It also requires an infrastructure for distribution, and disposal of the material, when spent.

2.1.2 Molecular sieve carbon/zeolites

Adsorptive separation of CO_2 from air, with solid sorbents, is usually achieved by the steric or molecular sieving effect. Since the effective diameter of water molecules (<3Å) is lower than that of CO_2 molecules (<4Å) the water molecules are adsorbed preferentially in all such cases (Yang[52-p4]). Separation due to the kinetic effect, that is the difference in rates of diffusion of the molecules through the pore structure, is done using molecular sieve carbon. The so called kinetic diameters for water and CO_2 are similar (Yang[52-p271]) and hence these are commonly removed together. Adsorption on solid sorbents is accompanied by release of adsorption energy. For the first molecular layer adsorbed, this energy is higher than for subsequent layers. For the subsequent layers the adsorption energy is the heat of vaporisation (Brunauer et al.[53]). The net adsorption energy is then higher than the heat of vaporisation, although the adsorption will occur at pressures below the vapour pressure of the adsorbate. The adsorptive capacity of the sorbent, and outlet composition of the gas, depends on the relative concentration of the gas mixture components, temperature and pressure. Adsorption and regeneration is achieved by temperature swing, pressure swing, purge gas, or any combination of the three. Most commonly several beds are cycled, the impurity saturated

beds being regenerated by a proportion of the purified gas, first heated to 250-350°C for desorption, and then cooled to increase capacity. These factors mean a large bed size, and high regeneration energy requirements.

Bockris and Appleby[54-p121] state that molecular sieves may be used to give CO_2 levels in the exit gas of 1ppm. Piperopoulou and Bloomfield[17] give the CO_2 partial pressure in the exit gas from Linde 4A and 5A molecular sieves as 1mm Hg, which is higher than that found in the atmosphere. They state categorically that due to this, molecular sieves may only be used for fuel side CO_2 removal.

2.1.3 In-cell electrochemical removal

A system for electrochemical regeneration of the electrolyte in the fuel cell itself, has been developed at Pratt and Whitney and is described by Appleby and Foulkes[13-p270]. In this system electrochemical removal of CO_2 can be achieved, after electrolyte carbonation has occurred. This is done by operating the fuel cell at high current densities for some time. This creates a very low hydroxyl ion concentration at the anode causing the formation of bicarbonate and free carbonic acid which is then decomposed into CO_2. The CO_2 evolved at the anode is flushed out with H_2 gas and vented from the system. To increase the operating time prior to regeneration, electrolyte circulation is used. The OH^- gradient is enhanced by membrane diffusion barriers. The necessary wider electrode gaps and diffusion barriers reduce the performance of the fuel cell.

It is unclear whether the overall performance of the cell still degrades over time. The authors state that with each regeneration the cell voltage returns *almost* to that prior to the test. It is also unclear what the effect is of operating the cell at four times ($400mA/cm^2$) its normal current density for the regeneration period 100 hours.

Other methods such as CO_2 removal using membrane processes have been proposed for air side CO_2 removal. Some of these have been evaluated by McCray et al.[55]. and Lee et al.[56] for CO_2 removal from breathing atmospheres in space applications. These meet the stringent criteria of minimum weight, volume and energy consumption for that application. They have not been demonstrated for CO_2 removal to concentrations as low as a few ppm.

2.2 Refrigeration purification calculations

2.2.1 Basic calculations

2.2.1.1 Cooling required

The maximum allowable concentration of CO_2 for alkaline fuel cell feed air according to Bockris and Appleby[54-p98], is generally taken as 10ppm. Elenco nv. specified 50ppm as being permissable for their standard AFC module[57]. An equation describing the vapour pressure curve may be derived from the Clausius-Clapeyron equation and used in conjunction with the appropriate constants for water and CO_2 listed by Barron[58-p225], to determine that air at a pressure of 1 atm must be lowered to a temperature of 112K to obtain a CO_2 concentration of 10ppm. 384ppm CO_2, the normal concentration in air, becomes saturated at 130K. The concentration of water is <1ppm at the normal sublimation temperature for CO_2, 194.68K. The vapour pressure curves for the temperature range of interest are shown in Figure 2.1 and Figure 2.2.

The cooling required ($\dot{Q}$) to lower air to a temperature of 112K, condense moisture and sublime CO_2 may then be calculated as shown in equation (2.2). This is done by taking the sum of the changes in enthalpy (h) of dry air and the product of the mixing ratio (w) and enthalpy of the components condensed or sublimed for a temperature change from ambient to 112K.

$$\frac{\dot{Q}}{\dot{m}} = (h_{a,2} - h_{a,1}) + (w_{CO_2,2} h_{CO_2,2} - w_{CO_2,1} h_{CO_2,1}) - (w_{H_2O,1} h_{H_2O,1}) \tag{2.2}$$

The mixing ratio for water at a temperature of 112K is negligible and so ignored in (2.2). Taking the worst case for moisture content in air and ambient temperature to be 100% relative humidity at 33°C (0.033kg/kg dry air), and the CO_2 content in air to be 384ppm, the cooling required is -279.5kJ/kg of air, the water alone requiring -84.52kJ/kg of air. The appropriate values for enthalpy were obtained from the data listings of Din[59], and Rogers and Mayhew[60].

2.2.1.2 Exergy calculations

The thermomechanical exergy (B) available from liquid hydrogen is calculated as

$$B = (H_1 - T_0 S_1) - (H_0 - T_0 S_0) \tag{2.3}$$

for steady flow, where H and S are the enthalpy and entropy, and the subscript $_0$ refers to the reference state. Estimating the outlet state as 280K and 1.01325 bar and using storage conditions of 25.957K and 4 bar, the total thermomechanical exergy (ignoring kinetic and potential terms) is 10740.92 kJ/kg. Values of enthalpy and entropy are taken from the monograph by McCarty et al.[61]. If the hydrogen is used only as a heat

sink, only the thermal component of the exergy which is 4087.6 kJ/kg, 38% of the total, is used. Of this, 389.7 kJ/kg is in phase transition and 3697.9 kJ/kg is in gaseous heating.

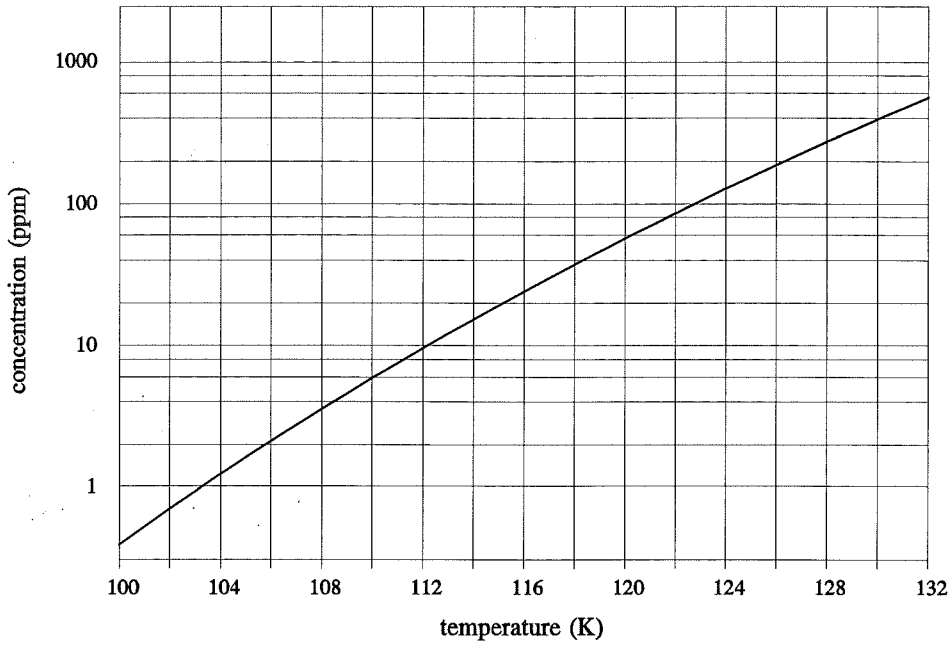

Figure 2.1 Equilibrium concentration for CO_2 in air at 1 atm pressure vs. temperature.

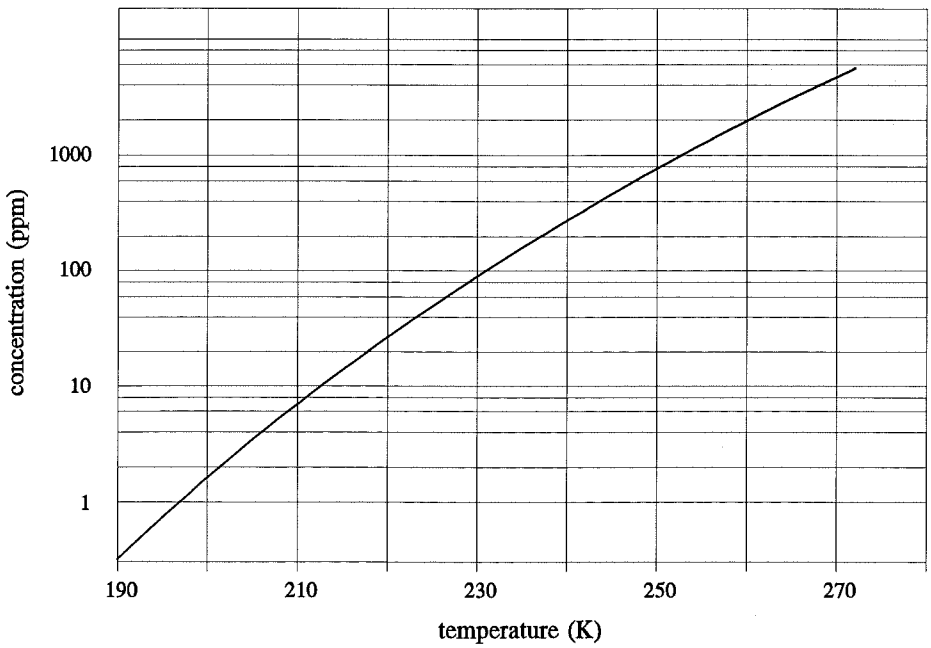

Figure 2.2 Equilibrium concentration of water in air at 1 atm pressure vs. temperature.

2.2.1.3 Cooling ratio

Air is supplied to the FC, in excess of the stoichiometric amount, by an amount equal to the ratio of hydrogen to oxygen utilisation factor. This ratio is usually, according to Giner and Swette[47-p87], taken as 2, or from Elenco's standard module data sheet[57] as 2.5, by volume. Taking the ratio to be 2.5 gives a hydrogen-air mass ratio ~1:85. The ratio of total cooling available to that required is obtained by multiplying the cooling available, the thermal component of exergy, with the mass ratio. For the case of boil-off only it is 0.154, and for vaporisation and boil-off it is 0.170.

2.3 Schematic description of the new process

Only 15-17% of the cooling required to lower air to the calculated cold end temperature, and condense the water and CO_2, is available. This will be further reduced by heat leak from the surroundings into the apparatus. The process of refrigeration purification is thus dependant on air to air heat exchange and the re-vaporisation of the condensed water to an effectiveness greater than at least 85%. The cooling available from the hydrogen is therefore only used to make up the irreversibilities in the heat exchange, the sublimation of CO_2, and any heat leak.

The system must therefore:-

- allow hydrogen-air, and air-air heat exchange at an effectiveness greater than 85%;
- provide for water re-vaporisation;
- be able to purge, periodically, the sublimed CO_2;
- be located at the point of venting of boil-off and insulated, to minimise heat leakage;
- have low mass and volume; and
- have minimal pressure drop to minimise pumping energy.

A heat exchanger apparatus to perform CO_2 removal from air has been designed in three parts as shown in Figure 2.3:

- one reversing heat exchanger operating above the CO_2 saturation temperature, between ambient temperature and ~200K, with flow switching to allow water condensation and re-vaporisation, and air-air heat exchange;
- two direct heat exchangers being cycled in the CO_2 sublimation region, between 200K and 112K; and
- one direct heat exchanger for hydrogen-air heat exchange.

The reversing heat exchanger is similar in principle to the standard reversing heat exchangers used in the air separation industry. It is a counterflow heat exchanger operating between ambient temperature and ~200K. Compared to regenerators, there is no heat storage in the packing, instead, the flow channels are exposed alternately to moist air, and then to dry air at a lower pressure after the CO_2 has been removed,

evaporating the previously condensed water. Therefore at any time, one channel is condensing water and transferring heat to the other channel where water is being evaporated. The flow is switched (inlet and outlet swapped) at a period dependent on how much water can be condensed before that channel needs to be dried, and the minimum volume flow required in each period to nullify cross-over contamination. Flow switching is achieved through two, four-way cross-over valves controlled electronically.

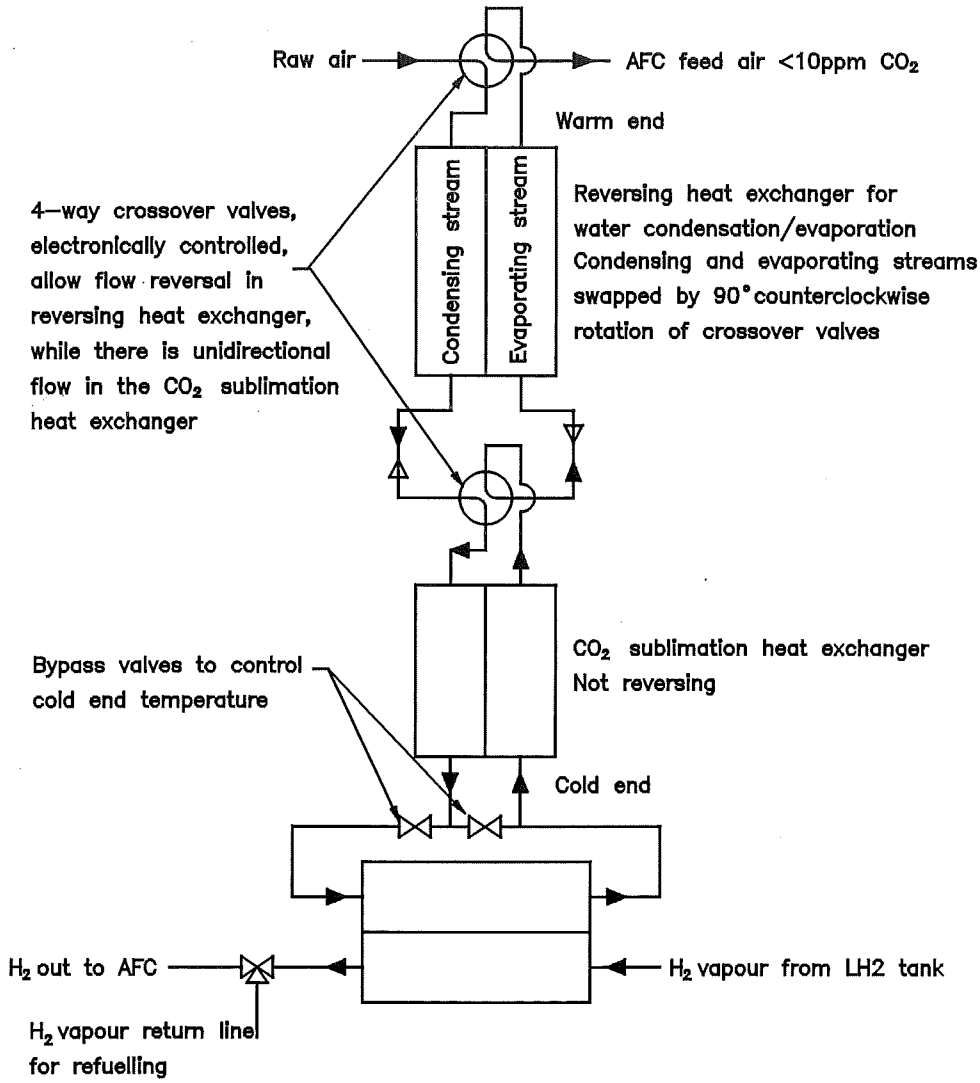

Figure 2.3 Schematic representation of heat exchanger apparatus for CO_2 removal. Off-line CO_2 subliming heat exchanger not shown.

In the CO_2 sublimation region, between 200K and 112K, there are two direct counterflow heat exchangers operating with no flow switching. One is on-line while the other is being dried by simply allowing it to warm up. The volume of solid CO_2 deposited is $0.372 ml/kg_{air}$.

For the experimental work liquid nitrogen (LN2) has been used to provide the amount of cooling which would be available from hydrogen. The air exiting the warm side of the CO_2 subliming heat exchanger passes into a coiled tube immersed in a LN2 bath. A bypass around the LN2 bath and two valves allow control of the proportion of air passing through the LN2 bath. This allows control of the cold end temperature.

The pressure drop between the air inlet and outlet, in addition to that due to the valves and core, may be increased to aid the re-vaporisation of water and the degree of CO_2 removal. This may be done using the bypass valves which also control the cold end temperature.

In practice, initial cool-down is envisaged being achieved by using the boil-off vapour, resulting from initial filling of the liquid hydrogen vessel. Subsequent re-cooling of the CO_2 subliming heat exchangers is done using a bypass from the hydrogen-air heat exchanger.

This schematic represents the general layout for a fully instrumented research apparatus used for this experimental project, not a prototype. The eventual layout may, for example, consist of only two 3 fluid (or 3 stream) heat exchangers with cross-over valves. For this project the CO_2 removal apparatus was sized based on a 1-1.2kW alkaline fuel cell.

2.4 Criteria for efficiency

The minimum work requirement (W) for separation of CO_2 from air may be calculated for a thermodynamically ideal separation system as

$$-W_j/n_m = \boldsymbol{R}T_m \sum_j y_j \ln(1/y_j) \tag{2.4}$$

where $y_j=n_j/n_m$=mole fraction of the j^{th} component, and the subscript $_m$ refers to the mixture. This equation, shown by Barron[58-p151], can be used to calculate for CO_2 the minimum work input which equates to 293 J/kg of air.

It is difficult to establish an equitable criteria for efficiency, or rather, Figure of Merit (FOM), of a CO_2 removal system. The use of expendable absorbers poses no immediate energy penalty other than that due to the pressure drop through the material. On this basis, it is difficult for any regenerable system to have a comparable FOM.

For this work, the FOM of the refrigeration purification method proposed may be calculated in several ways. The actual work input may be taken as:

- work for gas compression to overcome the pressure drop in the CO_2 removal device, and the work input for hydrogen liquefaction;
- the work input for gas compression only, since the hydrogen has already been liquified for storage; or

- the sum of gas compression work input and the total thermomechanical exergy since this exergy would otherwise be available to perform other work as shown by Fyke et al.[42] and Furuhama et al.[41].

It may be that if thermomechanical exergy recovery from cryofuels becomes the norm, the efficiency of processes in harvesting that exergy will become important.

In most cases, for fuel cell system analysis, the power consumed by peripheral equipment is calculated as a percentage of the power output of the FC, ie. as parasitic power consumption. In accordance with this, the parasitic power consumption of this refrigeration purification system may be calculated using only the power consumed by the air blower to overcome the pressure drop. For example, the air pump supplied by Elenco[62] for their standard AFC module (1.2kW) has a power consumption of 125W. The total pressure differential of 100mbar is due to 20mbar through the CO_2 scrubber and filter, and the rest (80mbar) through the fuel cell stack. At the same efficiency and flow rate, the power consumed for the CO_2 scrubber alone would be 25W or ~2% of the output. This is not directly scalable and may be 0.5-0.7% for higher power FC's[62]. An FOM calculated on this basis for the Elenco scrubber, works out to 0.023. Since the CO_2 removal apparatus for this project is sized based on the Elenco nv. standard module, this provides one simple comparison.

Chapter 3

Heat exchanger design and construction

CO_2 removal from air using thermomechanical exergy recovery from liquid hydrogen relies on very high effectiveness heat exchange. Matrix type heat exchangers made from perforated plates were chosen to achieve this. Their application as reversing heat exchangers is discussed. Methods for analysis of their thermal and hydraulic performance are reviewed. A new analytical method for their design has been adopted. This method and its adaptation to this problem are presented. A new method for the construction of MHE's has been devised and is described. Optimization of MHE geometry is discussed.

3.1 Introduction

Calculations for using the thermomechanical exergy of liquid hydrogen to effect CO_2 removal from air, described in the chapter two, show that the process depends on heat exchange to an effectiveness greater than at least 85%. Since the condensation of moisture in the process air represents up to ~30% of the cooling required it is essential that this water be re-vaporised. The description of the required heat exchange apparatus given in chapter two, requires that two heat exchangers operate in separate temperature ranges since the temperature range for refrigeration purification of air by condensation of water and sublimation of CO_2 are quite separate; a reversing section for the water range, above ~200K, and a non-reversing section below 200K.

Reversing heat exchangers have been used commonly in air separation plants for the removal of water and carbon dioxide from the inlet air. Their design and operation is reviewed briefly, and discussed as relevant to this design.

The two heat exchangers to be used are both perforated plate matrix heat exchangers (MHE) to enable high effectiveness heat and mass transfer. Their structure, heat transfer and flow friction characteristics of the surfaces used, and methods of analysis for the thermal and hydraulic performance of matrix heat exchangers are reviewed. A sizing procedure for the heat exchangers is established and a simple program to calculate the size and pressure drop, for various design variables, is developed. It incorporates an iterative procedure for taking into account temperature dependant gas properties.

Unavailability of suitable materials to manufacture wire mesh cores for the matrix heat exchangers led to the development of a new method for construction for perforated plate MHE's. This method allows a metal - plastic construction which was found to be very successful. The construction is described.

Optimization of matrix heat exchanger geometry is complex. An exhaustive search method was used. This optimization was used to check the viability of the new

construction method and its results are presented.

3.2 The reversing heat exchanger

3.2.1 Operating principles

The reversing heat exchanger in its simplest form, is a two channel counterflow heat exchanger in which an impure feed gas at high pressure is cooled by the pure product gas at a lower pressure. Automatic valves at either end periodically switch the two gas streams between channels so that the impurities deposited by the high pressure feed stream are re-vaporised by the low pressure product, without interfering with the heat transfer duty of the unit. The application of reversing heat exchangers to air purification in air separation plants has been described by Lobo and Skaperdas[63]. A detailed description of construction and design details of a reversing heat exchanger are given by Trumpler and Dodge[64]. Denton and Ward[65] have given design details for plate-fin heat exchangers to be used as reversing heat exchangers.

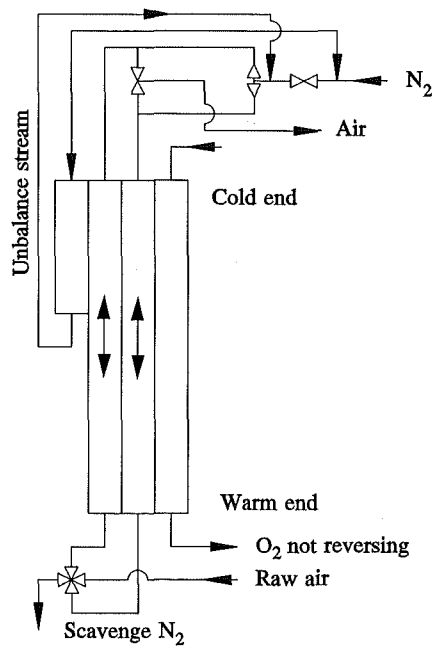

Figure 3.1 Schematic of typical reversing heat exchanger as used in air separation plant.

The complete re-vaporisation of the deposited impurity depends on:

- the difference in pressure between the streams, since this determines the partial pressures and effects the mass transfer rate;
- the temperature difference between the two streams, since this effects the

concentration difference between the surface and bulk gas, and hence the concentration difference at the same temperature level between the two streams, and

- deviation from ideality of partial vapour pressures at low temperature.

Deviation from ideality of the specific heat of the high pressure gas stream at temperatures approaching its boiling point causes the temperature difference between the two streams to increase and this has a deleterious effect on the re-vaporisation.

Temperature differences at the cold end can be controlled by a method proposed by Trumpler, discussed by Lobo and Skaperdas[63]. In this arrangement, applied to air separation, the reversing heat exchanger is a multi-stream heat exchanger with four passages carrying air, nitrogen, product oxygen, and an unbalance stream. A schematic representation of this arrangement is shown in Figure 3.1. The process inlet air is cooled by the other three streams. The streams carrying air and nitrogen are switched, or reversed periodically, so that the water and carbon dioxide deposited by the air are re-vaporised and purged by the nitrogen. The nitrogen, being at a much lower pressure than the air, can hold more water and carbon dioxide than was deposited by the air, at the same temperature as the nitrogen. This is so, even though the mass flow rate of nitrogen is lower than that of air. At low temperature however, the specific heat of air at high pressure (typically 6-7 bar) is greater than that of its components (oxygen and nitrogen) at low pressure (1-2 bar). Therefore the temperature difference between the air, and the nitrogen and oxygen streams increases with decreasing temperature. The nitrogen at this low temperature is unable to re-vaporise all the deposited impurities. The unbalance stream is a portion of the nitrogen stream which is recirculated at the low temperature end thereby increasing the net mass flow rate of nitrogen in that region of the heat exchanger and reducing the temperature difference. This allows complete re-vaporisation, and enables the heat exchanger to continue functioning without becoming blocked and inoperable.

3.2.2 Mass transfer

In this process of removing CO_2 and water from a stream of air by refrigeration purification, the lowest temperature required for sufficient condensation of water is high enough for the bulk air to be considered non-condensible. The temperature ranges in which the condensation of water and then sublimation of CO_2 occur are quite separate so at any given time there is only a single vapour condensing or evaporating. An analysis of the mass transfer processes for the case of condensation of a vapour from a non-condensible gas may be found in the books by Kern[66] or Webb[67].

Figure 3.2 shows a schematic of a cross section of a condenser wall. Two main effects are observed: a depression of the partial pressure of the vapour in the vicinity of the wall, and a depression of the interface temperature. The mass transfer and heat

transfer do not occur independently of each other. The heat (h) and mass (h_D) transfer coefficients are related by

$$\frac{h}{h_D} = \rho c_p \left(\frac{Sc}{Pr}\right)^{2/3} \tag{3.1}$$

showing that the mass transfer coefficient is directly proportional to the heat transfer coefficient. Enhancement of heat and mass transfer by choosing the appropriate surface geometry must be done keeping in mind, as Webb[67] points out, that the effects of surface geometry may be lost due to the liquid or solid film thickness. Whatever geometry is chosen, its effects must be at the gas-condensate interface.

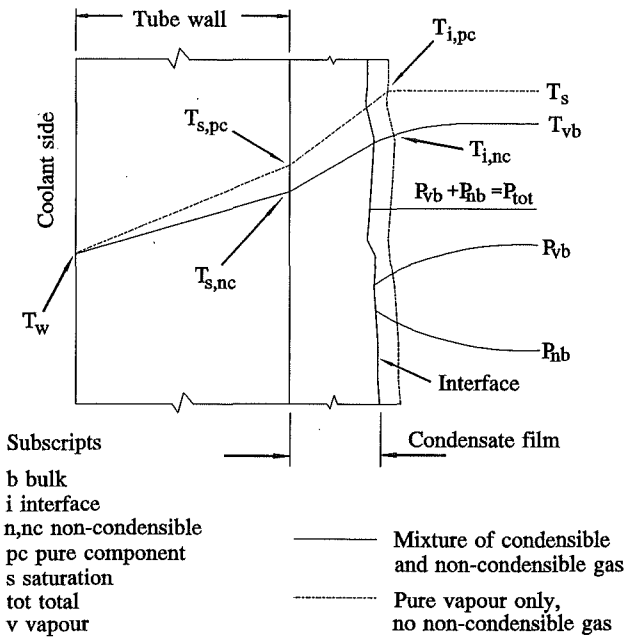

Figure 3.2 Drawing showing partial pressure and temperature profiles for condensation of vapour from a mixture with a non-condensible gas.

Denton et al.[68] have developed a general theory for the operation of reversing heat exchangers. The limiting temperature difference (ΔT) between feed and return gas is given by

$$\Delta T \leq \frac{2T_s^2 \left(\frac{C_s^L}{C_s^H} - 1\right)}{Le\left[\left(\frac{C_s^L}{C_s^H}\right) B^H + B^L\right]} \tag{3.2}$$

The switching time may be determined using the equation for mass deposition rate (m)

$$m=\left(\frac{M_I}{M}\right)\frac{\dot{m}\,C_s^{\,H}CRe^{\,-a}Sc^{\,-b}}{\frac{T_s^2}{Le}\Delta TB^{\,H}-1} \tag{3.3}$$

where T_s is the absolute surface temperature, C_s is the impurity concentration, B is the constant from the concentration equation $C_s=e^{A-B/T}$, M is molecular mass, a,A,b,B and C are constants, the subscript $_I$ refers to the impurity, and the superscripts ^{H} and ^{L} refer to the high and low pressure streams.

For this work the design of the reversing heat exchanger is such that the inlet stream and the purge stream are almost identical. In the inlet air, the CO_2 is 0.057% by mass and the worst case considered for humidity is 3.3% water by mass. The mass flow rate of the purge stream is lower than that of the inlet stream by an amount equal to the sum of the mass of carbon dioxide removed in the non-reversing heat exchanger, and the water not re-vaporised, if any, in the reversing section. The pressure difference is that due to the pressure drop in the non-reversing heat exchanger, the cross-over valve, and the water condensed in the reversing heat exchanger (~5kPa). Thus the flow stream capacity (product of mass flow rate and specific heat) for both streams is almost identical, giving a minimal and constant temperature difference over the length of the heat exchanger. In this case an unbalance stream may be redundant. The cross-over valve will introduce some heat leak into the gas and this will effect the local temperature profile at the cold end of the reversing heat exchanger. Since the mass flow rate and pressure of the inlet and purge streams are very similar and the effect of the cross-over valve is unknown, without experimental measurements it is not possible to predict the minimum obtainable temperature difference. However, in practice, the complete re-vaporisation of water should be able to be controlled by controlling the pressure difference between the two streams if required. This is achieved using the bypass and LN2 heat exchanger valves discussed in chapter two.

Plate fin heat exchangers are used as reversing heat exchangers in air separation plants because of the need for high heat transfer coefficients, low pressure drop, compact volume and low thermal mass. For this work matrix surfaces were chosen because the effectiveness, weight and volume are even more important. Matrix surfaces may be expected to result in higher pressure drop, but at the low flows encountered in this design, the pressure drop is minimal. Low volume was also important from the view of minimising heat leak into the heat exchangers from their surroundings. The flow passages in matrix surfaces are smaller and blockage may be a problem if cycle times (time before flow reversal) are too long.

3.3 Switched dual heat exchangers

The heat exchanger operating in the CO_2 sublimation region is non-reversing. Instead, in this region two heat exchangers are operated alternately. While one is on-stream with solid CO_2 being deposited, the other is off-stream being cleaned. They may be switched periodically using automatically operated valves. Use of switched dual heat exchangers for air purification for oxygen production has been described by Crawford[69] and for purification of hydrogen by Denton et al.[68]. The off-stream unit is cleaned by allowing it to warm up through a temperature range of 17K to 130K, the saturation temperature corresponding to the normal concentration of CO_2 in air. This imposes some additional refrigeration load for re-cooling the off-stream unit before bringing it back on-line.

3.4 Matrix heat exchangers

Matrix heat exchangers were developed to meet the need for very high effectiveness heat exchangers of very low volume. First described by McMahon et al.[70] in 1949, they are now the basis of many cryogenic processes. Detail theory, design method, and heat transfer and flow friction data for compact heat exchangers is presented by Kays and London[71]. An excellent review of matrix heat exchangers is presented by Venkatarathnam and Sarangi[72].

At low performance levels, heat exchanger effectiveness is governed by film heat transfer coefficients. For effectiveness >90% other factors such as;

- axial conduction,
- flow distribution, and
- heat exchange with the surroundings

become important. Kroeger[73] has presented a method for accounting for performance deterioration due to axial conduction. Kays and London[71] present curves for performance deterioration due to axial conduction for balanced flow, $C_{min}/C_{max}=1$, and $C_{min}/C_{max}=0.95$, based on a performance study of periodic flow heat exchangers by Bahnke and Howard[74]. Predicting performance as a function of flow distribution is difficult because flow distribution varies so much. The effect of flow maldistribution for some simple cases has been studied by Fleming[75]. For cryogenic heat exchangers the large temperature difference between ambient and operating conditions is conducive to heat leak. Performance deterioration due to heat leak has been analyzed by Barron[76], and Chowdhury and Sarangi[77].

3.4.1 Matrix heat exchanger structure

The structure of a matrix heat exchanger is shown schematically in Figure 3.3. It consists of a stack of high thermal conductivity (copper or aluminium) perforated plates or wire mesh screens alternating with low thermal conductivity spacers (plastics, stainless steel) bonded together to form leak free passages for the gas streams exchanging heat.

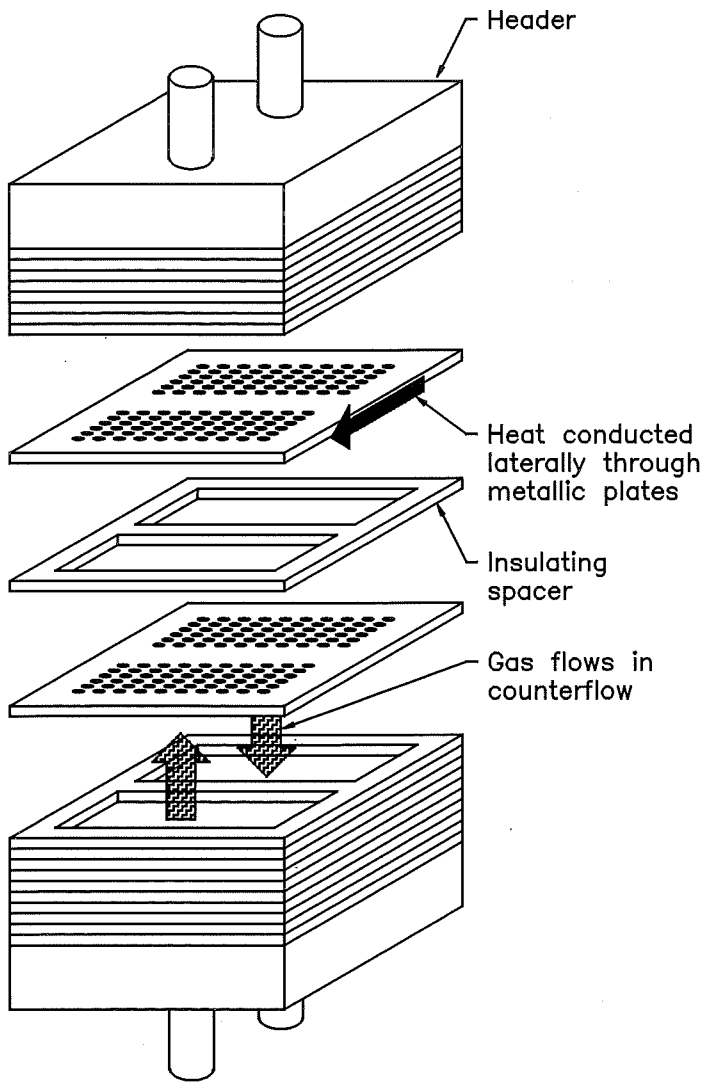

Figure 3.3 Matrix heat exchanger schematic

Gas flows longitudinally in counterflow, and heat transfers laterally from one stream to the other through the plates. The small flow passages (typically 0.3-1.0mm) and successive gaps maintain developing flow ensuring the highest possible heat transfer

coefficients besides providing very high heat transfer areas. The gaps between the screens also ensure uniform flow distribution by continuous re-headering, provided the passages of the same stream are connected internally, rather than at headers at the ends only. The spacers, being of low thermal conductivity, also reduce axial conduction and the associated deterioration in thermal performance.

There is no unique geometry for the plates/screens or the arrangement of process streams. Multiple flow passages are used to reduce fin height (increase fin effectiveness). The low volume and mass of the matrix heat exchanger are important for reducing the exposed area and thus heat leak, and cool-down time.

3.4.2 Choice of perforated plate over wire mesh

As a part of this work, while analytical models of thermal and hydraulic performance were being evaluated, construction materials and methods, for matrix heat exchangers were also tested. Given that the thermal hydraulic properties of wire mesh are superior to those of perforated plate: higher porosity, higher surface area per unit volume, and lower drag coefficient; and that wire mesh has been studied more extensively in connection with its use in regenerators, the initial work focused on wire mesh. Although spacers made from several materials were tried, bonding and sealing problems persisted. Subsequently a suitable method for construction using perforated plates was developed. The rest of this chapter is therefore focused mainly on perforated plate matrix heat exchangers. Construction techniques are covered in the latter part of this chapter.

3.4.3 Matrix heat exchanger analysis

Matrix heat exchangers were initially treated as conventional heat exchangers employing an extended fin surface on both sides. The standard hyperbolic tangent formula was used for fin effectiveness by McMahon et al.[70] Subsequently Fleming's[78] relation, based on the assumption that the temperature difference between the fluid and the matrix, rather than the fluid temperature itself remains constant over the length of the fin, has been used. Axial conduction was accounted for by the method of Kroeger[73]. Sarangi and Barclay[79] treated the MHE as a discrete set of plate-spacer pairs, instead of being uniform in the axial direction, and found a substantial ineffectiveness to be related to the finite number of plates. They assumed, however, that fin effectiveness was unity.

In the most recent analysis available, Venkatarathnam[80] has derived two second order ordinary differential equations and four algebraic equations describing the energy balance and heat transfer for every plate, based on the assumptions that the axial temperature gradient in the plate is negligible and hence the full temperature drop takes

place across the spacer. He has developed an algorithm to solve these equations in an iterative manner.

Venkatarathnam's analysis for the thermal performance of MHE's has been used as the basis for designing the MHE's for this project for two reasons:

(a) Venkatarathnam's analysis represents the latest and most complete work on MHE's, in terms of accounting for the discrete plate-spacer pair sets and fin effectiveness.

(b) His analysis was developed specifically for thermal performance of >~90% effectiveness. He was, however, unable to manufacture an MHE of high enough effectiveness to perform suitable experimental correlation. The effectiveness of the MHE reported in his results was only 65%. Using his analysis represents an opportunity for experimental correlation to his theoretical work.

Using Venkatarathnam's analysis posed some problems. The source code of the program incorporating his solution algorithm for the energy balance and heat transfer equations, as presented in his thesis, does not run. He has developed an approximate analytical solution as well. This analytical solution was used, with modification, to derive a sizing equation for designing perforated plate MHE's for this project.

The matrix heat exchangers built for this project used perforated plates made from copper and spacers made from glass laminate. The thermal mass of these heat exchangers is quite high and thus warranted a comparison with regenerator performance. In regenerators, the fluid and packing temperatures depend on time in addition to position. Mathematical analysis is even more complex and as a result several approximate and numerical solutions have been developed. These have been reviewed, and a summary of design theory presented, by Coppage and London[81]. No complete analytical solution is available for the equations describing the energy balance in the gas and packing except for the case $C_r/C_{min}=\infty$. In this case the behaviour becomes identical in form to that of a direct type counterflow heat exchanger.

$$\varepsilon=\frac{1-e^{-Ntu(1-C_{min}/C_{max})}}{1-\frac{C_{min}}{C_{max}}e^{-Ntu(1-C_{min}/C_{max})}} \tag{3.4}$$

Further if $C_{min}/C_{max}=1$ then

$$\varepsilon=\frac{Ntu}{Ntu+1} \tag{3.5}$$

where C is the product of mass flow rate and specific heat, and the subscripts $_r$, $_{min}$, and $_{max}$ refer to the regenerator and the minimum and maximum value of the product for the two gas streams, respectively. The mass flow rate of the regenerator is given by the product of its mass, specific heat and the number of regenerator cycles per second. For a fixed-bed regenerator the number of regenerator cycles per second is the reciprocal of the period of one complete flow reversal. Numerical finite-difference methods have been used by Lambertson[82] and Bahnke and Howard[74] to extend the results to cover

$1 \geq C_{min}/C_{max} \geq 0.1$, $1 \leq C_r/C_{min} \leq \infty$ and $1 \leq Ntu \leq 100$. For $C_r/C_{min} > 5$ the solution is very close to the limiting solution of $C_r/C_{min} = \infty$ and hence to that of a direct type counterflow heat exchanger.

3.4.4 Heat transfer and flow friction data

The total heat transfer resistance between the fluid streams is made up of: convective heat transfer between the gas and the perforated plates; and conduction along the screens, and across the separator. The convective heat transfer process and flow friction characteristics of a matrix heat exchanger are complex. The flow cross section changes substantially, continuously, between that of the mesh or perforated plate and that of the spacer. Consequently, the fluid undergoes alternate expansion and contraction as it flows through the exchanger. Two stacking arrangements for the perforated plates or wire mesh are possible, the perforations of adjoining plates being aligned or staggered. Mikulin et al.[83] and Venkatarathnam and Sarangi[84] suggest that for the staggered case, and the aligned case where spacer thickness is greater that the pore diameter, the boundary layer is interrupted at every screen maintaining developing flow. In the aligned case, if the spacer thickness is less than or equal to the pore diameter the flow through the perforations tends to become developed turbulent flow, with a secondary recirculation or stagnant zone occurring in the gaps.

3.4.4.1 Convective heat transfer

Convective heat transfer occurs at the front and back faces of the plates and in the tubular surface of the perforations. The fluid impinging continuously on the front face of the plates gives heat transfer coefficients that are an order of magnitude higher than those normally associated with gaseous heat transfer.

Heat transfer data and empirical correlations for perforated plates have been determined by McMahon et al.[70], Mikulin et al.[83], Orlov et al.[85], Shevyakova and Orlov[86], and Hubbell and Cain[87]. These are tabulated in Table 3.1. Heat transfer data and empirical correlations for wire mesh have been determined by Coppage and London[88], Tong and London[89], and Mikulin and Shevich[90].

The general approach has been to find an empirical relation of the form

$$Nu = C\ Re^{\,n} \tag{3.6}$$

to fit the data, where C and n are functions of geometric parameters and Re is based on the flow velocity in the perforation and the perforation diameter as the characteristic dimension. For this work the equation (3.7) derived by Venkatarathnam[80], combining empirical equations for heat transfer from impinging jets on facing and lee sides of a plate and the cylindrical surface of perforations, has been used for the design of the perforated plates. This was done with correlation of the experimental work to his

analytical work in mind.

$$Nu=\frac{7.32\frac{\delta}{d}+\frac{0.146Re}{1+0.012(Re\ d/\delta)^{0.8}}+\frac{0.475Re^{0.476}}{\sqrt{p}}+0.0237Re^{0.72}\frac{1+\sqrt{p}}{\sqrt{p}}}{\frac{1-p}{p}+\frac{2\delta}{d}} \quad (3.7)$$

where p is the porosity, d the diameter of the perforation, and δ is the thickness of the plate.

Table 3.1 Heat transfer correlations for perforated plate matrix heat exchangers

Correlation	Restrictions	Source
$h=a\ Re^n$, $0.88<n<1.14$	$800<Re<4000$, $p=0.403$	McMahon et al.[70]
$Nu=0.2\ Re^{0.64}$	$70<Re<2100$, shifted holes	Mikulin et al.[83]
$Nu=0.22\ Re^{0.69}$	$30<Re<1600$, shifted slots	
$Nu=0.065\ Re^{0.74}(s/d)^{0.21}$	$200<Re<1000$, $0.11<s/d<1$, aligned holes	
$Nu=0.045\ Re^{0.87}(s/a)^{0.5}$	$200<Re<1400$, $0.075<s/a<0.88$, aligned slots	
$StPr^{2/3}=1.2\ Re^{-0.62}$	$300<Re<3000$, $p=0.3246$	Orlov et al.[85]
$StPr^{2/3}=C\ Re^n$, $C=3.6\times10^{-4}[(1-p)p-0.2]^{-2.07}$ $n=-4.36\times10^{-2}p^{-2.34}$	$300<Re<300$, $0.3<p<0.6$, $0.4<s<1.6$	Shevyakova and Orlov[86]
$Ntu/plate=b\ Re^{-m}$ $b=2.104, 3.549, 3.747$ $m=0.372, 0.503, 0.569$	$Re<100$, $p=0.09, 0.236, 0.245$	Hubbell and Cain[87]

3.4.4.2 Conduction along perforated plates

The conductivity of a perforated material may be determined by Lord Rayleigh's[91] expression

$$\frac{k_p}{k}=\frac{1-p}{1+p} \quad (3.8)$$

where p is the porosity of the material, k it's conductivity, and the subscript $_p$ refers to the perforated material. For high porosity the numerical solution of Keller and Sachs[92] for p>0.5 for a square array of holes, shown in equation (3.9) may be used.

$$\frac{k_p}{k}=\left(\frac{\pi}{[2-(16p/\pi)^{0.5}]^{0.5}}-1.95\right)^{-1} \tag{3.9}$$

3.4.4.3 Flow friction

Flow friction data and empirical correlations for drag coefficient for perforated plate have been determined by several authors. The results of McMahon et al.[70], Mikulin et al.[83], Shevyakova and Orlov[86], and Hubbell and Cain[87] all show that flow friction varies minimally with Reynolds number at Re>200, indicating that form drag predominates.

Venkatarathnam[80-p98] in his thesis has presented a graph of drag coefficient versus plate porosity determined from the results of Shevyakova and Orlov, Mikulin et al., and Hubbell and Cain. These are compared against values calculated from entry and exit pressure loss coefficients for multiple-circular-tube cores and apparent friction factor for the hydrodynamic entry length of a circular tube presented by Kays and London[71:Fig.5-2,p111;Fig.6-23,p138]. He concludes that the values calculated from the data of Kays and London are substantially higher than those for real MHE's. However, for his calculations, he has used the *apparent* friction factor which already includes entry and exit loss, and he has ignored their recommendation of using values for Re=∞ for interrupted fin surfaces. His data points attributed to Mikulin et al., and Hubbell and Cain do not appear correct. Furthermore, the choice of a Re of 80 for comparison seems unreasonable since Mikulin et al.'s correlation is only valid for Re>100 above which ξ is independent of Re, and Shevyakova and Orlov's correlation applies to Re<160 once again above which ξ is independent of Re. Venkatarathnam's graph is re-plotted here as Figure 3.4, for Re=160 and $\delta/d=1$. Hubbell and Cain's data is not included since it is not for $\delta/d=1$ and thus not directly comparable.

3.4.4.4 Geometric dependence of heat transfer and flow friction: lack of consistency in results

The convective heat transfer and flow friction characteristics of perforated plate and wire mesh are strongly dependent on the shape and size of the perforations, porosity, plate and spacer thickness, alignment of perforations on adjoining plates, as well as the method of manufacture. Hubbell and Cain[87] show different heat transfer results for perforated plate manufactured by punching, with the perforation breakout material facing upstream, and downstream. This strong geometric dependence of heat transfer and flow friction characteristics is in keeping with the lack of agreement in the results of the various researchers, which is evident from Table 3.1 and Figure 3.4. The results of

Coppage and London[88] and Tong and London[89] collated by Kays and London[71] for heat transfer with wire mesh and crossed rod matrices have been correlated with porosity by Qvale and Smith[93]. They were able to find some degree of correlation for the random stacking case but not the aligned case.

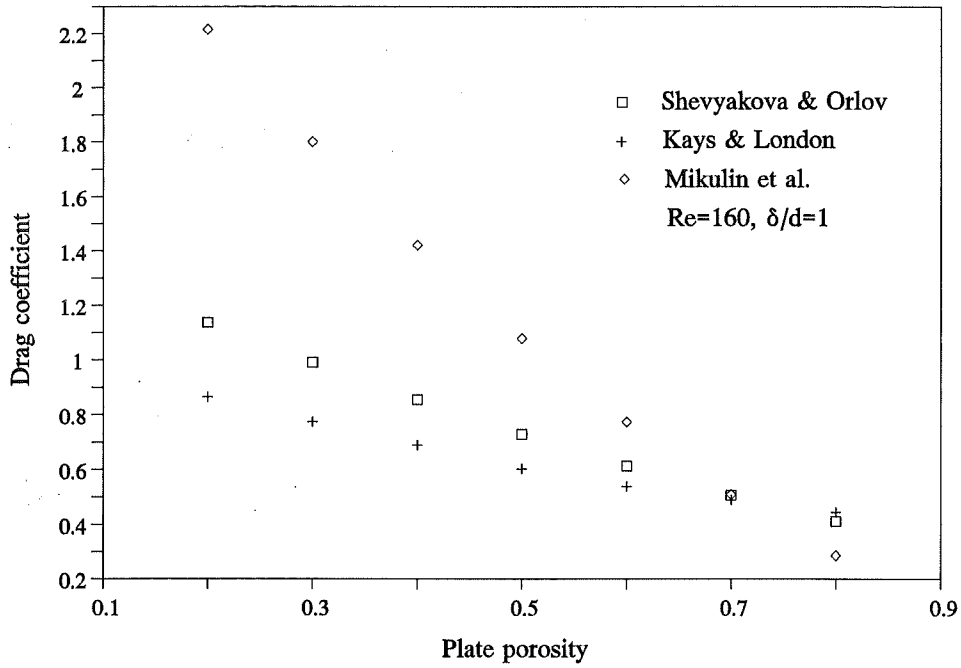

Figure 3.4 Graph of drag coefficient vs. plate porosity at Re=160.

The effects of spacer thickness on the heat transfer coefficient and flow friction depend on the manner of stacking. For the staggered case increasing the spacer thickness to pore diameter ratio can be expected to reduce the drag coefficient while not substantially effecting the convection heat transfer coefficient. This is backed up by the results of Mikulin et al.[83], Orlov et al.[85] and Shevyakova and Orlov[86]. For aligned holes increasing the spacer thickness to pore diameter ratio may be expected to increase both the heat transfer and drag coefficient, and this is confirmed by the results of McMahon et al.[70] and Mikulin et al.[83].

3.5 Sizing procedure development

3.5.1 Heat transfer

Venkatarathnam's approximate analytical solution for the equations for energy balance and heat transfer, accounting for the heat transfer coefficient, axial conduction, number of plates, and fin effectiveness in MHE's, for balanced flow is shown in

equation (3.10).

$$Ntu_{eff}=\frac{n(1-\alpha_1)(1-\alpha_2)}{\lambda n(1-\alpha_1)(1-\alpha_2)+1-\alpha_1\alpha_2+(1-\alpha_1)(1-\alpha_2)/Ntu_{po}} \tag{3.10}$$

where

$$\alpha_i = e^{-Ntu_{fi}} = e^{-2Ntu_D/n} \tag{3.11}$$

and Ntu_{po}, the overall plate Ntu is defined as:

$$\frac{1}{Ntu_{po}} = \frac{1}{\lambda_p}+\frac{1}{3\phi_1 Ntu_{f,1}}+\frac{\nu}{3\phi_2 Ntu_{f,2}} \tag{3.12}$$

with

$$\lambda_p=\frac{k_{plate}\delta W}{bC} \tag{3.13}$$

$$\lambda=\frac{k_s bW}{nsC} \tag{3.14}$$

Plate and spacer dimensions relevant to these equations are shown in Figure 3.5.

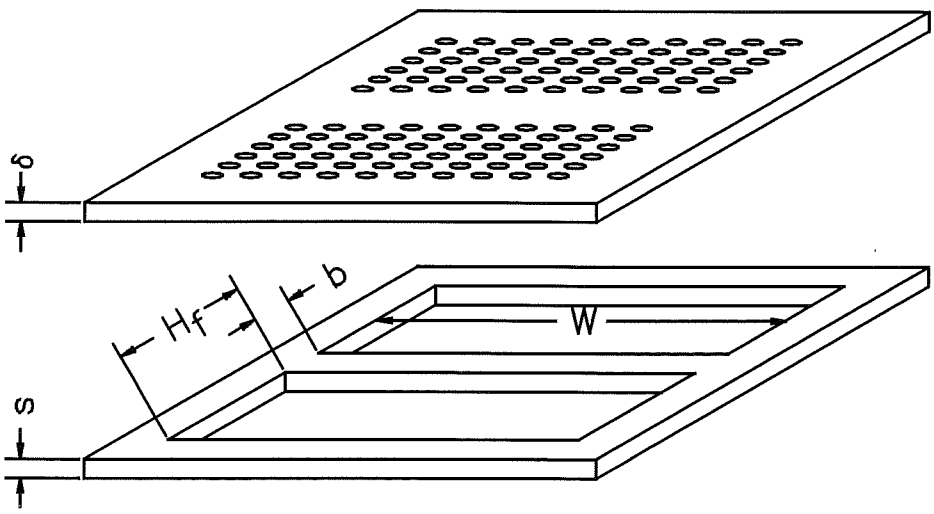

Figure 3.5 Perforated plate and spacer dimensions

Venkatarathnam has used the simplification of neglecting transverse resistance in the separator, by assuming the plate conduction parameter $\lambda_p=\infty$. Thus

$$Ntu_{po}=\frac{3}{2}Ntu_{p,i}=\frac{3k\delta}{2G_o pc_p H_f^2} \tag{3.15}$$

The axial conduction parameter defined in (3.14) incorporates a spacer area equivalent only to that of the separator (bW). This is a small proportion of the area over which axial conduction occurs. In keeping with the definition of the axial conduction parameter used by Kays and London[71] and Kroeger[73] the overall axial conductivity and total

area for axial conduction have been used to re-define the axial conduction parameter.

$$\lambda = \frac{k_{ax} A_{cr}}{nsC} \tag{3.16}$$

where

$$k_{ax} = \frac{\delta + s}{\frac{\delta}{k_{plate}} + \frac{s}{k_s}} \tag{3.17}$$

The sizing equation can then be derived from equation (3.10) by re-arranging the terms and solving by substitution. The sizing equation gives the surface area required for any known desired Ntu. From (3.10), (3.11) and (3.15)

$$Ntu_{eff} = \frac{n(1 - e^{-2Ntu_D/n})}{n\lambda(1 - e^{-2Ntu_D/n}) + (1 + e^{-2Ntu_D/n}) + \frac{(1 - e^{-2Ntu_D/n})}{3/2Ntu_{p,i}}} \tag{3.18}$$

Using (3.15) and (3.16)

$$Ntu_{eff} = \frac{n}{\frac{k_{ax} A_{cr}}{\delta C} + \frac{1 + e^{-2Ntu_D/n}}{1 - e^{-2Ntu_D/n}} + \frac{2G_o pc_p H_f^2}{3k\delta}} \tag{3.19}$$

Taking the number of plates as

$$n = \frac{A}{\beta A_{fr} \delta} \tag{3.20}$$

which gives

$$\frac{-2Ntu_D}{n} = \frac{-2U\beta A_{fr}\delta}{C} \tag{3.21}$$

Equation (3.19) can then be solved as

$$A = [e^{2\tanh^{-1}(-2U\beta A_{fr}\delta/C)} + \frac{k_{ax} A_{cr}}{\delta C} + \frac{2G_o pc_p H_f^2}{3k_{plate}\delta}]\beta A_{fr}\delta Ntu_{eff} \tag{3.22}$$

The variation of properties of air over the temperature range in the heat exchanger is taken into account by going through the calculations for chosen increments of temperature. The effect of humidity in air has been included in the calculations. For a known number of increments, n, the hot and cold side inlet temperature, $T_{h,i}$, $T_{c,i}$, and the effectiveness the size of the temperature increments, ΔT, is calculated.

$$T_{c,o} = \varepsilon(T_{h,i} - T_{c,i}) + T_{c,i} \tag{3.23}$$

$$\Delta T = \frac{T_{c,o} - T_{c,i}}{n} = \frac{T_{h,i} - T_{h,o}}{n} \tag{3.24}$$

Since the heat exchanger required is a counterflow arrangement exchanging heat between

two streams of the same fluid, $C_{min}=C_{max}$, and with negligible longitudinal conduction, the temperature vs. length profiles of both streams will be necessarily identical though slightly shifted, ie. the temperature difference between the hot stream and the cold stream, $T_{h,i}-T_{c,o}$, is constant over the length of the heat exchanger (Kays and London[71,p34]). The heat transferred is given by

$$UA(T_{h,i}-T_{c,o})=C(T_{c,o}-T_{c,i})=C(T_{h,i}-T_{h,o}) \tag{3.25}$$

ΔNtu, the number of transfer units for each temperature increment, then becomes

$$\Delta Ntu=\frac{(T_{c,o}-T_{c,i})/n}{T_{h,i}-T_{c,o}}=\frac{\Delta T}{T_{h,i}-T_{c,o}} \tag{3.26}$$

3.5.2 Pressure drop

The core pressure drop is derived from the relation given by Kays and London[71,p36]

$$\Delta P=\frac{nG_o^2}{2\rho}(4f\frac{\delta}{d}+k_c+k_e) \tag{3.27}$$

For matrix surfaces the entrance and exit effect is usually included in the friction factor then referred to as the equivalent friction factor or drag coefficient, wherein the drag coefficient is defined as

$$\xi=2f\frac{\delta}{d}+\frac{1}{2}(k_c+k_e) \tag{3.28}$$

3.5.3 General approach to the sizing problem

The required effectiveness of the heat exchanger is the starting point for the sizing problem. For a user specified geometry the total surface area required and hence the volume, number of plates and pressure drop can be calculated using equations (3.22), (3.26) and (3.27). The schematic approach to this sizing procedure is shown in Table 3.2. Temperature dependant fluid properties are read in from a file and interpolated if necessary. A listing of the source code is given in appendix A.

3.6 Matrix heat exchanger - construction

Several methods for construction of MHE's have been used since they were first made in 1950 by McMahon et al.[70]. Venkatarathnam and Sarangi's excellent review[72] of matrix heat exchangers covers the various methods and hence these are

Table 3.2 Schematic approach to heat exchanger sizing including temperature related variation of fluid properties

Input	Calculate for each temperature increment	Output
• effectiveness • hot and cold end temperatures • number of temperature increments • plate geometry • flow rate	• average bulk fluid temperature • fluid properties • local flow and geometry dependant variables • overall heat transfer coefficient • area required • pressure drop	• total area • volume • number of plates • total pressure drop

only reported here briefly or as pertinent. McMahon et al. used commercially available punched plates in a demountable assembly with neoprene gaskets. Vonk[94] used paper impregnated with cresol (phenolic) resin to form spacers between wire mesh screens. The MHE was fabricated by hot pressing (curing at elevated temperature and pressure) a stack of screens and spacers in a suitable jig. These MHE's are still in use in Phillips Helium Liquefiers. Since then, adhesive bonding has been used for providing leak free bonds between metal plates and plastic spacers. Detailed information on types of adhesives and joining techniques are not generally available in open literature. Lately vacuum diffusion welding has been used to make all metal MHE's. An example of this is described by Voronin et al.[95].

For this work the method described by Vonk[94] was used in an attempt to fabricate wire mesh cores. The hot press constructed for this purpose is shown in Plate 3.1. Several materials were tried as spacers: paper based pre-impregnated material, epoxy resin films, epoxy resin with thickeners to reduce flow, Xylan flouropolymer, etc.. None of these materials met the criteria of providing leak free bonding and ease of application.

Following the failure of attempts to manufacture wire mesh cores in-house, a new method for fabricating perforated plate heat exchangers was devised using materials and processes that were available locally. Perforated plates were manufactured by photo-chemical etching. Spacers were made from fibre glass laminate used for printed circuit boards (PCB). This laminate has 70μm thin copper film pre-bonded on either side. Spacers were manufactured by punching. The plates and spacers were screen printed with Indalloy® (Sn Pb Ag) solder paste, stacked in a jig and baked to flow the solder.

This resulted in a very successful soldered metal-plastic MHE construction.

Plate 3.1 Hot press built for fabricating wire mesh and thermosetting plastic pre-preg spacer MHE cores.

This method of construction placed certain limitations on the MHE geometry. Copper was used for the perforated plates instead of aluminium, for ease of soldering. Two thicknesses of copper sheet were commercially available, 0.5mm and 0.2mm. The 0.2mm sheet came as a roll and was flimsy to handle. Several samples of 0.5mm thick perforated plates were manufactured by photo-chemical etching to explore the lower limits of perforation diameter and perforation spacing which could be achieved by this process and the allowances required for the etchant under-cutting the photo-resist. Plate 3.2 shows two of these samples. The lower plate shows the effect of under-cutting, the concave surface of the hole created by the etchant, even in a double sided etch. The

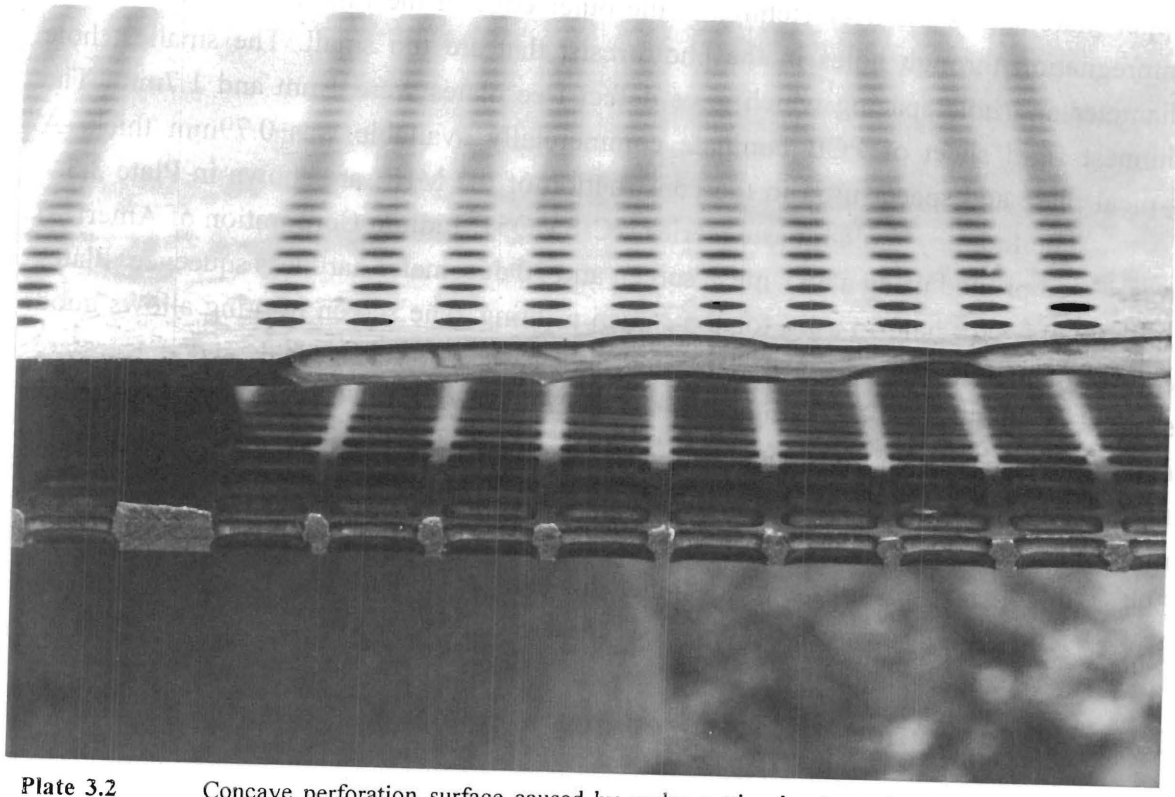

Plate 3.2 Concave perforation surface caused by under cutting by the etchant. Over etching at the edge caused by holes in photo-resist being too small

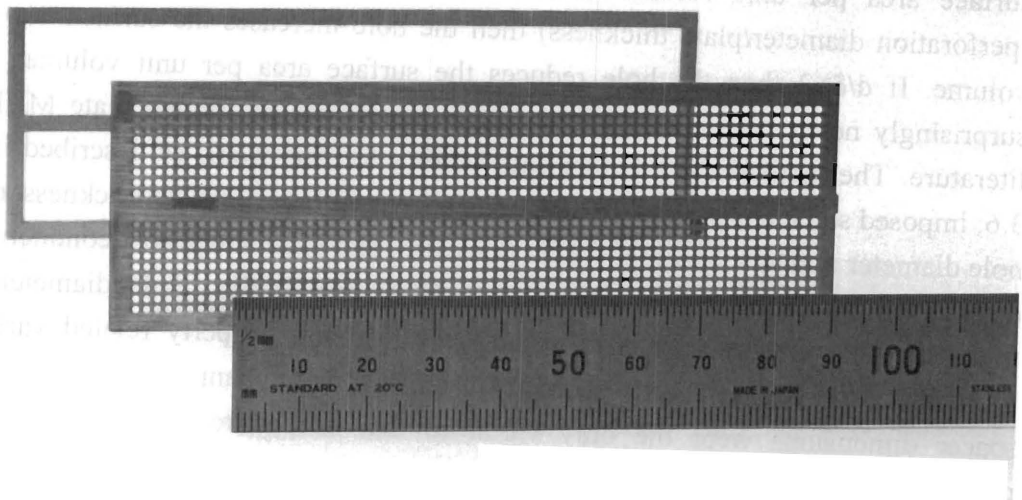

Plate 3.3 Plate and spacer used for MHE construction.

upper plate shows the over etching of the outer edge in the time allowed for etchant impregnation through holes in the photo-resist that are too small. The smallest hole diameter and hole spacing which gave defect free plates were 1mm and 1.7mm. The thinnest rigid sheet of PCB laminate commercially available was 0.79mm thick. A typical plate and spacer used in the construction of the MHE are shown in Plate 3.3.

The Indalloy® solder paste (series NC-SMQ51, Indium Corporation of America) was screen printed using a 36T mesh screen and 70 durometer hardness squeegee. Plates and spacers were held in a jig for the screen printing. The screen printing allows good control of the amount of solder deposited on each surface. The plates and spacers are stacked in another jig for holding them in place in the oven while the solder flows. A dry run (prior to being screen printed) of the stack of plates and spacers with thermocouples placed at various points in the stack was used to set the temperature-time ramp-up profile prescribed for the solder paste. The headers, which are constructed from 304 stainless steel, were previously tinned for ease of soldering.

3.7 Optimization of MHE geometry

Optimization of MHE geometry is extremely difficult because of the large number of variables. Equation (3.22) gives the surface area required for any known desired Ntu. There are 13 independent variables in this equation, and the interrelationships between these variables are extremely complex. One of the main requirements is to make the heat exchangers as small as practicable. To achieve this the surface area per unit volume must be maximised. For perforated plate if $d/\delta<2$ (perforation diameter/plate thickness) then the hole increases the surface area per unit volume. If $d/\delta>2$ then the hole reduces the surface area per unit volume. This has surprisingly never been stated previously in any of the perforated plate MHE related literature. The method used to fabricate MHE's for this work, as described in section 3.6, imposed some constraints on the geometric variables. The plate thickness, minimum hole diameter and hole spacing, spacer thickness, and plate and spacer conductivity were determined by process limitations and material availability. Hole diameter to plate thickness ratio was two ($d/\delta=2$). Fluid flow rate and property related variables are predefined in this case. Gross geometry variables: flow channel width, fin height and spacer dimensions were the only variables that needed to be defined for optimal performance.

Optimization of MHE geometry was done by using an exhaustive search to minimize a *Goodness* factor. The factor used was a weighted combination of MHE volume, number of plates and pressure drop. The weightings reduced the numbers to the same order of magnitude so that their contribution to the Goodness factor was even. A

simple program was written to calculate the Goodness factor for a user defined number of dimensions (variables), range and intervals for each dimension. The program stores a user defined number of optimum solutions from the entire lattice. Regions of interest may then be explored by defining smaller intervals. This is by no means an efficient method for optimization, but given the complex interplay of several variables, is simple and should allow a definitive mapping of the Goodness factor. Equal intervals were used for incrementing each variable and so sets of best results were recorded to eliminate highly localised minima. A copy of this program is listed in appendix A.

Prior to a method of construction being devised this exhaustive search optimization was done for plate thickness δ, hole diameter d, hole spacing x_t, spacer pitch x_l, channel width W and fin height H_f. This was done for wire mesh cores as well, for wire diameter and spacing instead of δ, d and x_t. The results for wire mesh are not reported here as no experimental work was done to give comparable values. The best results calculated in this way for perforated plate are shown in Table 3.3. These results show that high surface area per unit volume (β), high porosity (p), high frontal area ($W \times H_f$) and low fin height (H_f) alone do not give an optimum MHE geometry. They ratify the complex interplay of various variables entering into the design of heat exchangers with very high effectiveness.

The optimum geometry for the two MHE's required in this project was not identical. The difference is due to the variation of air properties with temperature. The two MHE's operate in different temperature ranges and lower values of δ and d were indicated for the lower temperature MHE. To minimize construction costs, the same plates were used for both MHE's. This gave, theoretically, a Goodness factor 18% higher than for the optimum case, for the lower temperature MHE.

The results of this optimization were used as a guide to establish the viability of the fabrication of the MHE by the new method. They showed that plates made by photo-chemical etching and spacers made from PCB laminate were of suitable dimensions. The optimization was re-done with the material, material availability and process constraints in place. This gave a Goodness factor 19% higher than for the optimum case. The dimensions used for construction are shown against the optimization results in Table 3.3.

Table 3.3 Optimization results

Variable	Best case	Range tested	This design
plate thickness δ	0.3mm	0.2-1.0mm	0.5mm
hole diameter d	0.9mm	0.2-2.0mm	1.0mm
hole pitch x_t	1.6	1.18-7	1.7
spacer pitch x_l	2	1.5-3	2.14
channel width W	85mm	40-110mm	110mm
fin height H_f	15mm	10-30mm	15mm
Goodness factor	0.736		0.875

Chapter 4

An apparatus to test CO_2 removal from air by refrigeration purification

Heat exchanger effectiveness, CO_2 removal by refrigeration purification, including water condensation and re-vaporisation in a reversing heat exchanger, are to be investigated experimentally. The development of a fully instrumented apparatus to test matrix heat exchangers in these applications is described.

In order to establish the efficacy of the heat exchangers and their application to the proposed process of CO_2 removal by refrigeration purification, an apparatus was required to be designed and built to measure:

(a) Heat transfer and pressure drop performance of the matrix heat exchanger.
(b) Heat transfer and pressure drop performance of two MHE's coupled together with the cross-over valves that are required for the CO_2 removal process configuration.
(c) CO_2 concentration to 10ppm in air, to determine CO_2 removal by refrigeration purification.
(d) H_2O concentration in ambient humid air to 10ppm, to determine the performance of the reversing heat exchanger in water cycling.

To monitor the CO_2 removal process as a whole, including reversing heat exchanger performance, the CO_2 and H_2O concentrations must be able to be measured continuously.

The apparatus developed for this project is essentially in two parts: one consisting of the matrix heat exchangers and associated equipment; and the other, consisting of a mass spectrometer and its associated equipment. The two parts are completely independent of each other. When the matrix heat exchanger apparatus is tested for the CO_2 removal process as a whole, the mass spectrometer is used for monitoring continuously, CO_2 and H_2O concentrations in the process air stream.

4.1 Apparatus for heat exchanger testing

4.1.1 Method for testing matrix heat exchanger effectiveness

Heat exchanger effectiveness, at steady state, may be calculated directly from inlet and outlet temperatures. At high effectiveness however, errors in temperature readings become amplified in terms of Ntu or heat transfer coefficient[80-p136]. In addition, in this application it was uncertain what, if any, variation there might be of the

inlet and outlet temperatures as part of the process. Gifford et al.[96] developed an alternative method to measure the effectiveness of regenerators operating at cryogenic temperatures. In this method the warm fluid exiting the test regenerator flows through a liquid nitrogen (LN2) bath before entering an identical regenerator as the cold fluid. The LN2 is used to provide a constant cold end temperature and the boil-off of LN2 fom this bath provides a direct measure of the *ineffectiveness* of the regenerator. Venkatarathnam[80-p138] has developed an apparatus for measuring MHE effectiveness which is similar in principle. He has introduced a by-pass which allows, only part of the fluid flow, to be diverted through the LN2 bath while the rest goes through the by-pass. The relative flows in the by-pass and the LN2 bath are each controlled by a valve. This allows control of the cold end temperature. The two valves can also be used to increase the pressure difference between the cold and hot streams. The working principle is shown in Figure 4.1. The test rig used for this project has been developed on this principle.

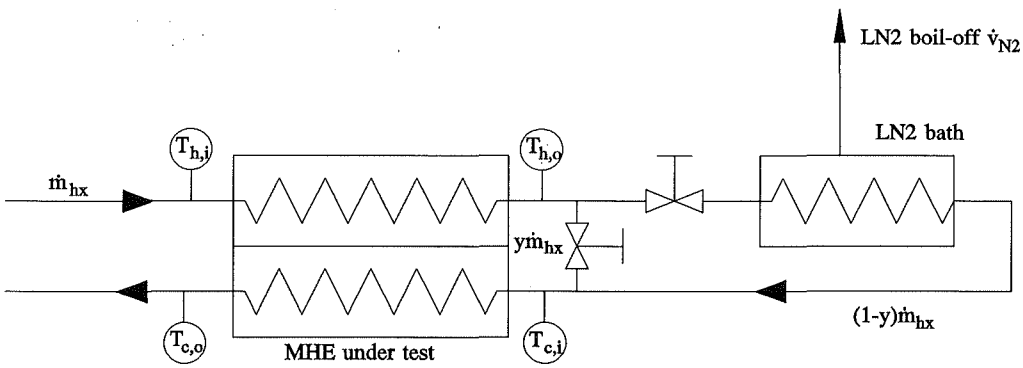

Figure 4.1 Working principle of cryogenic heat exchanger test apparatus. Cold end temperature is controlled by varying the amount of the flow passing through the LN2 bath.

The effectiveness is calculated from the boil-off of liquid nitrogen as

$$\varepsilon_{LN2}=1-\frac{\dot{v}_{N2}\rho h_{fg}}{\dot{m}_{MHE}c_p(T_{h,i}-T_{c,i})} \tag{4.1}$$

where $\dot{v}_{N2}$ is the volume flow rate of the boil-off from the LN2 bath, $\dot{m}_{MHE}$ is the mass flow rate in the heat exchangers and $T_{h,i}$ etc. refer to the temperatures of the fluid in the heat exchanger.

4.1.2 Description of apparatus: set-up and operation

The test apparatus is shown schematically in Figure 4.2 and Figure 4.3. Plate 4.1 shows the actual apparatus layout.

The working fluid enters the reversing heat exchanger (H2O-MHE) through the

first cross-over valve at room temperature. On exiting the reversing heat exchanger it passes through the second cross-over valve and into the CO_2 subliming heat exchanger (CO2-MHE). On exiting the CO2-MHE the gas stream is divided into two parts. One part passes through the by-pass valve and enters the return channel of the CO2-MHE. The other part is diverted through the LN2 heat exchanger valve, and through the liquid nitrogen heat exchanger (LN2-HX). The LN2-HX is simply a copper tube immersed in a LN2 bath. The proportion of the fluid diverted through the LN2-HX is controlled by the by-pass and LN2-HX valves. The combined stream then flows through the return channel of the CO2-MHE, through the second cross-over valve, through the return channel of the H2O-MHE and is exhausted to atmosphere through the first cross-over valve.

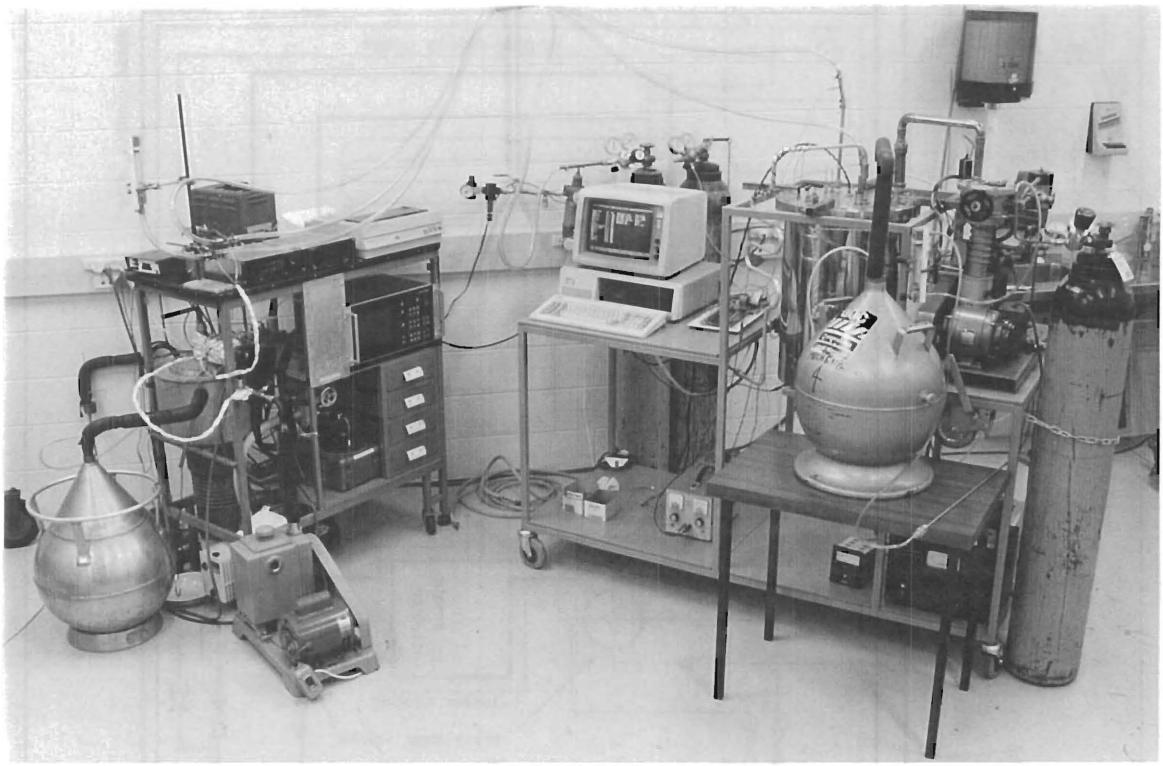

Plate 4.1 Photograph showing overall apparatus layout.

The cross-over valves may be rotated through 90° using the actuator. They are both rotated simultaneously. Every rotation of the cross-over valves swaps or reverses the inlet and outlet streams of the H2O-MHE while retaining unidirectional flow in the CO2-MHE.

The liquid nitrogen bath is thermally shielded by a second liquid nitrogen bath referred to as the outer bath or guard vessel. This is done to minimise boil-off in the inner bath, due to heat leak from the surroundings.

The heat exchangers, cross-over valves, actuator, by-pass and LN2-HX valves, and LN2 baths are suspended inside, from the lid of, a stainless steel vacuum vessel. The

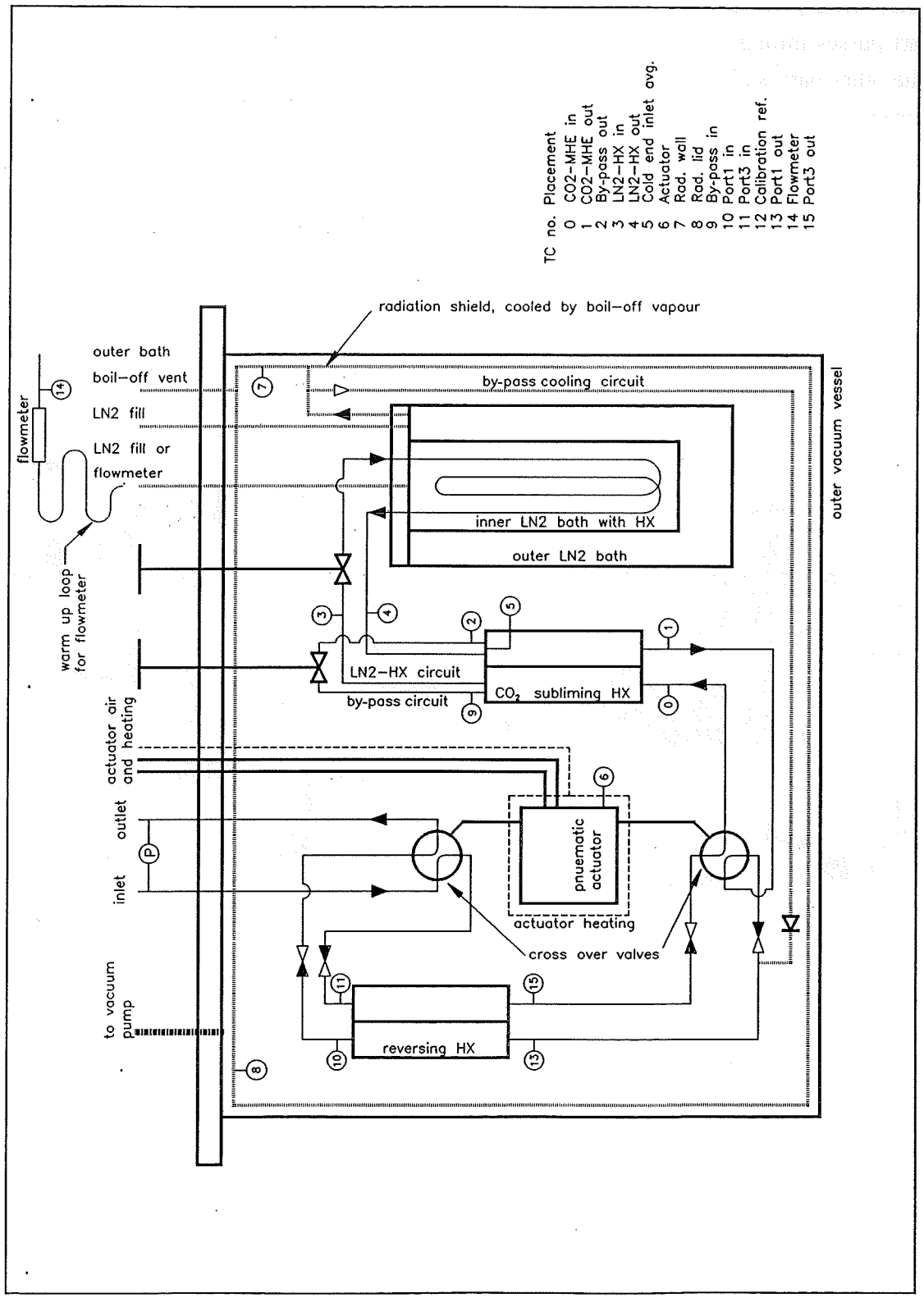

Figure 4.2 Schematic layout of heat exchanger test vessel.

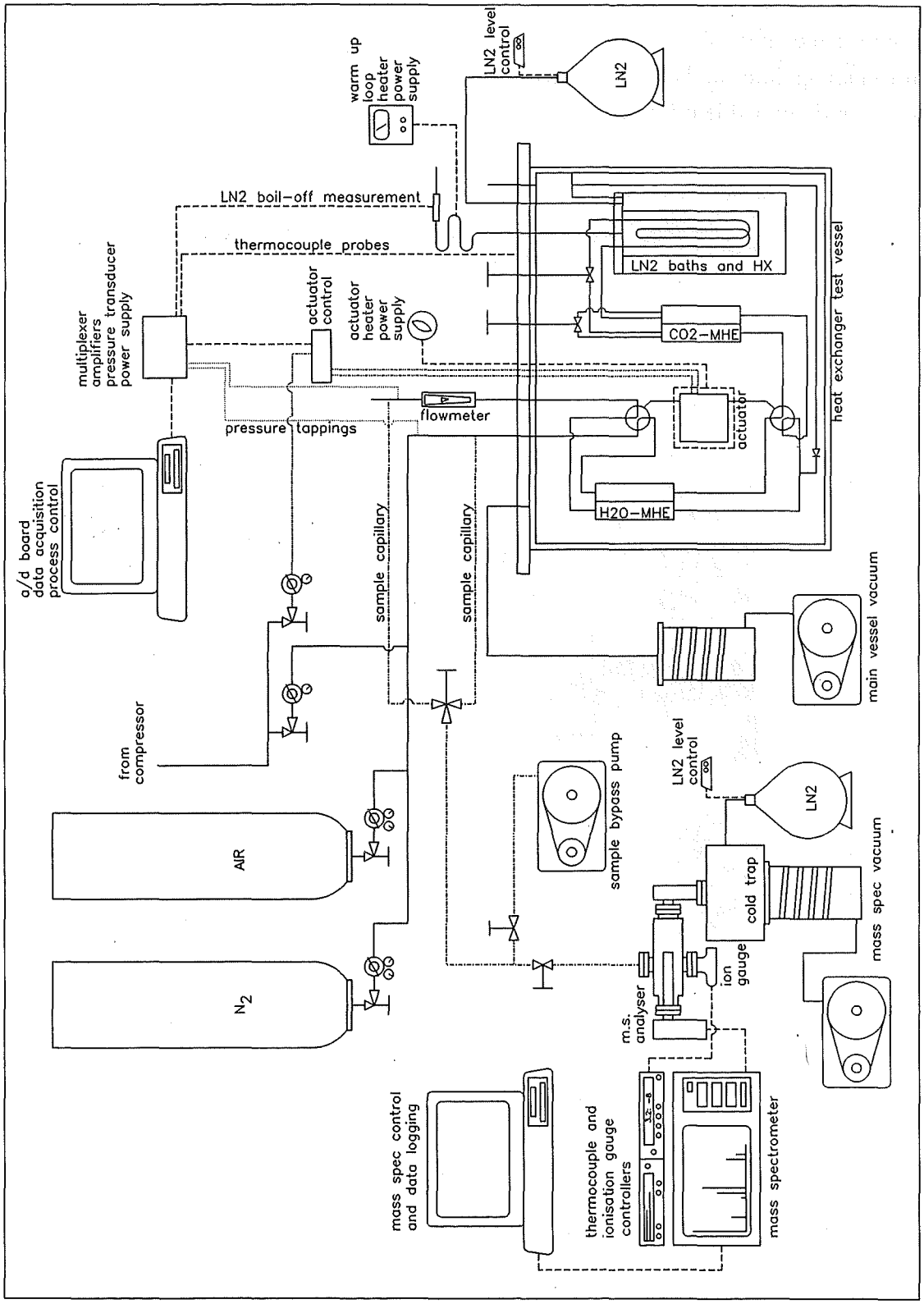

Figure 4.3 Schematic layout of test apparatus.

vessel is approximately 400mm in diameter and 600mm high. The vessel is maintained at a pressure of 10^{-3} to 10^{-6} torr by a diffusion pump vacuum system. The vacuum provides the thermal insulation necessary to eliminate excessive heat leak from the surroundings into the heat exchangers under test. The insulation is aided by a polished copper radiation shield immediately inside the vessel. The radiation shield is cooled by boil-off vapour from the guard vessel.

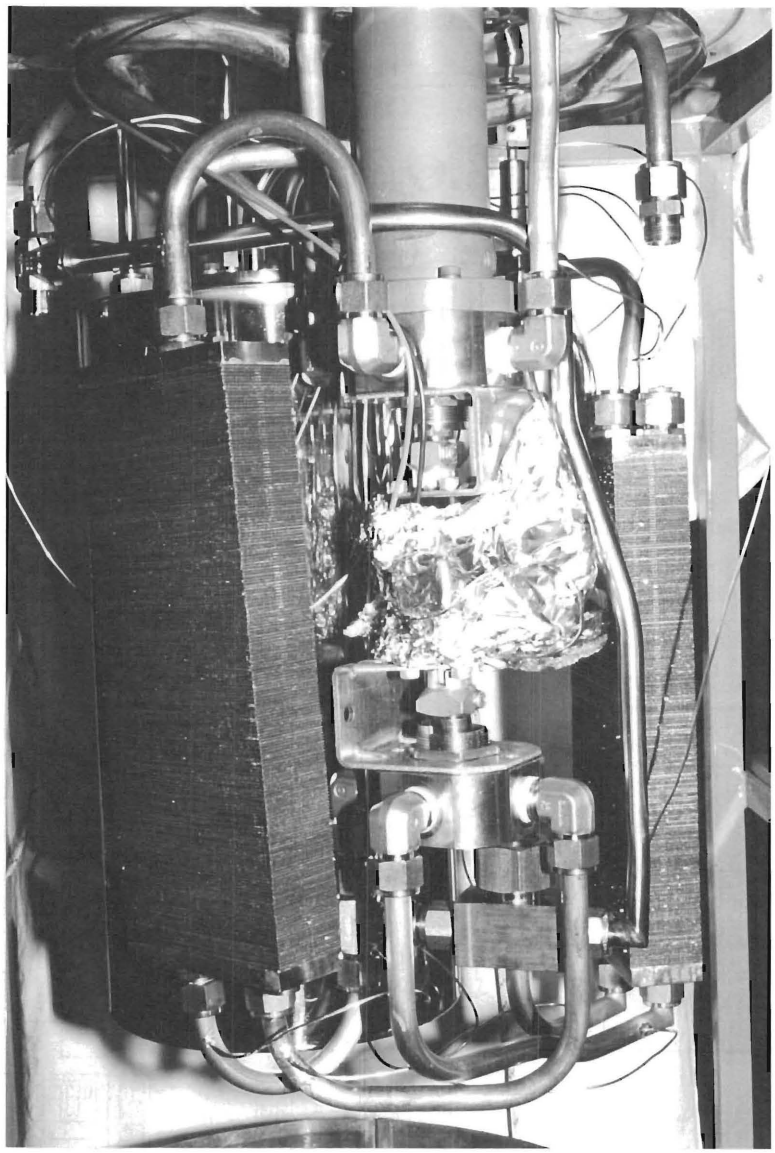

Plate 4.2 Photograph showing the heat exchanger apparatus for the two heat exchanger configuration. Note the cross-over valves, and actuator wrapped in heating coil.

The by-pass and LN2-HX valves are bellows sealed needle valves (Nupro SS-8BG). The cross-over valves are TFE gland packed ball valves (Whitey SS-45YF8). The actuator is pneumatic and double acting (Whitey MS-133-DA). The actuator is controlled using a solenoid actuated directional control spool valve (Norgren MH01CDB34ALXX).

The vacuum vessel; LN2 baths; electrical, gas, rotary actuation and LN2 feed-throughs; and other rig components, were all designed and built in-house for this project. Workshop drawings for these components are not included in this thesis as they are based on standard design practice and procedures for vacuum and cryogenic equipment. The apparatus with the outer vessel removed is shown in Plate 4.2.

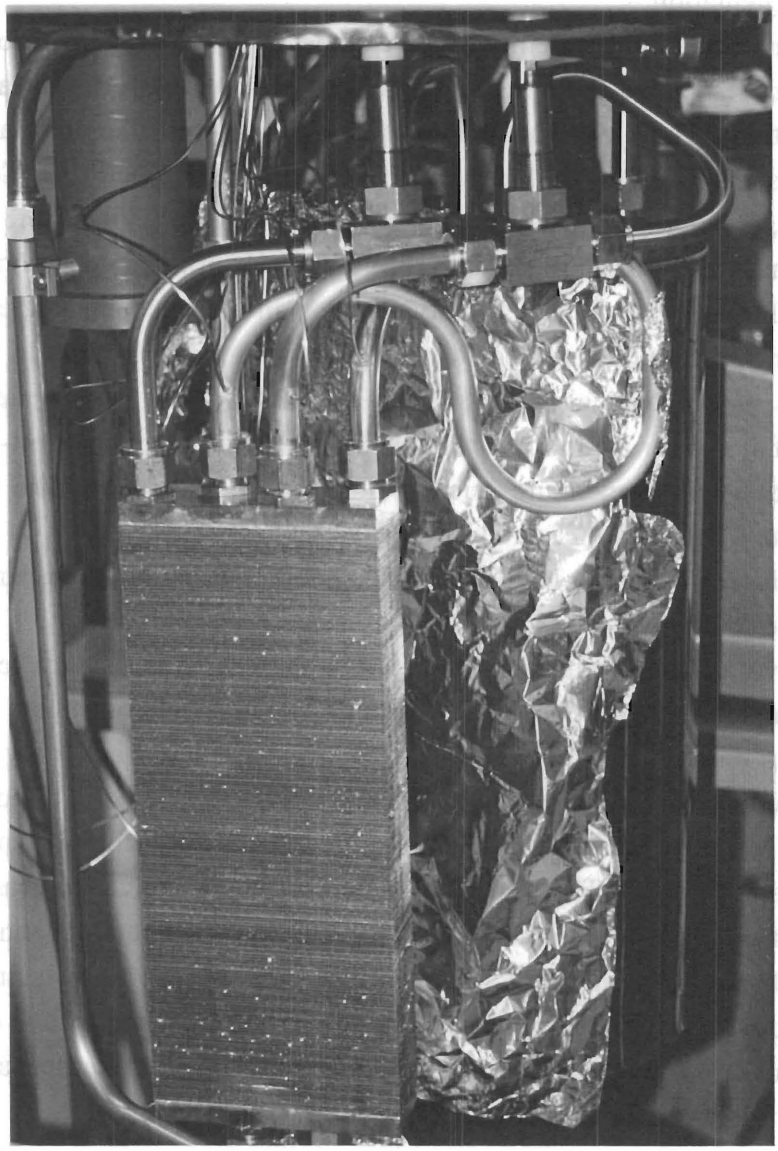

Plate 4.3 Photograph showing single heat exchanger configuration.

The apparatus configuration for the single heat exchanger effectiveness tests is slightly simpler than that shown. The difference being that the reversing heat exchanger and associated cross-over valves and actuator are not present in this configuration. This configuration is shown in Plate 4.3.

The working fluid used for various tests was:

- bottled dry N_2 for effectiveness tests to ensure that no phase change or mass transfer

occurs;

- bottled dry air for initial CO_2 removal tests; and
- compressed moist air from a laboratory air supply for water cycling/reversing heat exchanger tests.

4.1.2.1 Instrumentation

All temperature measurements were done using K type thermocouples. The temperature probes inside the vacuum vessel are in stainless steel sheaths and have grounded junctions. These were built in-house for this project. The flow rate of the boil-off of LN2 was measured using a pelton wheel turbine meter (McMillan Co.; Flo-sensor model 100-10, 4-20 l/min) or a thermal mass flow meter (Honeywell Microswitch; Microbridge mass airflow sensor AWM5101VN, 0-5 l/min), depending on the flow rate range. Since the temperature and density of the boil-off vapour change rapidly as it warms up, some precautions are necessary for flow rate measurement. In this apparatus the boil-off is passed through a length of aluminium tubing with a heater wrapped around part of it (warm up loop), to allow the temperature of the boil-off vapour to equilibrate with room temperature prior to flow rate measurement. The working fluid flow rate in the MHE was measured using a variable area flowmeter. A piezoresistive pressure transducer (Motorola; MPX5050DP, 0-50kPa) was used to measure the pressure drop across the MHE.

The level of liquid nitrogen in the baths is controlled using a level controller based on a temperature sensitive BSY38 transistor. The level controllers were built in-house based on a design from the Physics Department at this University.

Data acquisition is done using a Universal Pulse Processor I/O board (designed and built by J.Murphy, Technician, Dept. of Mechanical Engineering) which plugs into an 8 bit ISA slot in a PC. This provides analog to digital conversion (a/d), 20 analog input channels and 32 digital i/o channels. It is interfaced with a 16 channel multiplexer and amplifier board (Advantech; PCLD-889) and other purpose built electronics to allow data to be recorded on a IBM XT personal computer. The programmable digital outputs allow control of cross-over valve actuation. The program written for data acquisition and process control is listed in appendix B.

4.1.3 Aspects of rig performance

The performance of the heat exchanger test apparatus has considerable effect on the tests. Some aspects of the performance of this rig are discussed in this section.

4.1.3.1 Ultimate vacuum and heat leak

The vacuum vessel containing the heat exchange apparatus can be evacuated to 10^{-4} torr by the vacuum pumping system (Edwards; Speedivac 203B and ISC50B). When

the LN2 baths are filled, the guard vessel acts as a cryopump, and the pressure in the vessel is reduced to 10^{-6} torr.

The total heat leak into the vacuum vessel was measured by the boil-off from the LN2 baths. The LN2 baths are at the lowest temperature inside the vessel and so form the final heat sink. The measured heat leak from the inner bath during test conditions was ~2W.

4.1.3.2 Cross-over valves

The design operating temperature ranges for the two MHE's are; room temperature to ~-73°C, and -73°C to -160°C. The cross-over valve located between the H2O-MHE and the CO2-MHE, began to leak during initial testing, at a temperature of about -15°C. The leak rate was higher than the vessel vacuum system could pump, and the pressure in the vessel would rise rapidly. The leak could be alleviated by allowing the temperature of the valve to rise. By tightening the gland packing and applying silicone vacuum grease to the valve stem, a temperature of -60°C could be maintained with no leak. When the valve was operated it began to leak at a temperature of -40°C.

No appropriate cross-over valve designed for cryogenic service was readily available. During testing the temperature at this valve was limited to -60°C for the tests not involving its operation. For the testing concerning reversing heat exchanger operation the temperature at this valve was limited to -40°C.

4.1.3.3 Cross-over valve actuator

The pneumatic actuator used for the cross-over valves is sealed using O-rings. During testing it cools slowly losing heat by conduction through the cross-over valves to the working fluid which may be at temperatures as low as -60°C. It also loses heat by radiation to the LN2 baths. During initial testing it was found that this actuator would become in-operable, and leak. The actuator temperature during these tests would drop as low as -35°C over 3½ hours. It was thought to become in-operable as a result of the water in the pneumatic air supply freezing. Operating it using compressed N_2 instead of air alleviated the freezing and it remained operable at low temperatures, but it still leaked. In the absence of any other suitable actuator, a heating arrangement was installed and this actuator was heated to keep it from freezing and leaking. With this provision it did not leak, provided it was maintained above -10°C.

4.1.3.4 Additional cool-down circuit

In the single heat exchanger test configuration, the initial cool-down of the matrix heat exchanger was achieved by directing most of the flow of gaseous nitrogen through the LN2-HX until the prescribed cold end temperature was achieved. For the double heat exchanger configuration, the cool-down was initially attempted the same way as for the single heat exchanger. It was thought that the two heat exchangers in series would act,

for the purposes of cool-down, as one larger heat exchanger. Since the heat transfer duty has been approximately doubled, it was expected that the accompanying decrease in effectiveness of the cold end heat exchanger, or CO2-MHE, would cause the warm end heat exchanger, or H2O-MHE, to cool down. It was found that this did happen and that the reduction in effectiveness of the cold end heat exchanger was of the order of 10%. However complete cool-down to the desired temperatures was not achieved because this process was very slow.

A new gas flow circuit was added to aid the cool-down of the H2O-MHE. A T-junction was established in the line carrying boil-off vapour from the guard vessel to the radiation shield. A pipe from this T-junction leads through a lift check valve (Nupro SS-58S8) to the cold fluid inlet of the H2O-MHE. Plugging the boil-off vent of the guard vessel causes gas from the guard vessel to flow through this new circuit into the cold fluid inlet of the H2O-MHE. Gaseous N_2 is bubbled through the LN2 in the guard vessel. The resulting cold N_2 gas flows into the H2O-MHE. This circuit is shown in Figure 4.2. By adjusting the flow rate of gaseous nitrogen in the new cool-down circuit relative to the flow rate in the MHE's the desired cold end inlet temperature for the H2O-MHE can be obtained. When the guard vessel boil-off vent is unplugged the pressure of the working fluid keeps the lift check valve closed. This new circuit allowed the H2O-MHE to be cooled much faster.

4.2 Gas analysis using a mass spectrometer

A Spectramass dataquad DAQ200/DXS quadrupole mass spectrometer was used for continuous monitoring of CO_2 and H_2O concentration in the process air stream. The set-up of the mass spectrometer[1] is described in this section. A variable throughput continuous sampling system was devised for introducing gas samples to the mass spectrometer. The design of this sampling system is described. A schematic layout of the mass spectrometer and associated equipment is shown in Figure 4.3. The actual layout is shown in Plate 4.4.

The Dataquad mass spectrometer has an RS232 interface. This has been used to down load data while testing. The program for data transfer is listed in appendix C.

---

[1] Two 180° deflection mass spectrometers were available in the Engineering Faculty (AEI Mimimass, AEI MS10), but on setting up were found to produce shifted background spectra. This was ascribed to gradual demagnetization or variation of field strength in the permanent magnets. Attempts at re-magnetizing them were unsuccessful. The Dataquad quadrupole mass spectrometer was therefore purchased.

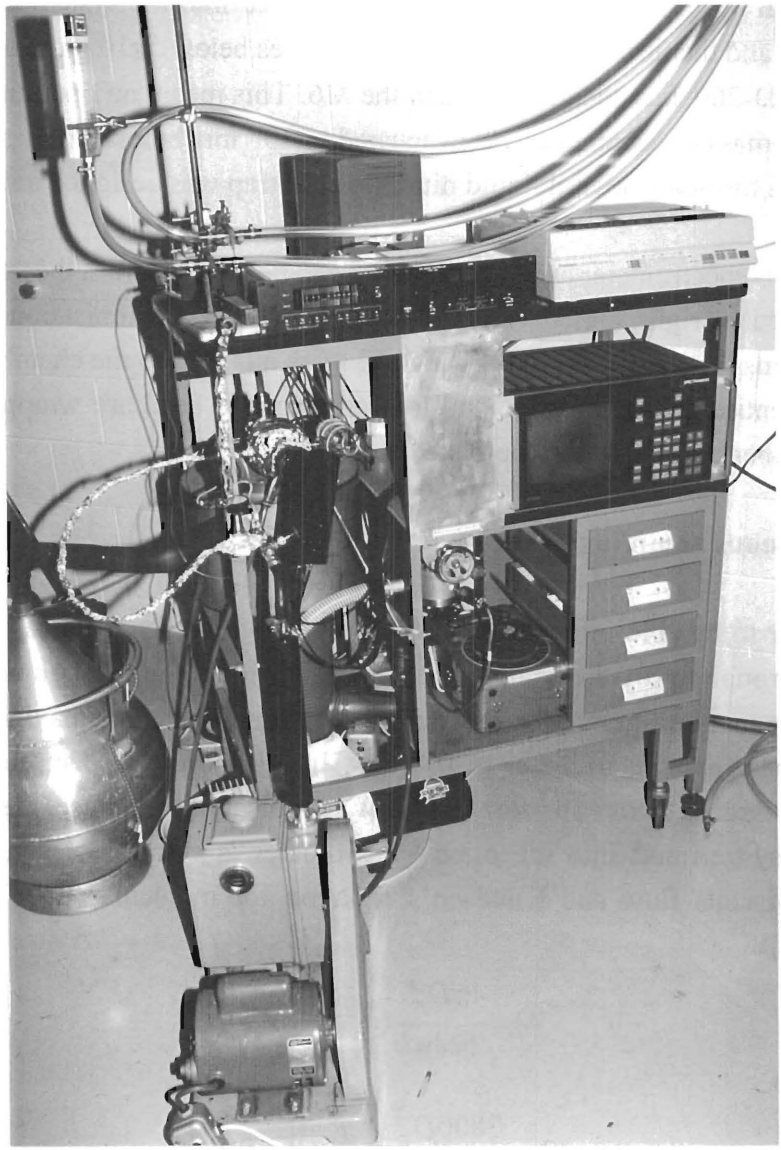

Plate 4.4 Photograph of mass spectrometer and associated equipment.

4.2.1 Vacuum set-up

The mass spectrometer was initially set up with a vacuum provided by an Ulvac PFL-02 oil diffusion pump backed with a Varian SD-200 two stage rotary pump. The PFL-02 was cold trapped with a 3l liquid nitrogen cylindrical cold trap, designed and built in-house. System ultimate pressure was 10^{-8} torr. Sampling was done through a 800mm long capillary of 0.010" (0.254mm) bore with a needle valve at the mass spectrometer end. Sample pressure had to be reduced to 100 mbar else the throughput of the sampling system exceeded that of the PFL-02 and the system pressure would rise above the mass spectrometer operating pressure. This system was suitable for sampling in batch mode but not in continuous mode.

A Varian M6 oil diffusion pump was substituted into the system to increase the pumping speed and the throughput. At system pressures below $5x10^{-3}$ torr the throughput of the Varian SD-200 was adequate to back the M6. This meant an operating precaution of ensuring the mass spectrometer was evacuated to 10^{-3} torr before bringing the M6 on-line. A new 6½l toroidal-louvred liquid nitrogen cold trap was designed and built for use with the M6.

The mass spectrometer analyser chamber can be isolated from the vacuum system by a bellows sealed right angled valve (Varian 951-5027). An ionisation gauge (MKS Instruments, SensaVac 290C-06, IG-4 gauge head) is attached to the chamber to monitor pressure. The entire chamber, valve and ionisation gauge head are wrapped in heating coil. The chamber and valve can be baked to 350°C.

4.2.2 Continuous sampling system

In order to be able introduce a gas sample continuously for mass spectrometric analysis the throughput of the sample must be matched to the throughput of the mass spectrometer vacuum system at the desired sampling pressure. The maximum operating pressure for the mass spectrometer is 10^{-5} torr. Inside the mass spectrometer analyser chamber, at pressures below 10^{-5} torr, the flow is molecular in nature. Gas flow rate in the sampling system and into the mass spectrometer is calculated using Poiseuille's equation for viscous flow and Knudsen's equation for molecular flow (Brunner and Batzer[97-p14]).

$$Q_v = \frac{\pi D_T^4}{128 \mu L}(P_1^2 - P_2^2)/2 \tag{4.2}$$

$$Q_m = \frac{3800 D_T^4}{L}\sqrt{\frac{T}{M}}(P_1 - P_2) \tag{4.3}$$

where Q is the throughput in bar cm^3/s, the subscripts $_v$ and $_m$ denoting viscous and molecular flow; D_T is the tube diameter and L is its length; P_1 and P_2 denote the high and low pressure respectively.

The equation for molecular flow (4.3) shows the dependence of the flow rate on the molecular mass (M) of the gas. Hence if a gas sample consisting of a mixture of gases is introduced to a mass spectrometer and undergoes a transition from viscous to molecular flow at some point, mass fractionation of the gas sample will occur, as reported by Honig[98]. Nier et al.[99], while developing a gas sampling system for continuous sampling from a process stream, found fractionation to occur in the transition from viscous to molecular flow if the fractionated gas was allowed to back diffuse into the sample stream. Fractionation was eliminated by using a capillary 5¼" long, 0.006" ID. This maintained a high enough gas velocity up to the constriction where the

transition would occur, and prevent back diffusion of the fractionated gas. Halstead and Nier[100] suggest that the most feasible way of improving a viscous leak is to maintain viscous flow to the lowest possible pressure, by decreasing the diameter of the capillary and/or increasing its length. As long as the two are changed by the same factor the time response of the sampling system (ie. the transit time of the sample through the sampling system) is unchanged.

A continuous sampling system incorporating a by-pass pump was designed for a maximum operating pressure for the mass spectrometer of 10^{-6} torr. A schematic representation of the sampling system is shown in Figure 4.4. P_1 is taken as atmospheric pressure; D_1 is 0.010" (0.254mm); D_2 is 0.007" (0.178mm); and P_3 is 10^{-6} torr. The sample by-pass pump (single stage rotary pump; Japan Electron Optics Laboratory Co. Ltd., JR-150; speed 75 l/min, ultimate vacuum 0.001 torr) allows viscous flow to be maintained to a low intermediate pressure, P_2. As long as $P_2>10^{-2}$ torr, the flow in the 0.010" capillary is viscous in nature, the transition from viscous to molecular flow occurring in the 0.007" capillary. At 10^{-6} torr the maximum throughput for the M6 is

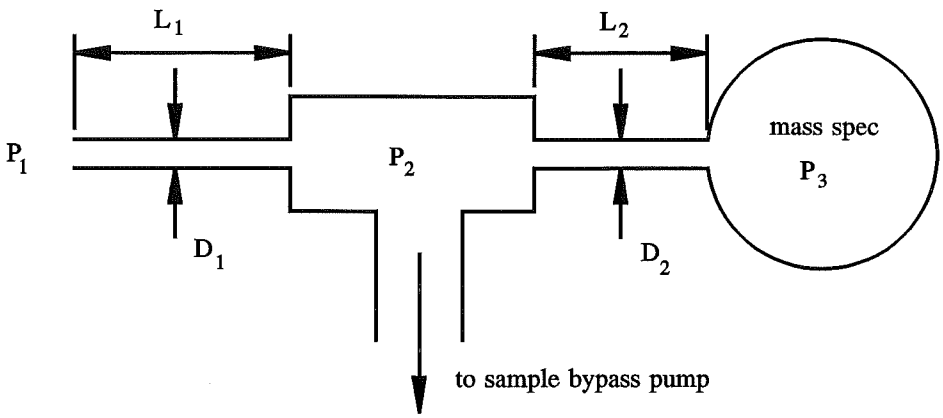

Figure 4.4 Schematic layout of continuous sampling system.

$2x10^{-5}$ bar cm^3/s. Then for $Q = 2x10^{-5}$ barr cm^3/s and using equation (4.2) $L_2 \approx 100mm$, assuming $P_2 \approx 4$ torr. For the by-pass pump operating at 4 torr its maximum throughput is estimated at 0.4 torr-l/s. From equation (4.2) $L_1 \approx 550mm$.

In this design a flow regulating valve was used to control the throughput to the sample by-pass pump. This allows control of the intermediate pressure P_2, and hence of the sample throughput to the mass spectrometer. A sampling pressure in the range of 10^{-5} to 10^{-8} torr can be chosen by the operator.

Chapter 5

Performance evaluation: heat exchanger performance and CO_2 removal process; and discussion of results

Results of experimental testing on heat exchanger performance and the CO_2 removal process are presented and discussed. Measurements of heat exchanger effectiveness are presented, and the associated minimum experimental uncertainty is calculated. The performance of the cross-over valves and associated actuator is discussed. Difficulties encountered in trace CO_2 analysis using the mass spectrometer, and the steps taken to circumvent some of these problems are described. Results of tests conducted to investigate functioning of the reversing heat exchanger and CO2-MHE regeneration are presented.

5.1 Introduction

The main focus of this work was to establish whether CO_2 removal from air may be effected by refrigeration purification, with only about 15% of the cooling required available. Implicit in this work is a new sizing equation and a new construction method for perforated plate matrix heat exchangers. The experimental work was conducted as four separate series of tests to determine:

(a) Heat transfer and pressure drop performance of the matrix heat exchanger. To establish that the heat transfer effectiveness of the designed heat exchangers was greater than at least 85%, as required for the CO_2 removal process. To compare the measured performance with performance predicted by the sizing procedure developed and other theoretical predictions. This performance was measured by conducting tests on a single heat exchanger.

(b) Heat transfer and pressure drop performance of two MHE's coupled together. The CO_2 removal process design requires two MHE's to be connected in series with a cross-over valve between them. It was not known what effect this configuration would have on the combined performance and this had to be determined experimentally.

(c) The feasibility of CO_2 removal from air to 10ppm by refrigeration purification. These tests were carried out using bottled dry air so that the CO_2 removal alone could be measured.

(d) CO_2 removal from ambient humid air, and the performance of the reversing heat exchanger in water condensation and re-vaporisation (water cycling). These tests were carried out using wet air from a laboratory compressed air supply.

This chapter is set out in six parts. The first three parts on:

- MHE effectiveness and pressure drop measurement, and MHE construction evaluation, cover heat exchanger performance.

The next three parts on:

- CO_2 removal, water cycling, and CO_2 MHE regeneration tests, cover CO_2 removal process evaluation.

Errors in experimental measurements for each case are discussed. The general treatment of errors is described in the first section. Data files from the various tests are not included, to save space.

A mass spectrometer was used to monitor CO_2 and water concentration in the inlet and outlet streams for the tests on CO_2 removal and water cycling. Both CO_2 and water are strongly adsorbed on surfaces in vacuum systems and the effect of this on the results obtained is discussed.

5.2 Heat transfer and pressure drop performance of the matrix heat exchanger

5.2.1 Effectiveness test results

The experimental results of single heat exchanger effectiveness tests show that the measured effectiveness for the tested range of flow rates is 97% ±1.9%. Within the limits of minimum experimental uncertainty this is not measurably different from the predicted values. These results are shown in Figure 5.1 and Figure 5.2. Measured and predicted effectiveness are plotted for a range of flow rates of gaseous nitrogen. Dry gaseous nitrogen was used for these tests to ensure that no condensation, ie. no mass transfer, occurred in the MHE. Each experimental data point on the graph represents the mean of data recorded over 10 to 20 minutes of steady state operation.

The two theoretical performance predictions are calculated from:

(a) A running version of the program in Venkatarathnam's doctoral thesis[80]. This running version was obtained through correspondence with the author[101]. He stated that the program included in his thesis is a pared down version of a larger program and suggested changes to the source code.

(b) The modified approximate analytical solution used in the sizing procedure. This sizing procedure has been described previously in chapter three.

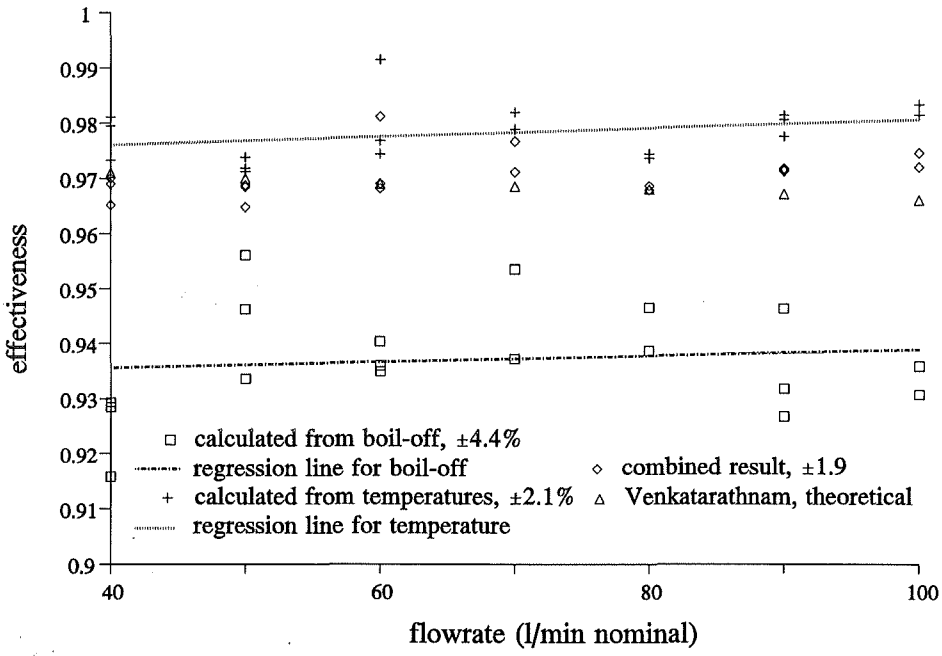

Figure 5.1 Heat exchanger effectiveness vs. nominal flow rate, for single matrix heat exchanger heat transfer performance.

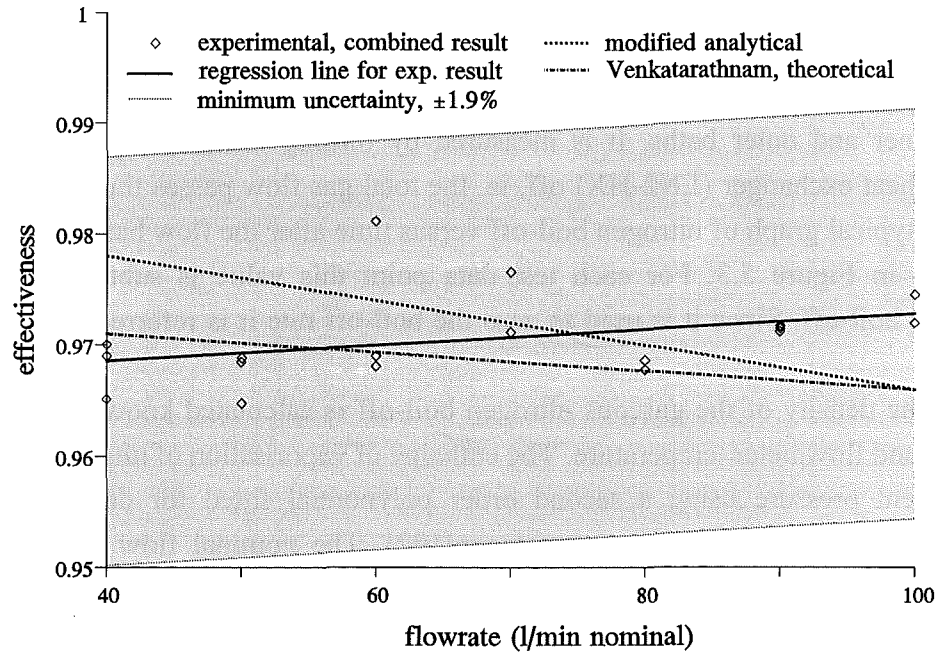

Figure 5.2 Comparison of measured heat transfer performance with Venkatarathnam's solution and the modified analytical solution.

5.2.2 Measurement of effectiveness

In order to see what effect experimental errors have on the measured effectiveness, the manner in which this effectiveness is calculated is outlined here. Apparatus for temperature and flow rate measurement has been described earlier along with the apparatus set-up and method used to test for heat transfer effectiveness of a single matrix heat exchanger, in chapter four. Thermocouple locations and gas flow paths are shown in Figure 5.5. The effectiveness is calculated from the boil-off of liquid nitrogen as

$$\varepsilon_{LN2}=1-\frac{\dot{v}_{N2}\rho h_{fg}}{\dot{m}_{MHE}c_p(T_{h,i}-T_{c,i})} \tag{5.1}$$

where $\dot{v}_{N2}$ is the volume flow rate of the boil-off from the LN2 bath, $\dot{m}_{MHE}$ is the mass flow rate in the heat exchangers and $T_{h,i}$ etc. refer to the temperatures of the fluid in the heat exchanger. The effectiveness is also calculated from temperature differences as

$$\varepsilon_{temp}=\frac{T_{h,i}-T_{h,o}}{T_{h,i}-T_{c,i}} \tag{5.2}$$

or

$$\varepsilon_{temp}=\frac{T_{c,o}-T_{c,i}}{T_{h,i}-T_{c,i}} \tag{5.3}$$

In addition to the boil-off induced by the ineffectiveness of the heat exchanger, there is some boil-off from the inner liquid nitrogen bath due to heat leak from the surroundings. This is measured at the end of each test run since it varies depending on the liquid level in the inner and outer baths. It is measured by turning the flow through the liquid nitrogen heat exchanger (LN2-HX) off, ie. the total gas flow passes through the bypass valve. A typical graph of nitrogen boil-off versus time after the flow has been turned off is shown in Figure 5.3. For each test data point this value is subtracted from the measured boil-off. Since it is used to zero the boil-off rate it is referred to as the zero-rate.

The density of the gaseous nitrogen boil-off is calculated knowing the ambient pressure and flowmeter temperature. The enthalpy of vaporisation of nitrogen is adjusted for ambient pressure using a second order polynomial fitted for data listed in the IUPAC, Chemical Data Series on nitrogen[102]. The nominal flow rate of gaseous nitrogen in the MHE's is distinguished from the actual flow rate only by a correction to account for variation of ambient pressure and flowmeter temperature. For these tests the maximum difference between nominal and actual flow rate was 3.7% (12°C,1025mbar). All plotted values are calculated using the actual flow rate.

5.2.3 Experimental errors

Experimental errors have been treated in accordance with Barford[103]. The approach has been to calculate the minimum uncertainty attainable for the measured results.

5.2.3.1 Random error

In a typical test 152 data sets were recorded over ~18 minutes of steady state operation. The random error has been calculated for a 99.7% confidence level using

$$S_n = \frac{3\sigma}{n^{1/2}} \tag{5.4}$$

where S is the standard error for n samples, and σ is the standard deviation.

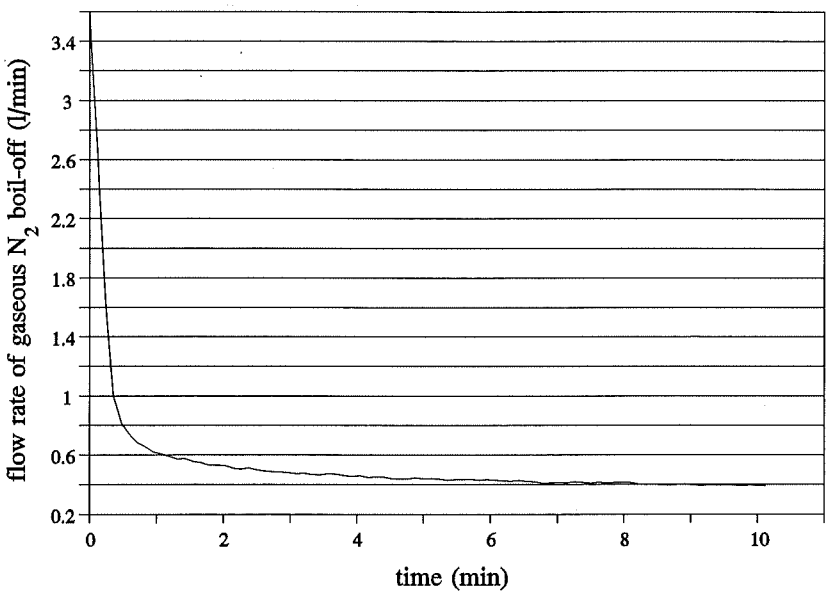

Figure 5.3 Flow rate of nitrogen boil-off from LN2 bath with no flow through liquid nitrogen heat exchanger.

5.2.3.2 Systematic error

The only un-rectifiable systematic error was found in the thermocouple calibration. Due to the lack of a cryogenic temperature calibration facility (ie. controlled temperature conditions and any other method of cryogenic temperature measurement) only four reference temperatures were used. Cold junction compensation temperature was adjusted to ambient, while an ice bath, solid CO_2, and liquid nitrogen were used as the other three reference states. At liquid nitrogen temperature the thermocouple showed an error of 2%.

First order uncertainty, or random error, and systematic error have been combined using the least error (least squares) principle, to give the N^{th} order uncertainty. These results are shown in Table 5.1. The two main results from the error analysis are that the effectiveness calculated from temperatures is at best ±2.1%, and that the effectiveness calculated from the boil-off rate is at best ±4.4%.

Table 5.1 Random and systematic errors associated with various experimental measurements and results

Reading	**Random error (%)**	**Including systematic error (%)**
Inlet temperature	0.73	1.2
Outlet temperature	0.33	1.0
Bypass temperature	0.11	1.0
Cold end inlet temperature	0.10	1.0
Effectiveness, temperature based, calculated	0.81	2.1
Effectiveness, temperature based, measured	0.47	-
Boil-off rate	2.29	-
Mass flow rate in heat exchanger	2.9	3.2
Effectiveness, LN_2 based, calculated	3.8	4.4
Effectiveness, LN_2 based, measured	0.21	-

In this apparatus it has not been possible to estimate the error in temperature measurement caused by the balance of conduction, convection and radiation at each thermocouple junction, at the cold end of the matrix heat exchanger. This is because temperatures of the pipe-work and the various bodies inside the vacuum vessel are not known independent of the thermocouple measurements. Temperatures at the cold end and their influence on the measured results are discussed in section 5.2.4.

5.2.3.3 Combined result calculation

In accordance with Barford[103] the combined result from the temperature based and boil-off based effectiveness is calculated as

$$X_{n,m} = \frac{1}{S_n^{-2} + S_m^{-2}} \left(\frac{X_n}{S_n^2} + \frac{X_m}{S_m^2} \right) \tag{5.5}$$

where X is the mean value, and n and m represent the number of samples for the two

sets of results. This has been calculated for each test from the mean of the LN_2 boil-off and the mean of temperature based effectiveness, and is plotted in Figure 5.1 and Figure 5.2. The combined error is

$$S_{n,m}=\left(\frac{S_n^2\ S_m^2}{S_n^2+S_m^2}\right)^{1/2} \tag{5.6}$$

From Table 5.1 the errors for the effectiveness as calculated from LN_2 boil-off and temperatures, ±4.4% and ±2.1% respectively, give a combined error of ±1.9%.

5.2.4 Discussion of experimental effectiveness results

The experimental results show that heat transfer effectiveness for the flow range tested is 97% ±1.9%. Given the minimum uncertainty is ±1.9%, the experimental and theoretical results are not significantly different. Figure 5.2 shows the ±1.9% minimum uncertainty on the graph along with the combined experimental result and the theoretical predictions.

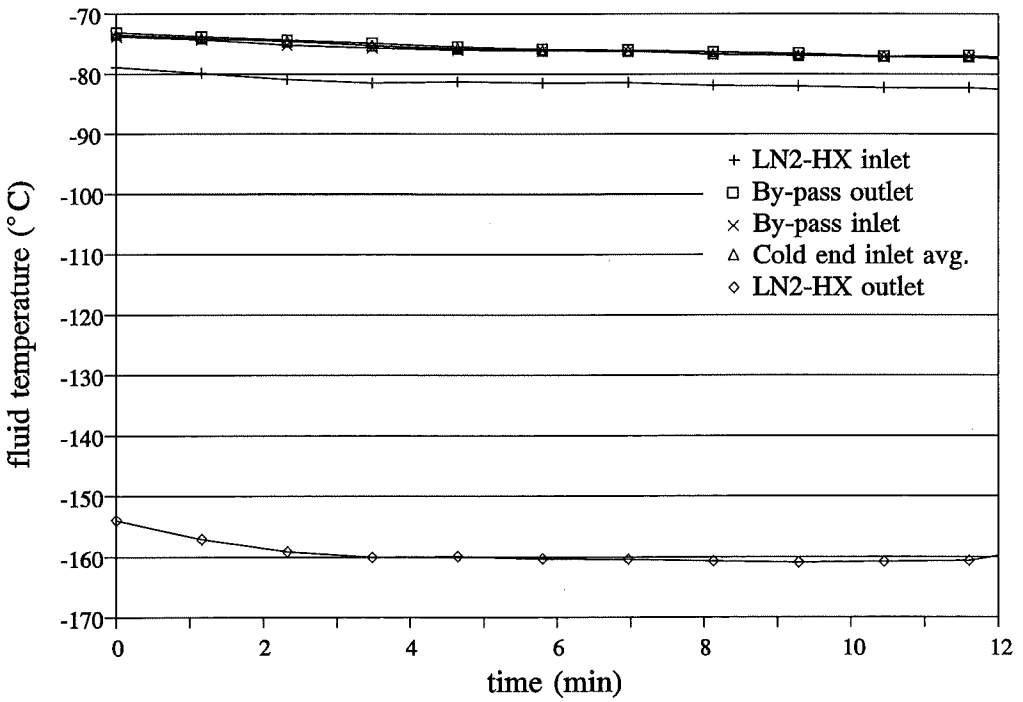

Figure 5.4 Fluid temperatures at various positions at the cold end during steady state test.

From Figure 5.1 it can be seen that in every case the effectiveness calculated from the boil-off of liquid nitrogen is lower than that calculated from the hot and cold end temperatures. This discrepancy was thought to be due to heat leak by conduction at the cold end through the by-pass and liquid nitrogen heat exchanger pipe-work and valves. Figure 5.5 shows the location of the thermocouples and the gas flow paths. It can

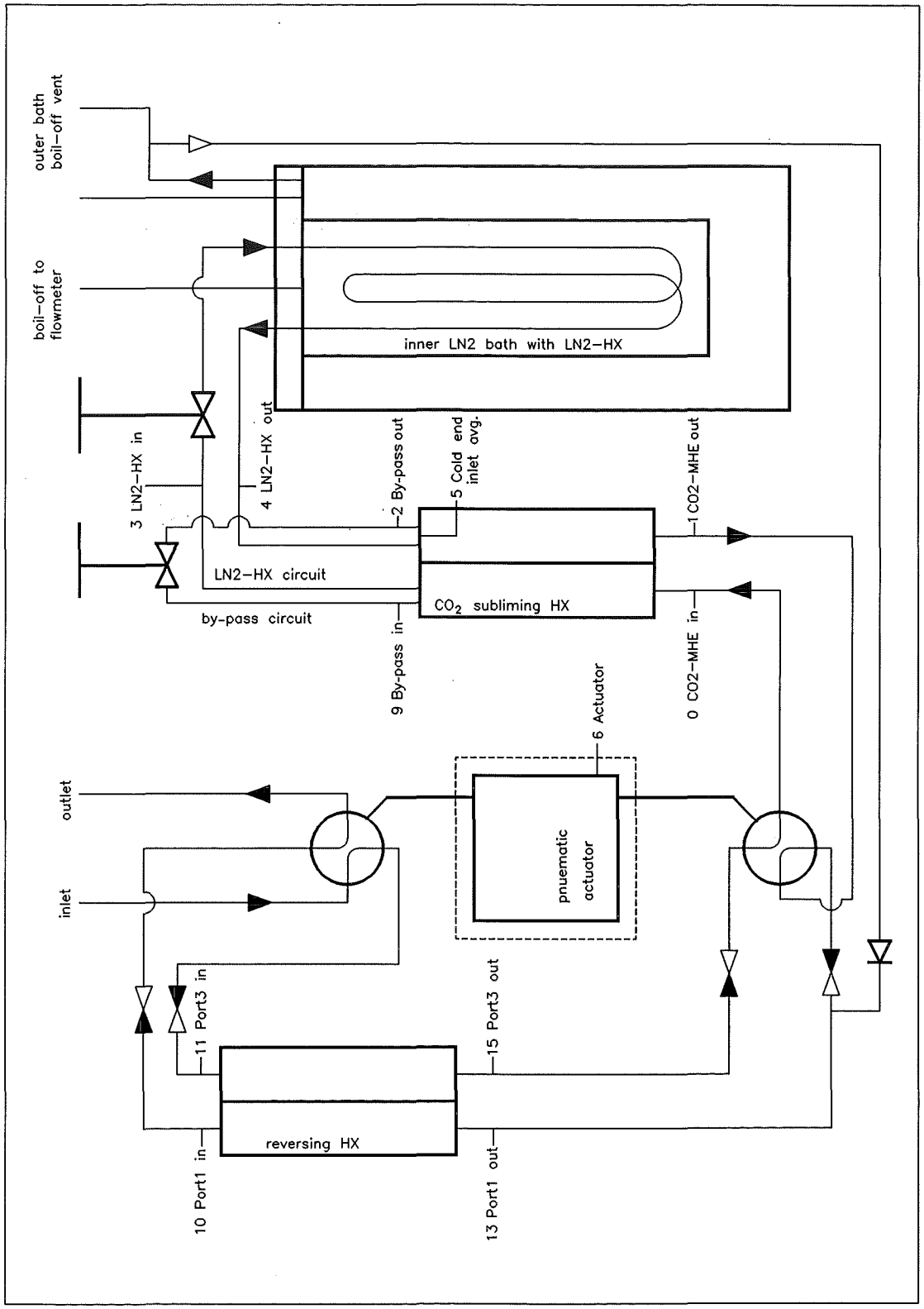

Figure 5.5 Schematic diagram showing thermocouple locations

be seen from Figure 5.4 that the temperature of the fluid in the by-pass inlet (T_{BPin}) and by-pass outlet (T_{BPout}) is substantially higher than the fluid temperature in liquid nitrogen heat exchanger inlet ($T_{LN2\text{-}HXin}$).

Further it can be seen from Figure 5.6 which is a record of temperature during the cool down period that T_{BPout} remains higher than T_{BPin} and that both of these in turn remain higher than $T_{LN2\text{-}HXin}$. It may be expected that the heat leak through the valves and pipe-work is higher when gas is flowing through these pipes. This would give higher net heat transfer due to added convection, over heat leak by conduction. At steady state conditions under which the tests are done the heat leak is balanced by added boil-off from the LN2 inner bath to maintain a constant cold end outlet temperature (taken as T_{BPin}). However, the zero-rate is measured with no flow through the LN2-HX. It therefore cannot represent completely the effect of this heat leak. A higher than measured zero-rate is consistent with calculated low LN2 boil-off based effectiveness.

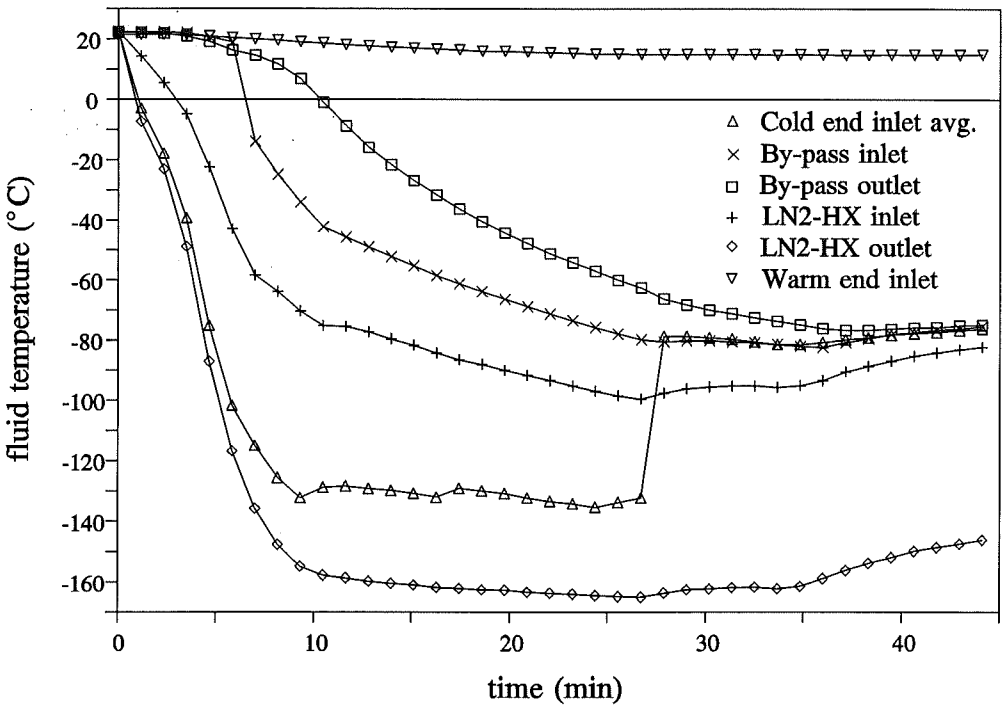

Figure 5.6 Fluid temperatures during cool down period. The step increase in cold end inlet avg. temperature marks the time at which the LN2-HX valve is turned almost completely off (by-pass valve full open).

5.2.5 Cool-down

Initial cool-down of the single heat exchanger is achieved by directing most of the flow of the dry gaseous nitrogen through the LN2-HX. As the cold end temperatures approach those required for the test the bypass valve is opened fully and the LN2-HX valve turned almost completely off. Cool-down temperatures versus time are shown in Figure 5.6. The step increase in cold end inlet average temperature (T_{CIavg}) indicates the

time at which the flow through the LN2-HX is turned almost off. Since the cold end temperature is controlled manually, rather than continually re-setting the cold end valves, a temperature drift of up to about 3°C was tolerated during steady state tests. Figure 5.4 shows typical temperatures during an effectiveness test.

5.2.6 Pressure drop measurement

Figure 5.7 shows the pressure drop across one side of the MHE as measured and predicted. One predicted result is from the empirical equation of Shevyakova and Orlov[86]. The other was calculated using graphs from Kays and London[71] for entry and exit pressure loss coefficients for multiple-circular-tube heat exchanger core[71:Fig.5-2,p111] and mean friction factor for the hydrodynamic entry length of a circular tube[71:Fig.6-23,p138]. Venkatarathnam[80] has used the same graphs from Kays and London, for pressure drop prediction, but contrary to the suggestion of Kays and London[71-p110] for interrupted fin surfaces, he has not used K_c and K_e values for Re=∞. Further, he has used the apparent friction factor from Figure 6-23[71-p138] which already includes the entry and exit loss, rather than the mean friction factor. As may be seen from Figure 5.7 the result predicted using the K_c and K_e values for Re=∞, and the mean friction factor are in excellent agreement with the experimental result.

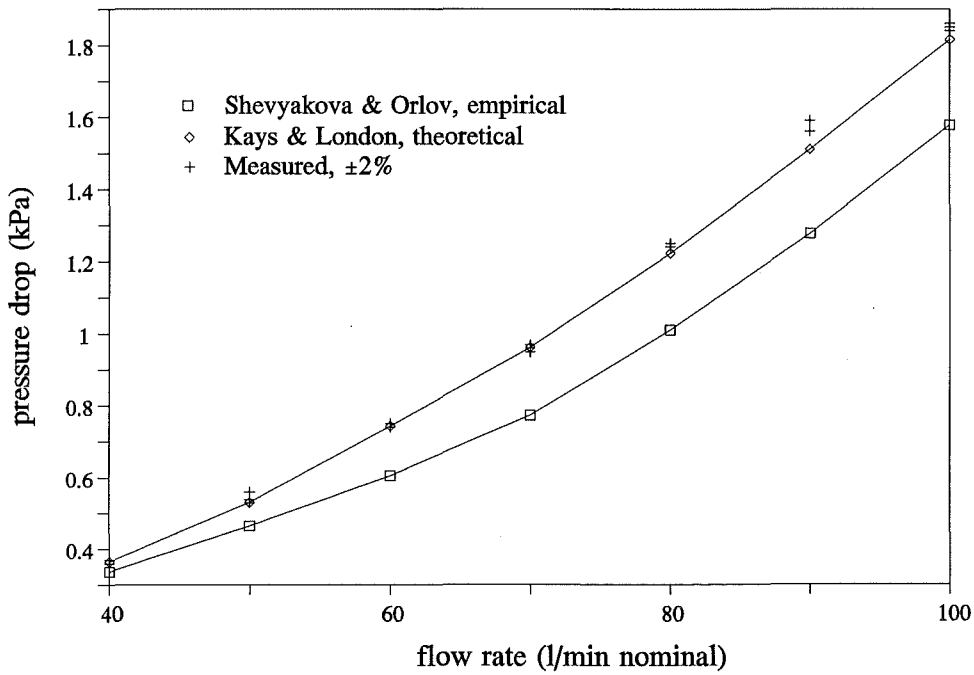

Figure 5.7 Pressure drop across a single matrix heat exchanger vs. nominal flow rate of nitrogen.

5.3 Heat transfer and pressure drop performance of two matrix heat exchangers coupled together

5.3.1 Effectiveness measurement

The measured effectiveness of the two MHE's operating in series was 93% ±2.5% over the tested range of flow rates of dry gaseous nitrogen. This result is shown in Figure 5.8. Of the two matrix heat exchangers in series, the first was operating at temperatures between ambient and -60°C, and the second between -60°C and -160°C. The -60°C limit was at the cross-over valve and has been discussed previously in the chapter four. The minimum uncertainty in the effectiveness calculated from liquid nitrogen boil-off is ±4.4%, as calculated before. For the two MHE's taken together the uncertainty in the temperature based value becomes ±3.0%, giving a combined minimum uncertainty of ±2.5%. As can be seen from Figure 5.8 most of the measured results lie within this minimum uncertainty.

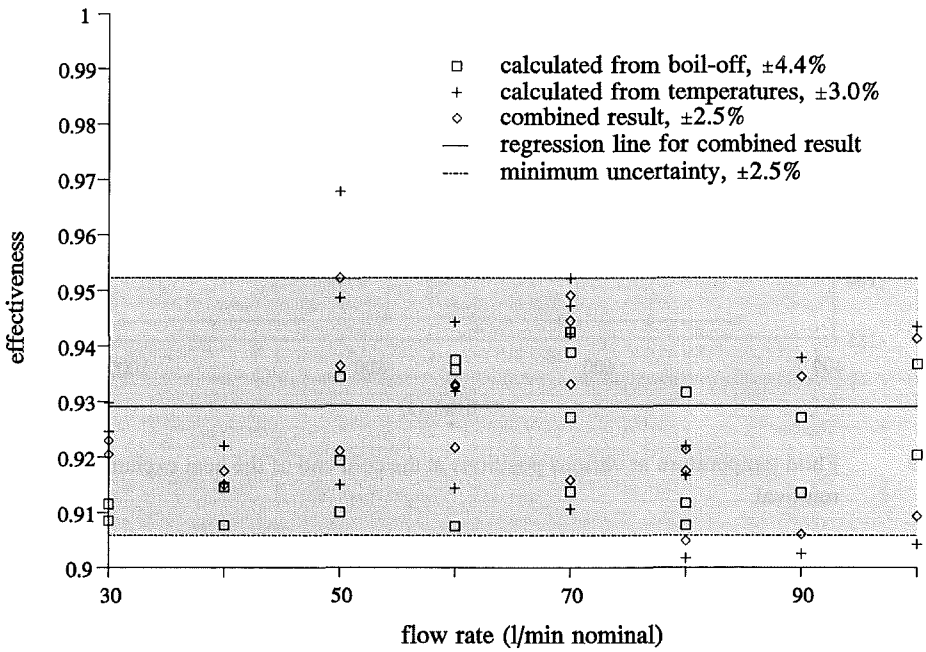

Figure 5.8 Combined effectiveness vs. nominal flow rate of nitrogen, for two matrix heat exchangers in series.

5.3.2 Effectiveness reduction due to heat leak

The 4% reduction in effectiveness of the two MHE's in series over the single MHE was thought to occur for two main reasons:

(a) The addition of the cross-over valve between the two MHE's. The cross-over valve

is operated by a pneumatic actuator. During the testing it was found that the actuator would freeze and become inoperable, and leak. In the absence of any other suitable actuator, a heating arrangement was installed and this actuator was heated to keep it from freezing and leaking. This additional heat adds a substantial heat leak into the nitrogen gas flowing through the cross-over valve by conduction through this valve. The temperature of the gas, on passing through this valve was measured to increase by about 1-2°C. It is not possible to quantify exactly the heat leak through the valve because there is some pressure drop across this valve as well, and associated cooling of the gas. The heat leak may be approximated from the measured temperature increase and knowledge of the flow rate, as 2-4W.

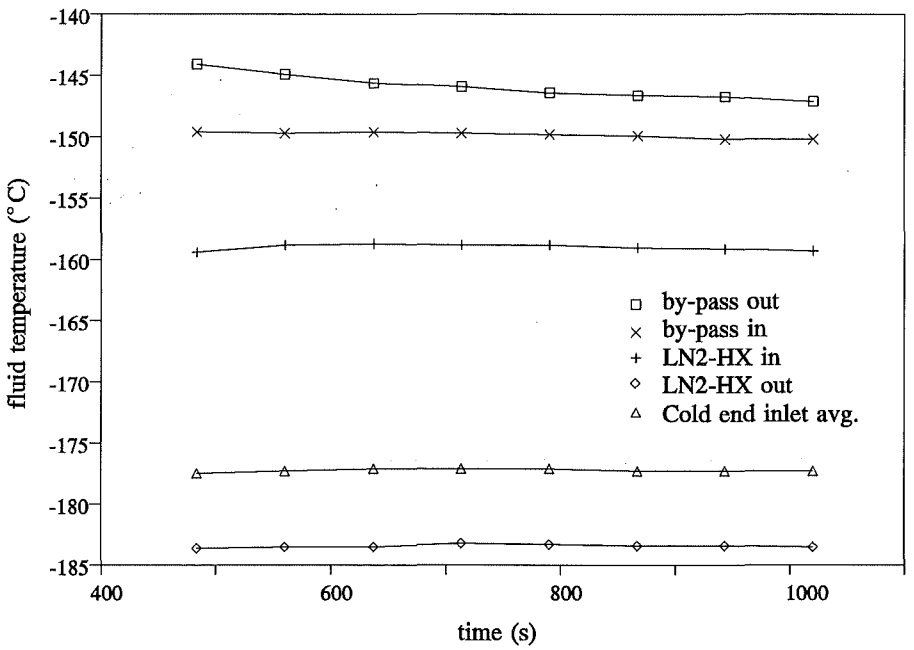

Figure 5.9 Fluid temperature at various positions at the cold end of the heat exchangers prior to by-pass removal.

(b) Increased heat leak at the cold end. The cold end temperature in this combined arrangement is -160°C in comparison to -75°C for the single MHE tests. The added temperature gradient increases the heat leak at the cold end through the by-pass and LN2-HX valves and pipe-work. Figure 5.4 and Figure 5.6 show the effect of heat leak on temperatures at the cold end in the single heat exchanger configuration. The presence and effect of this heat leak was explored by removing the by-pass valve and pipe-work. Figure 5.9 shows the cold end temperatures in the double heat exchanger configuration. Figure 5.10 shows the temperatures with the by-pass valve and pipe-work removed. The former by-pass inlet thermocouple has been inserted into the header at the cold end outlet. From these two graphs it can be seen that with the by-pass removed:

- the $T_{LN2\text{-}HXin}$ and cold end outlet average (T_{COavg}) temperatures are much closer together, 1.5° compared to 10°; and
- both these temperatures are lower, T_{COavg} is about 18° lower than T_{BPin}.

These temperatures appear to confirm the presence of the heat leak through the by-pass. The difference between $T_{LN2\text{-}HXin}$ and T_{BPin} and T_{BPout} is greater at lower temperature as can be seen by comparing Figure 5.4 and Figure 5.9 indicating that the heat leak is greater at lower cold end temperature.

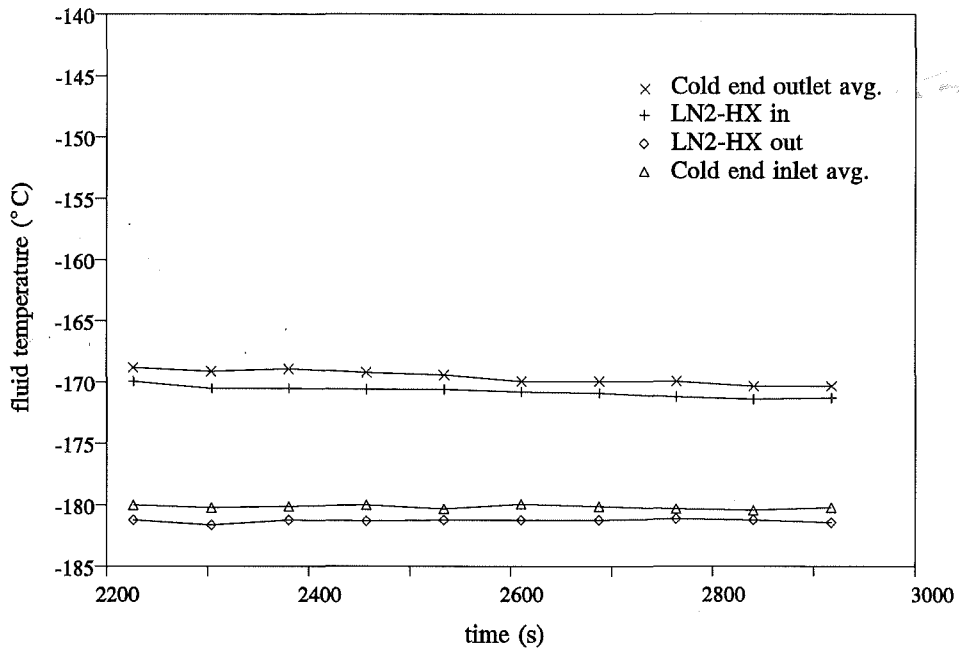

Figure 5.10 Fluid temperature at various positions at the cold end. By-pass valve and pipe-work removed. Cold end outlet avg. temperature is used instead of by-pass inlet temperature.

5.3.3 Cool-down

For the double heat exchanger configuration the cool-down was initially attempted in the same way as for the single heat exchanger. Most of the flow of the dry gaseous nitrogen was directed through the LN2-HX. It was thought that the two heat exchangers in series would act for the purposes of cool-down as one larger heat exchanger. Since the heat transfer duty has been approximately doubled, it was expected that the accompanying decrease in effectiveness of the cold end heat exchanger would cause the warm end heat exchanger to cool down. It was found that this did happen and that the reduction in effectiveness of the cold end heat exchanger was of the order of 10%. However complete cool-down to the desired temperatures was not achieved because this process was very slow.

A new flow circuit allowing cold nitrogen gas to be introduced into the warm

end heat exchanger was added to the rig. This circuit is shown schematically in Figure 4.2. Gaseous nitrogen is bubbled through the outer liquid nitrogen bath and through a one-way valve into the cold end inlet ($T_{Port1out}$) of the warm end MHE. By adjusting the relative flow rates in the new cool-down circuit and the main circuit the desired $T_{Port1out}$ temperature can be obtained. This method allowed the warm end MHE to be cooled faster. Figure 5.11 shows the temperatures during cool-down of the two MHE's. $T_{Port1out}$ shows the sharp temperature variations associated with changing the flow rate in the by-pass cooling circuit. The heat leak through the cross-over valve is also evident from $T_{CO2\text{-}MHEin}$ remaining much higher than $T_{Port3out}$.

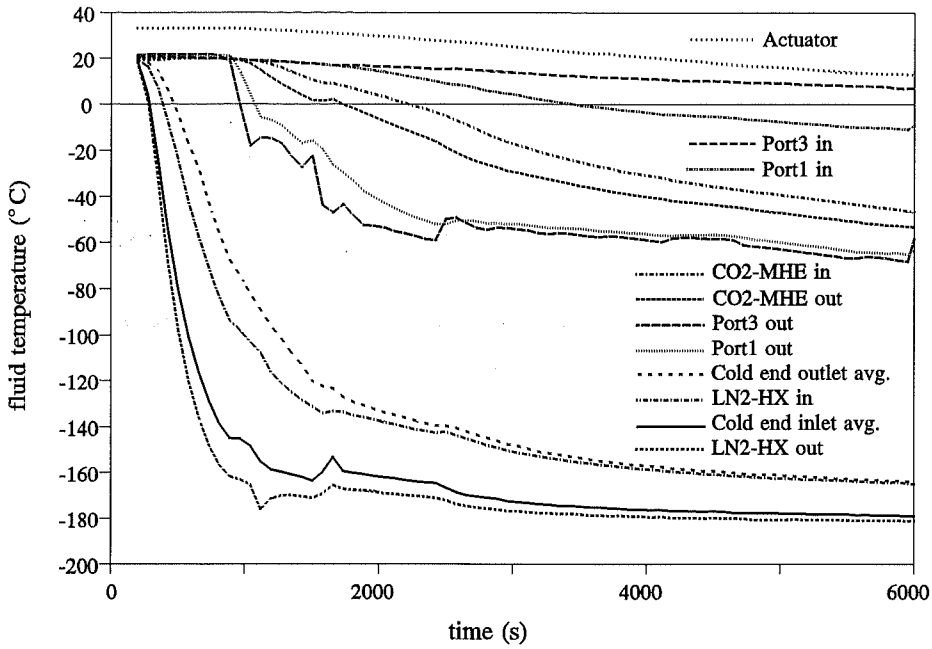

Figure 5.11 Fluid temperatures during cool-down period (refer to Figure 5.5). Warm end heat exchanger cool-down commenced at 1000s.

5.4 MHE construction evaluation

A new MHE construction was developed for this project. In addition to heat transfer effectiveness and pressure drop, heat exchanger performance evaluation included monitoring the MHE structure. The two MHE's built for this project, have been used over a period of two years. They have been cycled from ambient temperature to near liquid nitrogen temperature on at least 30 occasions, and have been tested in operation at cryogenic temperatures for approximately 120 hours. During early cool-down tests the H2O-MHE was deliberately flooded with liquid nitrogen. Later, during the initial tests using air, the cold end of the CO2-MHE was accidentally flooded with liquid oxygen.

The heat exchangers have been used at pressures of up to 4 bar. None of these factors has resulted in any leaks or any other visible degradation of their construction.

5.5 CO_2 removal from dry bottled air

5.5.1 Test format

The effectiveness tests on a single heat exchanger, and two heat exchangers with the cross-over valves in place, showed that the pre-requisite effectiveness for the CO_2 removal process can be achieved. CO_2 removal tests were carried out on dry bottled air. Inlet and outlet stream CO_2 concentration was measured using a mass spectrometer. The mass spectrometer set-up and continuous sampling system used has been described in chapter four. No flow switching was necessary because dry air was used for these tests. Dry gaseous nitrogen was used to effect the cool-down so that no mass transfer occurred in the transient stage. Once steady state was established the gas flow was switched from nitrogen to dry air. The pressure drop between the inlet and outlet was monitored for the effect of CO_2 deposition. All the tests were done at the design flow rate of 70l/min.

5.5.2 Trace CO_2 analysis

5.5.2.1 CO_2 concentration calculation

The mass spectrometer is used for quantitative analysis on the basis of there being a linear relationship between the concentration of a component of a gas mixture and its characteristic peak height. This peak height is the recorded ion current for a particular mass to charge ratio (m/e) ion. The specific geometry and tuning (acceleration potential etc.) of a mass spectrometer effect the absolute intensity of the recorded ion current for any ion species. For this work, a gas mixing facility of the required accuracy to obtain absolute sensitivities of the mass spectrometer for the gases of interest was not available.

Quantitative analysis may be done using relative ion current measurements. For a given electron accelerating voltage (eV) in the ion source the relative sensitivities of various ions are related to their ionization cross section only. Ionization cross sections for various substances have been measured and are available in listings such as that given by Kiser[104:Appendix III]. A mixture may therefore be analyzed by measuring the peak heights of all the components relative to one component assigned

a relative sensitivity of 1. The mole fractions are then calculated as

$$P_i = \frac{\frac{p_i}{s_i}}{\sum_j \frac{p_j}{s_j}} \tag{5.7}$$

where P_i is the actual partial pressure of the i^{th} component, p_i is the measured peak height, and s_i is its relative sensitivity, in a mixture of j components.

The ion current or measured peak height of any component is known at best to ±5%. Analysis of trace concentration by this method is therefore not possible to any accuracy. In this specific case for example, the gas to be analyzed is air. The measured peak height of N_2 will be 2000 times higher than that of CO_2. An error of ±5% in the N_2 peak could give an error in the calculated CO_2 concentration 100 times it's concentration.

Alternatively if the concentration of one component of the mixture is known and is similar to the component of interest, the relative analysis can be used with better accuracy. In air the concentration of argon is known and constant. The saturation temperature for argon at 1 atm is 87.28K. This means that the concentration of argon itself is not changing as part of this process, ie. the Ar does not condense at any stage in the heat exchangers. The concentration of CO_2 may then be calculated as

$$P_{CO_2} = \frac{p_{CO_2}}{4.31} \frac{3.52}{p_{Ar}} P_{Ar} \tag{5.8}$$

where the relative sensitivities of CO_2 and Ar are 4.31 and 3.52. The partial pressure or mole fraction of argon in air is 9340ppm. This method reduces the maximum error in the calculated CO_2 concentration to ±10%.

Table 5.2 Primary peaks of air components

Substance	H_2O	N_2	O_2	Ar	CO_2
m/e	18	28	32	40	44

5.5.2.2 CO_2 concentration measurement: establishing a sampling method

In the process of setting up the mass spectrometer and sampling system several samples of room air were introduced to the mass spectrometer for trial analysis. It was found that the CO_2 concentrations recorded were much higher than expected, of the order of 2000ppm. The background spectrum showed disproportionately high peaks at m/e 18, 28 and 44. The background spectrum is the spectrum of ion currents or peak

heights of the residual gases in the mass spectrometer with no sample introduced. The total pressure of the background was ~$3x10^{-8}$torr. The primary peaks for air components are given in Table 5.2. The m/e 18 peak is due to the H_2O^+ ion and its presence in the background indicates the adsorption of water on surfaces inside the vacuum chamber of the mass spectrometer. Residual vacuums which have been open to air all show elevated 18 and 44 peaks because water and CO_2 are the most strongly adsorbed components. All mass spectrometer vacuums are conventionally baked (held at elevated temperature for several hours, 250-350°C for 8-16 hours) to eliminate adsorbed gases. Baking in this case reduced the 18 peak height but those for 28 and 44 remained. The presence of 28 and 44 peaks was explained by the Spectramass quadrupole mass spectrometer literature[105] as the adsorption of CO (CO^+ m/e 28) and CO_2 on the filaments in the mass spectrometer and ion gauge. Both the mass spectrometer and the ion gauge have a de-gas facility. De-gassing them reduced the 28 and 44 peaks in the background. Total pressures as low as $2x10^{-9}$ were obtained. Introducing air samples for analysis in the mass spectrometer caused the high 28 and 44 peak to re-appear. These results are shown in Table 5.3.

Table 5.3 Background spectrum for various vacuum conditions

peak height, torr	m/e 18 H_2O	28 N_2	32 O_2	40 Ar	44 CO_2
post bake	1.6e-9	1e-9	7e-11	7e-11	3.6e-10
filaments degassed	1.5e-10	1.5e-10	4.9e-11	7e-11	1.2e-10
post sample	1.2e-9	4.2e-9	5.4e-10	1.7e-10	3.2e-10

It was found further that the 44 peak height increases with time while continuously sampling. This is shown in Figure 5.12 and Figure 5.13. This increase of the 44 peak may occur due to:

- mass discrimination in the sampling system or vacuum chamber,
- contamination in the mass spectrometer chamber,
- chemical reactions occurring in the mass spectrometer chamber, or
- adsorption on the chamber walls or filaments.

At mass 44, CO_2 is the heaviest molecule from the normal components of air. Mass fractionation may occur in the sampling system. The capillaries used in the sampling system are 0.18 and 0.25mm in diameter and may act as a chromatography column. In the results obtained the chromatogram associated with frontal analysis of a

continuous sample is not observed. Alternatively the pumping speed of the vacuum system for gases is related to their mass and may cause mass discrimination. In both these cases argon at mass 40 may be expected to show trends similar to CO_2. This is not evident from the results.

There may be some contaminant present in the mass spectrometer chamber which is interfering with the 44 peak. A background scan up to m/e 100 was done and showed no unusual peaks. It may be that at some time in the operation of the vacuum-mass spectrometer system back-streaming of diffusion pump oil vapour has occurred leaving fractionated components in the mass spectrometer chamber. Si^+ at m/e 28 and SiO^+ at 44 may be expected fractionated components of the silicon based DC705 diffusion pump oil used. The main peaks in the actual spectrum for DC705 as listed by VG Quadrupoles[106] are given in Table 5.4.

Table 5.4 Main peaks in DC705 diffusion pump oil spectrum.

m/e	39	43	76	78
relative abundance	73	59	83	100

Of these peaks the only interference may be expected from the 43 peak. Figure 5.13 shows that the 43 peak does not show any comparable increase with time.

A possible reaction mechanism involving CO and CO_2 could be

$$CO+H_2O \rightleftharpoons CO_2+H_2 \qquad (5.9)$$

At sample pressures of $1x10^{-6}$ torr the average mean free path for air molecules at 20°C may be approximated at 50m. Under these conditions the occurrence of any chemical reaction is considered extremely unlikely.

Preferential adsorption of CO_2 from the introduced sample may occur. To avoid this all surfaces in the mass spectrometer chamber are maintained at 60-90°C while sampling. This procedure, reported used previously by Reed[107], reports the use of mass spectrometer chamber heating up to 150°C for continuous process monitoring of water, CO_2 and NH_3. Adsorption of CO_2 on the filaments in the mass spectrometer and ion gauge has been suggested earlier. Since the mass spectrometer filament is on and therefore hot during the measurements adsorption on this filament is unlikely. The ion gauge filament is maintained off while analysing samples because this filament functions as an ion source. The ions generated by this ion gauge filament interfere with the reading of ions generated by the mass spectrometer ion source. There is a second filament in the ion gauge which is the de-gassing filament. This filament is maintained off while sampling because operating at the high pressure of the sample (10^{-5}) will cause this filament to vaporize rapidly. De-gassing the ion gauge filament after sampling

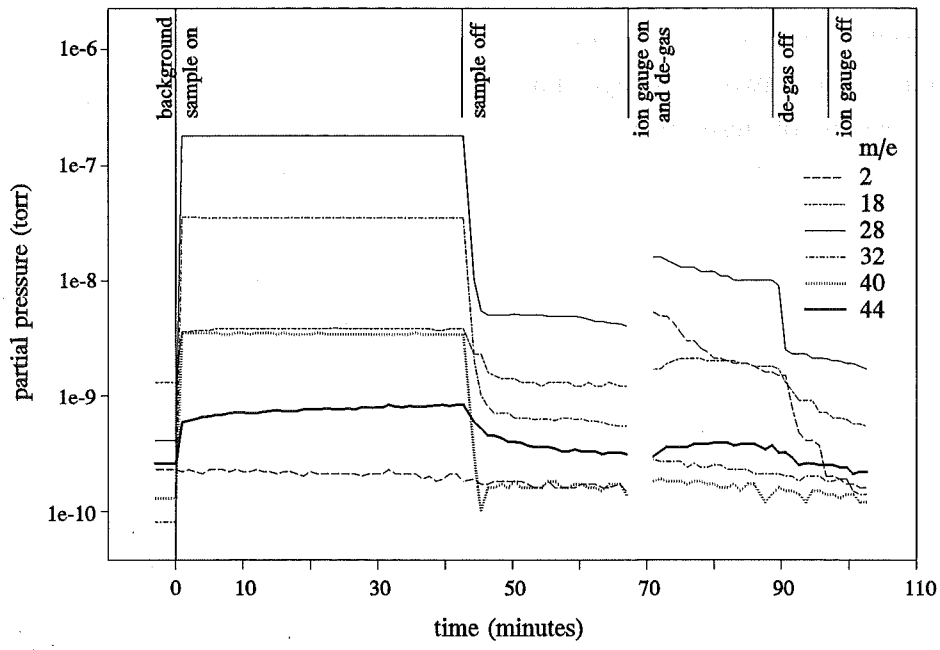

Figure 5.12 Mass spectrometer output for room air sample introduction, trend analysis and shut down (including ion gauge de-gassing).

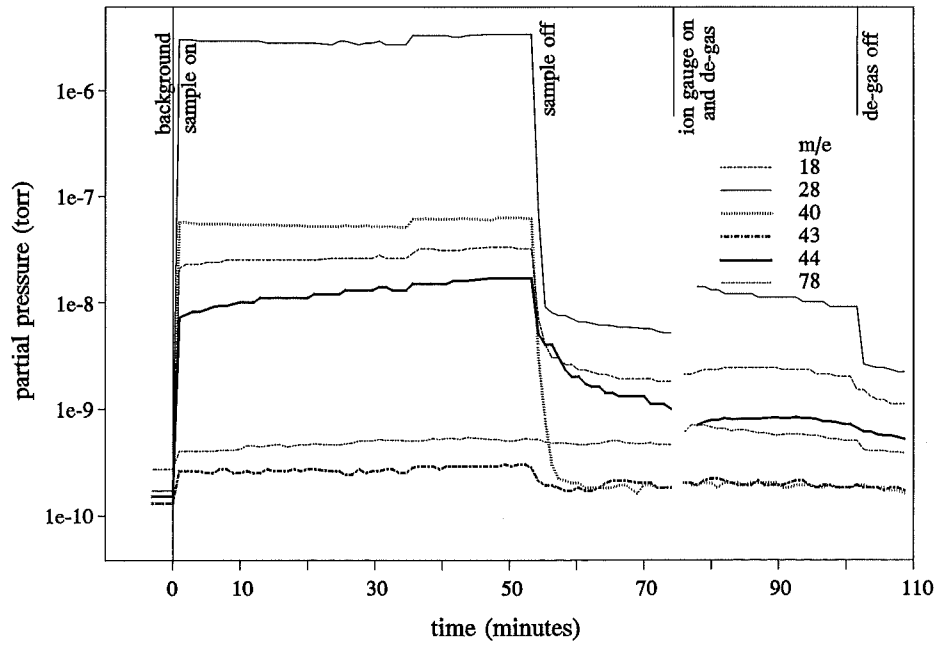

Figure 5.13 Mass spectrometer output for room air sample, as in Figure 5.12. Sample pressure is an order of magnitude higher and less stable. Mass peaks 78 and 43 are for DC705 diffusion pump oil.

causes pressure rises of up to 3 orders of magnitude in the vacuum (10^{-8} to 10^{-5} torr). Once the ion gauge filaments have been de-gassed, the total pressure returns to the normal background value of ~$1x10^{-8}$. This has been taken to indicate substantial adsorption in these two ion gauge filaments.

A series of tests was run to see if an increase in the background CO_2 concentration could be masked or swamped by:

- using a high sample pressure, or
- introducing a high CO_2 concentration gas to allow adsorption to occur prior to introducing the sample, or
- sampling with the ion gauge on to reduce the adsorption.

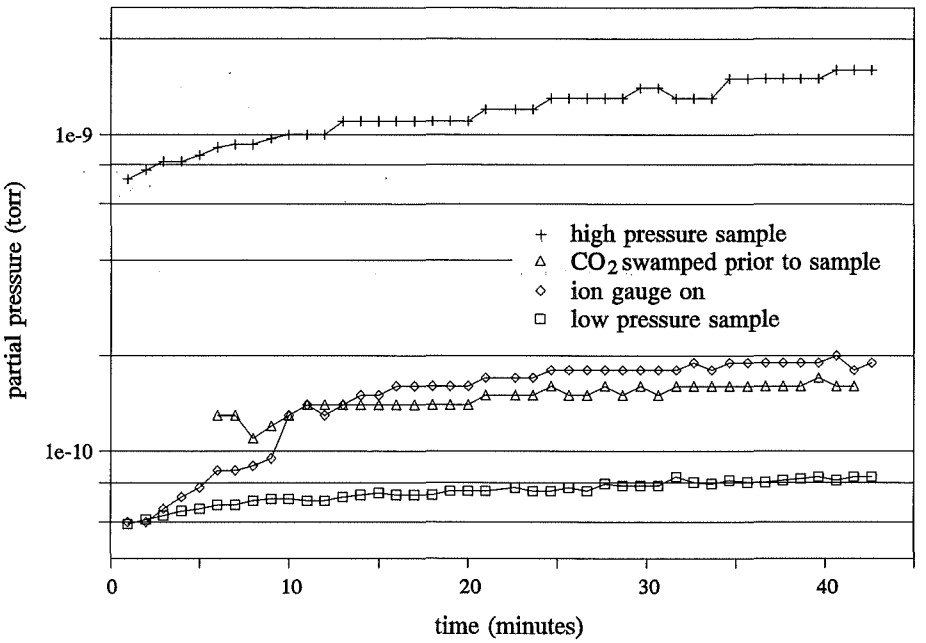

Figure 5.14 Comparison of change in measured CO_2 peak height with time, from a room air sample, for four approaches to sampling.

The results of these tests, compared to a low pressure sample, are shown in Figure 5.14. The low pressure sample and the CO_2 swamped sample appear to show lower rates of change of CO_2 concentration.

The factors outlined above made a meaningful reading of the absolute CO_2 concentration not possible. Since the re-appearance of the high CO_2 peak seemed linked to the introduction of CO_2 to the mass spectrometer a sequential sampling method was devised. In this method the difference in CO_2 concentration between two samples is measured. This is done by measuring the background, then introducing the sample containing no or low CO_2, and then the sample containing higher CO_2. This method was tested by comparing CO_2 scrubbed air with room air. The air was scrubbed by passing

it through two test tubes containing silica gel and NaOH respectively. The difference was also measured using Kitagawa gas detector tubes (tube no.126B, 100-1500ppm range). These contain alumina and NaOH with a pH sensitive indicator. The results are shown in Table 5.5. This method gave the most consistent results obtained for the various sampling methods tried and was used for all subsequent testing.

Table 5.5 Sequential sampling method results for measuring difference in CO_2 concentration.

ΔCO_2 Kitagawa	ΔCO_2 mass spectrometer
220±50ppm	224±45ppm

5.5.2.3 Variation of CO_2 concentration in bottled dry air

The bottled dry air (BOC Gases) acquired for MHE testing was sampled prior to each test to determine its CO_2 content. Two interesting results were obtained. First, the CO_2 concentration of each bottle was different, varying from 210-410 ppm. Second; the first two tests for CO_2 removal on the complete rig showed the inlet concentration of CO_2 to rise suddenly as the gas bottle became almost empty. The day after the second test run the residual content of the gas bottle used was sampled and found to contain 1100ppm of CO_2. The appearance of high concentration of CO_2 at reduced bottle pressure and when the bottle temperature has increased (equilibrated with room temperature) may indicate that this is due to adsorption of CO_2 on surfaces inside the cylinder.

5.5.3 Measured CO_2 removal

The discussion in the previous section outlines the problems encountered in trying to measure trace amounts of CO_2 in air samples. An example of actual test data collected is shown in Figure 5.15. Note how rapidly and well the Ar peak stabilizes by comparison to the CO_2 peak. Sampling sequence is background-outlet-inlet-background. Figure 5.16 shows more closely the peak heights for inlet and outlet CO_2 and Ar for one sample. In these readings alone a ±5% error in the Ar peak height could mean up to a ±50% error in the calculated CO_2 concentration difference between inlet and outlet. The only method left available to minimise errors in the readings was to take as many readings as possible and calculate mean results. The number of samples which may be read is limited by the time taken for readings to stabilize and to return to whatever is considered a reasonable background in the sampling sequence. For these tests each sample took about 15 minutes, allowing 6 samples per bottle. The time chosen for

averaging the results was the duration for which a gas bottle lasted since the initial CO_2 concentration in each bottle was always different. Test results obtained in this way, for three bottles of air, are shown in Figure 5.17. CO_2 concentration in the outlet stream calculated from the collective average of all the test results is shown in Figure 5.18.

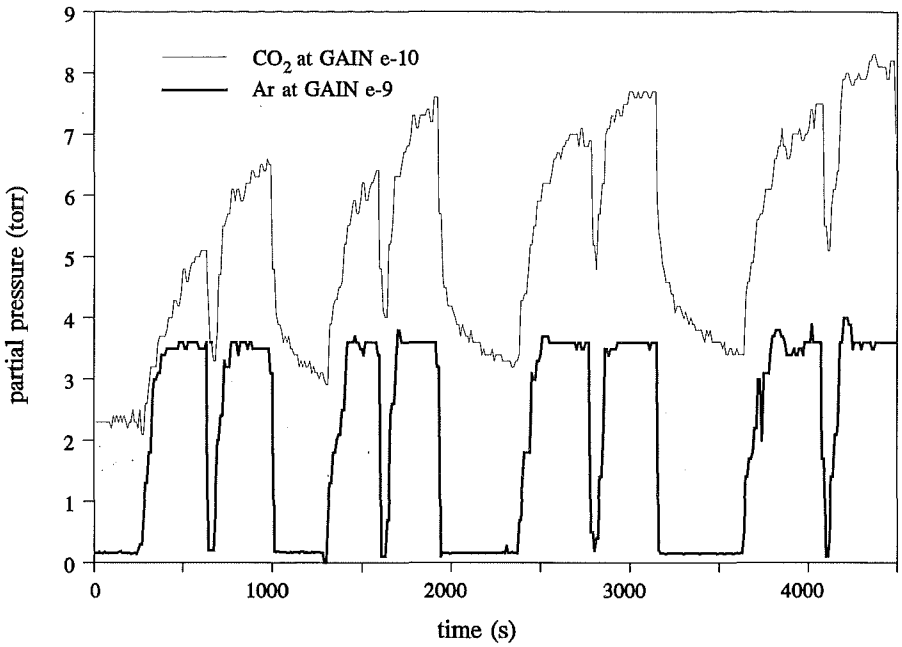

Figure 5.15 First four sequential samples for a CO_2 removal test.

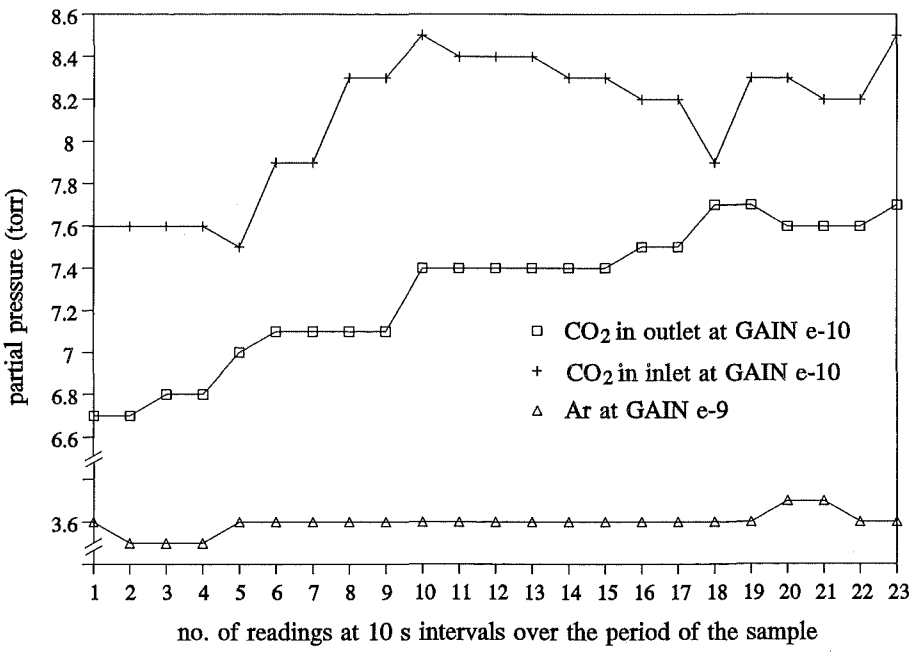

Figure 5.16 Inlet and outlet CO_2 peaks and Ar peak over the duration of one sample.

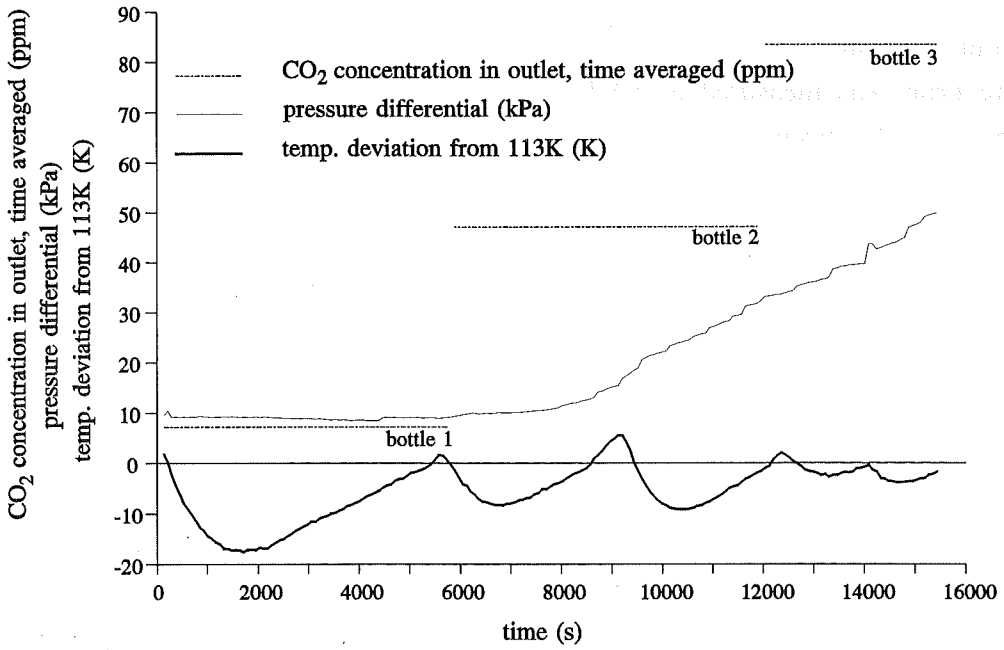

Figure 5.17 CO_2 concentration in outlet air, pressure differential between inlet and outlet, and cold end inlet avg. temperature plotted over the period of a test.

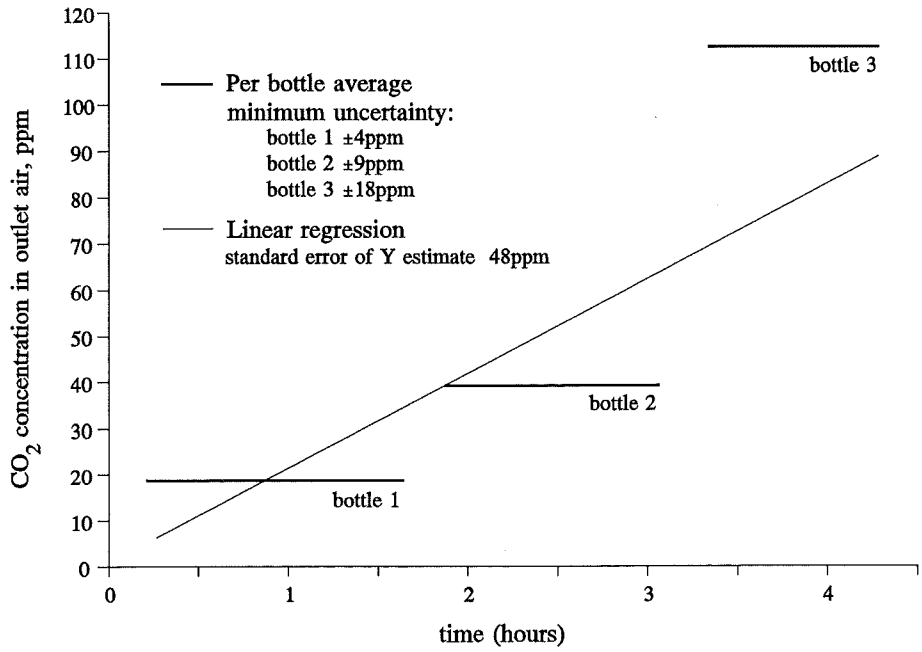

Figure 5.18 CO_2 concentration in outlet stream vs. time, averaged results from all tests.

Results show:

(a) CO_2 removal to below 10ppm is possible by this technique. Certainly levels below the 50ppm specified by Elenco nv.[?] can be obtained. For this apparatus levels below

50ppm can be maintained for up to at least 2 hours before regeneration is required.
(b) The pressure differential between inlet and outlet is linked to the CO_2 concentration in the outlet stream. It may be used as the indicator for regeneration times. Initial total pressure drop was measured at 10kPa. Pressure drop for each channel in the heat exchanger core has been previously measured at 1kPa. This indicates that ~6kPa pressure drop occurs in the cross-over valves.

5.6 Water cycling tests using compressor supplied air

Water cycling tests were done using air from a laboratory compressed air supply. Water concentration in the inlet and outlet streams was measured in the same way as the CO_2 concentration. A test sample is shown in Figure 5.19. It can be seen that the inlet and outlet H_2O readings were very similar. The difference between them was at most the 10% limit of resolution of the mass spectrometer. Once again the concentrations were averaged over time to see if a result was obtainable. These results are shown in Table 5.6.

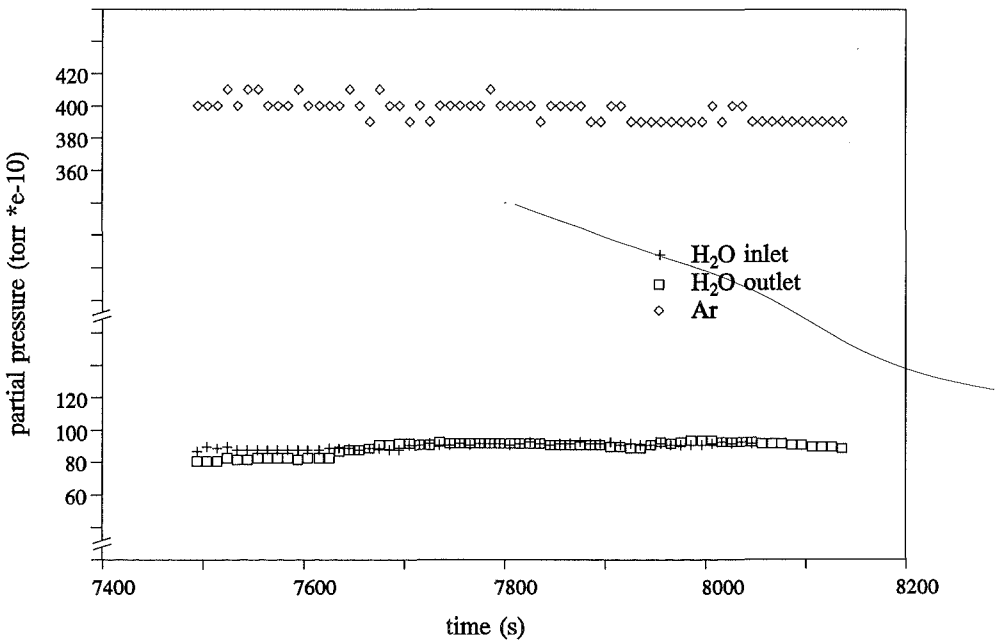

Figure 5.19 H_2O inlet and outlet, and Ar peak heights for a reversing heat exchanger test.

The cross-over valve located between the reversing heat exchanger and the CO_2 subliming heat exchanger had previously restricted testing to -60°C. Below this temperature the valve would begin to leak even when it was not operated. This has been discussed previously in chapter four. It was found that when this valve was operated, it

would in fact begin to leak at -40°C. During the test this temperature would rise to about -35°C over a period of 3½ to 4 hours.

Table 5.6 Reversing heat exchanger test results

Test no.	Average difference between inlet and outlet H_2O concentration, ppm
1	132
2	170
3	126

The saturation concentration of water in air at -40°C is 128ppm and at -35°C is 222ppm (Figure 2.2). It may be expected that this amount of water will be carried through, into the CO_2 subliming heat exchanger which is non-reversing. It can be seen from Table 5.6 that the results from each test lie within this range. This indicates that water condensation and re-vaporisation occurs in the reversing heat exchanger as expected.

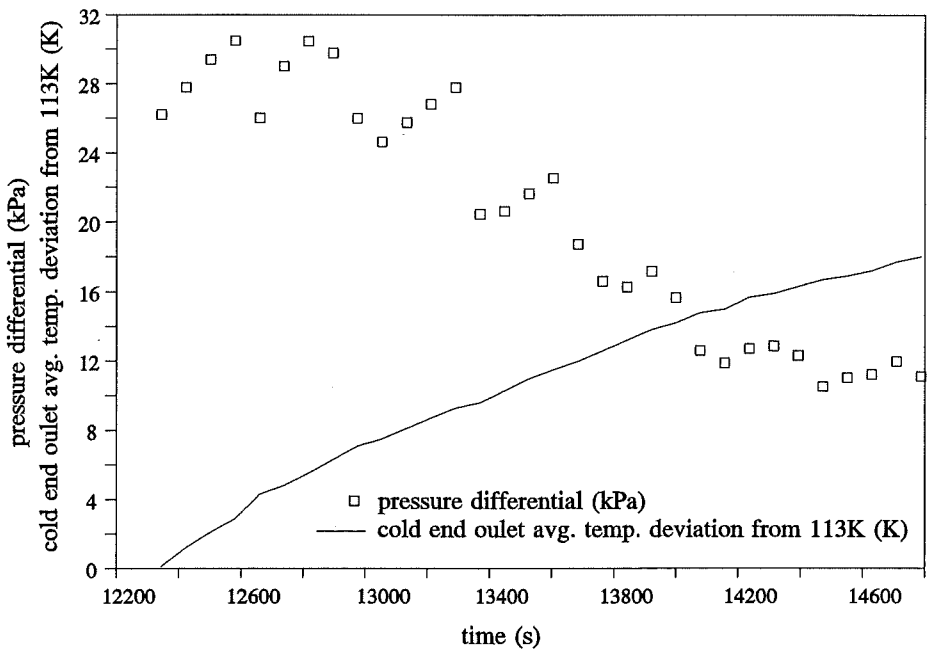

Figure 5.20 Pressure differential across inlet and outlet, and cold end outlet average temperature deviation for CO_2 MHE regeneration test.

5.7 CO_2 MHE regeneration tests

The CO_2 deposited in the heat exchanger may be expected to vaporise if the temperature at the cold end is allowed to rise. The saturation temperature for CO_2 in air is 130K (-143°C). A test was conducted to determine whether regeneration could be effected by allowing this temperature rise. At the end of a CO_2 removal and water cycling test, the cold end temperature was allowed to rise from its test value of -160°C. Figure 5.20 shows the measured pressure drop and cold end temperature with time. It can be seen that as the temperature rises from -160°C to -142°C the pressure drop across the heat exchangers returns from 30kPa to the original ~10kPa.

The fluctuation of the pressure differential readings seen in Figure 5.20 occurs for two reasons. Firstly, as the pressure differential decreases the flow rate of air through the heat exchanger apparatus increases. To compensate, the flow rate is decreased manually, and this causes a step decrease in the measured pressure differential. Secondly, the pressure of the air supply itself fluctuates.

Results summary

Single heat exchanger effectiveness 97%±1.9%
Pressure drop per channel 1kPa
Double heat exchanger effectiveness 93%±2.5%
Total pressure drop including cross over valves 10kPa
CO_2 removal to 20ppm for 1½ hours, 50ppm for 2-2½ hours
Pressure differential increase linked to outlet CO_2 concentration
Currently available cross over valve operating temperature limited to -40°C
Water cycling in reversing heat exchanger established, but water carry over to CO_2 subliming MHE occurs due to cross over valve temperature limit.
Regeneration of CO_2 subliming heat exchanger achieved by warming it by 18°C

Chapter 6

Conclusions and recommendations

It has been said that in a hydrogen economy, a time when hydrogen becomes widely available and used as a major transportation fuel, the use of alkaline fuel cells for transport power generation will be favoured over other types of fuel cells. This is because alkaline fuel cells are inherently more efficient and the range of materials which may be used as electrocatalysts or for structural elements is much larger for alkaline media than for acid media. The direct availability of hydrogen, ie. a supply independent of reformed hydrocarbon fuels, would alleviate the problem of CO_2 intolerance of alkaline fuel cells associated with the fuel. The CO_2 content of air remains a problem.

Research and demonstration projects on hydrogen-air alkaline fuel cell powered vehicles have so far used expendable adsorbers for scrubbing CO_2 from the air. These adsorbers represent a substantial added weight and occupy a large volume when used for other than low power or short duration applications. Large scale use of non-reusable scrubbers would create the added problem of distribution, and disposal of the spent adsorptive material.

The research undertaken in this project established that a regenerable process for CO_2 removal from alkaline fuel cell feed air by refrigeration purification, using the cooling available from thermomechanical exergy recovery from liquid hydrogen, is achievable.

6.1 Conclusions

The experimental work conducted showed that CO_2 removal from air to below 10ppm is possible using the proposed process. Water condensation and re-vaporisation which must occur as part of this process, has been demonstrated using a reversing heat exchanger. Regeneration for the heat exchanger in which the CO_2 was deposited was achieved by allowing it to warm up through a temperature range of 18°C. The increase of the pressure differential between inlet and outlet air streams was linked to outlet CO_2 concentration and thus offers a method for controlling regeneration timing. Heat transfer effectiveness was measured at 93%±2.5%. These results collectively indicate that the proposed CO_2 removal process functioned as designed, with a 93% internal refrigeration recovery. The testing has demonstrated that even with a hydrogen-air mass ratio as low as that for normal alkaline fuel cell operation, it is possible to effect CO_2 removal using exergy recovery if high effectiveness heat exchangers are used. With improved design of the cross-over valves and actuator used with the reversing heat exchanger, it is quite

feasible that such a process could be used in vehicular application.

For this project, matrix heat exchanger geometry was optimised giving equal weighting to heat exchanger volume, the number of plates and core pressure drop. The total pressure drop through the matrix heat exchanger cores was measured at 4kPa. This is twice that for Elenco nv.'s soda lime scrubber accompanying the BCB-1 1.2kW AFC module, on which basis the heat exchanger apparatus for this project was sized. A lower pressure drop could be achieved by optimising the heat exchanger geometry with a higher weighting for the core pressure drop.

The heat exchanger in which the CO_2 sublimation occurs, and the reversing heat exchanger, are both perforated plate matrix heat exchangers. For this work, in order to be able to build the required matrix heat exchangers, a new method for their construction was developed. This method of manufacturing copper perforated plate and fibre laminate spacer matrix heat exchangers, was highly successful.

Thermal and hydraulic performance evaluation experiments were conducted on the matrix heat exchangers built for this project. Single heat exchanger effectiveness was measured at 97%±1.9%. The experimental results for heat transfer performance were compared with those predicted by the new sizing equation developed and the numerical solution for heat transfer performance of matrix heat exchangers, developed by Venkatarathnam (*Ph.D thesis, IIT Kharagpur, India*). The predicted and experimental results lie within the limits of minimum experimental uncertainty.

6.2 Further work

6.2.1 Suggested modifications to equipment for further testing

Experimental results which may be improved and some possible ways of achieving this are suggested in the following sections.

6.2.1.1 Single heat exchanger effectiveness tests

The minimum experimental uncertainty in these tests was ±1.9%. In order to reduce this, two factors must be addressed. The first is thermocouple calibration at cryogenic temperature. The second is the discrepancy between heat exchanger effectiveness calculated from temperatures and that calculated from LN2 boil-off. This discrepancy, discussed in section 5.2.4 and section 5.3.2, is due to heat leak through the by-pass and LN2-HX valves. The two valves are positioned so that they can be operated from outside the vacuum vessel. Hence a large temperature gradient exists along the actuation mechanism used, causing an unavoidable heat leak. The two valves and the by-pass pipe-work may be eliminated if temperature control at the cold end can be achieved

by some other method such as LN2 level control. The positioning of an additional thermocouple inside the cold end outlet header may improve the accuracy of temperature based calculation.

6.2.1.2 Double heat exchanger configuration tests

The cross-over valve used for this project, that operates at low temperature, limited the temperature range over which the warm end heat exchanger (later used as the H2O-MHE) could be operated. The lower limit for fluid temperature passing through this valve, discussed in section 4.1.3, was -40°C or -60°C depending on whether it was operated or not. The actuator associated with this valve was pneumatic and would become inoperable and leak at low temperature. The cross-over valve and actuator induced an additional heat leak into the fluid passing through the valve.

The warm end heat exchanger cool-down, discussed in section 5.3.3, was very slow. Once again the fluid exiting the warm side of the warm end heat exchanger and passing into the (cold) cross-over valve is limited in temperature to -60°C, which limits the rate at which this heat exchanger is cooled down. Replacing the cross-over valves and actuator used, with an arrangement designed for operation at cryogenic temperatures may alleviate these problems.

6.2.1.3 Mass spectrometric measurement of trace CO_2 and water concentrations

The mass spectrometer and associated sampling method used, were limited in being able to monitor continuously trace CO_2 and water concentrations. The measurement of CO_2 was hampered by it's adsorption within the vacuum system and the variation in CO_2 concentration in the bottled air used for the tests. The limits on accuracy of concentration measurement were dependant on the ratio of the concentration to be measured to that of argon in air, since a relative analysis was used. The accuracy of the results obtained may be improved by performing an absolute calibration for these substances. This would allow functioning of the reversing heat exchanger at varied humidity levels to be investigated. Non-dispersive infrared analysis has been used elsewhere for trace CO_2 measurements and may prove to be a more suitable method for CO_2 measurement.

6.2.2 Vehicular application of the CO_2 removal process

Since this project has been successful in establishing the viability of the proposed new process for CO_2 removal, it is suggested that further development proceed by testing the apparatus with liquid hydrogen in a working system that includes an alkaline fuel cell. The issues of cross-over valves and actuator, cold end temperature control, and cross-over valve timing could be investigated in such a system. A working apparatus for vehicular application could be developed from this basis.

References

1. HOFFMAN,P.; *Hydrogen and Fuel Cell Letter*, vol.XI, no.3, 1996

2. SCOTT,D.S.; *Int J Hydrogen Energy*; vol.19, 1994: no.1,2,3,4,6,8,10; vol.20, 1995: no.12; vol.21, 1996: no.1

3. Source - Reuter, Christchurch Press, Newspaper, June 9, 1995, p33

4. PRESLEY,M.; First hydrogen fuel cell powered bus; *Hydrogen Today*, vol.5. no.1, 1994

5. Fuel cell vehicle; Daimler Benz 'High Tech' Report 2/1994

6. MARCENARO,B.; EQHHPP FC BUS: Status of the project and presentation of the first experimental results; *Hydrogen Energy Progress X*, vol.3, 1994, p1447-1456

7. De GEETER,E., VAN den BROECK,H., BOUT,P., WOORTMAN,M., CORNU,J., PESKI,V., DUFOUR,A. and MARCENARO,B.; Eureka fuel cell bus demonstration project; *Hydrogen Energy Progress X*, vol.3, 1994, p1457-1460

8. NADAL,M. and BARBIR,F.; Development of a hybrid fuel cell/battery powered electric vehicle; *Hydrogen Energy Progress X*, vol.3, 1994, p1427-1440

9. BILLINGS,R.E., SANCHEZ,M., CHERRY,P. and EYRE,D.B.; Lasercell prototype vehicle; *Int J Hydrogen Energy*, vol.16, no.12, 1991, p829-837

10. Phosphoric acid fuel cell bus program near completion at H Power; *The Clean Fuels Report*, Feb. 1996, p136

11. Hydrogen: company activities; *The Clean Fuels Report*, Nov. 1995, p125

12. WINTER,C.J. and NITSCH,J. (Eds.); Hydrogen as an energy carrier: technologies, systems, economy; Springer-Verlag, New York, 1988

13. APPLEBY,A.J. and FOULKES,F.R.; Fuel cell handbook; Van Nostrand Reinhold, New York, 1989

14. BLOMEN,L.J.M.J and MUGERWA,M.N. (Eds.); Fuel cell systems, Plenum Press, New York, 1993

15. WENDT,H. (Ed.); Electrochemical hydrogen technologies: electrochemical production and combustion of hydrogen; Elsevier, New York, 1990

16. CHUM,H.L. and SRINIVASAN,S. (Eds.); Executive summary; *Proc. Workshop on Renewable Fuels and Advanced Power Sources for Transportation*, June 1982; US Govt. Rep. no. SERI/CP-234-1707, DE83011988, p(vi)

17. PIPEROPOULOU,H. and BLOOMFIELD,D.; CO_2 management for alkaline fuel cells; *Proc. Workshop on Renewable Fuels and Advanced Power Sources for Transportation*, June 1982; US Govt. Rep. no. SERI/CP-234-1707, DE83011988, p149-166

18. ANAND,N.K., APPLEBY,A.J., DHAR,H.P., FERREIRA,A.C., KIM,J., MUKERJEE,S., NANDI,A., PARTHASARATHY,A., RHO,Y.W., SOMASANDARAN,S., SRINIVASAN,S., VELEV,V. and WAZIKOE,M.; Recent progress in proton exchange membrane fuel cells at Texas A&M University; *Hydrogen Energy Progress X*, vol.3, 1994, p1669-1679

19. SCOTT,D.S., ROGNER,H.-H. and SCOTT,M.B.; Fuel cell locomotives in Canada; *Int J Hydrogen Energy*, vol.18, no.3, 1993, p253-263

20. HOFFMAN,P.; *Hydrogen and Fuel Cell Letter*, vol.XI, no.2, 1996

21. BARENDRECHT,E.; Electrochemistry of fuel cells; in Fuel cell systems, BLOMEN,L.J.M.J. and MUGERWA,M.N. (Eds.), Plenum Press, New York, 1993

22. APPLEBY,A.J. and YEAGER,E.B.; Solid polymer electrolyte fuel cells; in *Energy*, PENNER,S.S. (Ed.), vol.12, no.1,2, 1986

23. APPLEBY,A.J.; Acid fuel cells: overview of the state of the art; *Proc. Workshop on Renewable Fuels and Advanced Power Sources for Transportation*, June 1982; US Govt. Rep. no.SERI/CP-234-1707, DE83011988

24. SRINIVASAN,S., DAVÉ,B.B., MURUGESAMOORTHI,K.A., PARTHASARATHY,A. and APPLEBY,A.J.; Over view of fuel cell technology; in Fuel cell systems, BLOMEN,L.J.M.J. and MUGERWA,M.N. (Eds.), Plenum Press, New York, 1993

25. AMPHLETT,J.C., BAUMERT,R.M., MANN,R.F. and PEPPLEY,B.A.; System analysis of an integrated methanol steam reformer/PEM fuel cell power generating system; *Proc. Inter-society Energy Conversion Conf.*, paper no.929212, 1992

26. WATKINS,D.S.; Solid polymer fuel cell systems; in Fuel cell systems, BLOMEN,L.J.M.J. and MUGERWA,M.N. (Eds.), Plenum Press, New York, 1993

27. DeLUCHI,M.A; Hydrogen vehicles: an evaluation of fuel storage, performance, safety, environmental impacts, and cost; *Int.J.Hydrogen Energy*, vol.14, no.2, p81-130, 1989

28. Daimler Benz AG Publication no.ÖWU/C 6705•2804-02•0790, not dated. The same figures attributed to Daimler-Benz are reported by Appleby[34]. His references are: POLZ,H., Presentation at the Hydrogen Vehicle Conf., New York, 1991; and QUADFLIEG,H. et al. (Working group), Alternative Energy Sources for Road Transport, Hydrogen Drive Test, TÜV Rheinland, Köln, 1990.

29. CARPETIS,C.; Comparison of the expenses required for the on-board fuel storage systems of hydrogen powered vehicles; *Int. J. Hydrogen Energy*, vol.7, no.1, 1982, p61-77

30. EDESKUTY,F.J. and STEWART,W.F.; Safety aspects of large scale handling of hydrogen; *Proc. 7th World Hydrogen Energy Conf.*, 1988, p1195-1208

31. PESCHKA,W; Operating characteristics of a LH_2-fuelled automotive vehicle and of a semi-automatic LH_2-refuelling station; *Int. J. Hydrogen Energy*, vol.7, no.8, 1982, p661-669

32. SWAIN,M.R. and SWAIN,M.N.; A comparison of H_2, CH_4, and C_3H_8 fuel leakage in residential settings; *Hydrogen Energy Progress IX*, vol.2, 1992, p1121-1130

33. BLANCHARD,E.R; The second century of cryogenics; *Int J Hydrogen Energy*, vol.2, 1977, p367-371

34. APPLEBY,A.J.; Fuel cells and hydrogen fuel; *Int J Hydrogen Energy*, vol.19, no.2, 1994, p175-180

35. EWALD,R.; Liquid hydrogen fuelled automobiles: on board and stationary cryogenic installations; *Proc. 13th ICEC, Cryogenics*, vol.30, 1990, p38-47

36. RÜDIGER,H.; Design characteristics and performance of a liquid hydrogen tank system for motor cars; *Cryogenics*, vol.32, no.3, 1992, p327-329

37. PEHR,K.; Aspects of safety and acceptance of LH_2 tank systems in passenger cars; *Hydrogen Energy Progress X*, vol.3, 1994, p1399-1413

38. STEWART,W.F.; Operating experience with a liquid hydrogen fuelled Buick and refuelling system; *Hydrogen Energy Progress IV*, vol.3, 1982, p1071-1093

39. ROTENBURG,Y.; Numerical simulation of self pressurization in a small cryogenic tank; *Advances in Cryogenic Engineering*, vol.31, 1986, p963-971

40. BRACHA,M., LORENZ,G., PATZELT,A. and WANNER,M.; Large scale hydrogen liquefaction in Germany; *Int. J. Hydrogen Energy*, vol.19, no.1, 1994, p53-59

41. FURUHAMA,S., NAKAJIMA,T. and HONDA,T.; Rankine cycle engines for utilisation of LH_2 car fuel as a low temperature source; *Int J Hydrogen Energy*, vol.18, no.2, 1993, p149-155

42. FYKE,A., LI,D., CRANE,P. and SCOTT,D.S.; Recovery of thermomechanical exergy from cryofuels; *Hydrogen Energy Progress X*, vol.2, 1994, p1007-1016

43. FURUHAMA,S., HIRUMA,M., KOYANAGI,K., TOMISAWA,N. and YAMAURA,K.; The power system of a computer controlled hydrogen car; *Proc. IMechE, Computers in engine technology*, C430/028, 1991, p179-188

44. TACHTLER,J. and SZYSZKA,A.; Car refuelling with liquid hydrogen (Neunberg Vorm Wald solar hydrogen project: experience and results of first project phase, concept for second phase); *Int. J. Hydrogen Energy*, vol.19, no.4, 1994, p377-385

45. RÜDIGER,H., SEIFERS,H., HOLZER,H. and WOLF,J.; Liquid hydrogen storage system for urban bus; *Hydrogen Energy Progress X*, vol.2, 1994, p967-973

46. VANDENBORRE,H. and SIERENS,R.; Greenbus: A hydrogen fuelled city bus; *Hydrogen Energy Progress X*, vol.3, 1994, p1959-1966

47. GINER,J. and SWETTE,L.; Evaluation of the feasibility of low cost carbon dioxide removal/transfer methods for fuel cell applications, EPRI EM-391; Electric Power Research Institute, Palo Alto (CA), 1975, p87

48. HOWARD,P.F., and GREENHILL,C.J.; Ballard PEM fuel cell powered ZEV bus; Paper 931817 in SAE SP-984, Electric vehicle power systems, 1993

49. KORDESCH,K.; Overview of the utilisation of alternative fuels in fuel cells and internal combustion engines; *Proc Workshop on Renewable Fuels and Advanced Power Sources for Transportation, June 1982*; US Govt. Rep. no. SERI/CP-234-1707, DE83011988

50. Fuel Cells; ELENCO nv., Company Brochure; Gravenstraat 73 bis, B-2480 Dessel, Belgium

51. De GEETER,E.; Private communication, July 1994

52. YANG,R.T.; Gas separation by adsorption processes, Butterworths, Boston, 1987

53. BRUNAUER,S., EMMETT,P.H. and TELLER,E.; Adsorption of gases in multimolecular layers; *J Am Chem Soc*, vol.60, 1938, p309-319

54. BOCKRIS,J.O'M. and APPLEBY,A.J.; Alkaline fuel cells, in PENNER,S.S. (Ed.) *Energy*, vol.12, no.1-2, 1986, p95-135

55. McCRAY,S.B., WYTCHERLEY,R.W., FRIESEN,D.T. and RAY,R.J.; Preliminary evaluation of a membrane based system for removing CO (*sic*) from air; SAE paper 901295, 1990, p159-166

56. LEE,N.C., SUDAR,M. and CUSICK,R.J.; Electrochemically regenerable carbon dioxide/moisture control technology for an Advanced Extravehicular Mobility Unit; SAE paper 871470, 1987

57. Data sheet for Standard Elenco AFC Module, ELENCO nv., Gravenstraat 73 bis, B-2480 Dessel, Belgium

58. BARRON,R.F.; Cryogenic systems, 2nd ed., Oxford University Press, New York, 1985

59. DIN,F. (Ed.); Thermodynamic functions of gases, vol.1&2, Butterworths Publications Ltd., London, 1956

60. ROGERS,G.F.C. and MAYHEW,Y.R.; Thermodynamic and transport properties of fluids, 3rd ed., Basil Blackwell, 1980

61. McCARTY,R.D., HORD,J. and RODER,H.M.; Selected properties of hydrogen (Engineering Design Data), NBS Monograph 168, US Dept of Commerce/National Bureau of Standards, Washington, 1981

62. VAN den BROECK,H.; Personal communication, 14/10/92

63. LOBO,W.E. and SKAPERDAS; Air purification in the reversing exchanger; *Chemical Engineering Progress*, vol.43, no.2, 1947, p69-74

64. TRUMPLER,P.R. and DODGE,B.F.; The design of ribbon-packed exchangers for low temperature air separation plants; *Chemical Engineering Progress*, vol.43, no.2, 1947, p75-84

65. DENTON,W.H. and WARD,D.E.; Applications of plate-fin heat exchangers; *British Chemical Engineering*, vol.5, 1960, p18

66. KERN,D.Q; Process heat transfer; McGraw Hill, 1990

67. WEBB,R.L.; Principles of enhanced heat transfer; John Wiley & Sons, New York, 1994

68. DENTON,W.H., SHAW,B. and WARD,D.E.; Purification of hydrogen for distillation; *Trans Instn Chem Engrs*, vol.36, 1958, p179-200

69. CRAWFORD,D.B.; Elliot oxygen process and impurity removal system; *Chem Eng Prog*, vol.46, no.2, 1950, p74-78

70. McMAHON,H.O., BOWEN,R.J. & BEYLE Jr.,G.A.; A perforated plate heat exchanger; *Trans ASME*, vol.72, 1950, p623-632

71. KAYS,W.M. and LONDON,A.L.; Compact heat exchangers, 3rd ed.; McGraw Hill, New York, 1984

72. VENKATARATHNAM,G. and SARANGI,S.; Matrix heat exchangers and their applications in cryogenic systems; *Cryogenics*, vol.30, no.11, 1990, p907-918

73. KROEGER,P.G.; Performance deterioration in high effectiveness heat exchangers due to axial conduction effects; *Advances in Cryogenic Engineering*, vol.12, 1967, p363-372

74. BAHNKE,G.D. and HOWARD,C.P.; The effect of longitudinal heat conduction on periodic-flow heat exchanger performance; *J. Engineering for Power, Trans ASME*, vol.86-A, 1964, p105-119

75. FLEMING,R.B.; The effect of flow distribution in parallel channels of counterflow heat exchangers; *Advances in Cryogenic Engineering*, vol.12, 1967, p352-362

76. BARRON,R.F.; Effect of heat transfer from ambient on cryogenic heat exchanger performance; *Advances in Cryogenic Engineering*, vol.29, 1984, p265-272

77. CHOWDHURY,K. and SARANGI,S.; Performance of cryogenic heat exchangers with heat leak from the surroundings; *Advances in Cryogenic Engineering*, vol.29, 1984,

p273-280

78. FLEMING,R.B.; A compact perforated plate heat exchanger; *Advances in Cryogenic Engineering*, vol.14, 1969, p197-204

79. SARANGI,S. and BARCLAY,J.A.; Analysis of compact heat exchanger performance; Cryogenic processes and equipment, KERNEY,P.J. et al (eds.); ASME, New York, 1984, p37-44

80. VENKATARATHNAM,G.; Matrix heat exchangers, Ph.D thesis, 1991; Indian Institute of Technology, Kharagpur

81. COPPAGE,J.E. and LONDON,A.L.; The periodic flow regenerator - a summary of design theory; *Trans ASME*, vol.75, 1953, p779-787

82. LAMBERTSON,T.J.; Performance factors of a periodic flow heat exchangers; *Trans ASME*, vol.80, 1958, p586-592

83. MIKULIN,E.I., SHEVICH,Yu.A., POTAPOV,V.N., SOLNTSEV,M,Ya. and YUSOVA,G.M.; Study of matrix-type heat exchangers made of perforated plates; (translation): *Chemical and Petroleum Engineering*, vol.16, pt.9-10, 1980, p514-519

84. VENKATARATHNAM,G. and SARANGI,S.; Heat transfer and flow friction correlations in perforated plate matrix heat exchangers; *Proc. 13th ICEC, Cryogenics*, vol.30, September Supplement, 1990, p313-317

85. ORLOV,V.K., SHEVYAKOVA,S.A. and VALEEV,G.W.; Heat exchange and hydraulic resistance in perforated-plate heat exchangers; (translation): *Chemical and Petroleum Engineering*, vol.14, pt.7-8 1978, p701-704

86. SHEVYAKOVA,S.A. and ORLOV,V.K.; Study of hydraulic resistance and heat transfer in perforated plate heat exchangers; (translation): *J Engineering Physics*, 1983, p734-737

87. HUBBELL,R. and CAIN,C.L.; New heat transfer and friction factor design data for perforated heat exchangers; *Advances in Cryogenic Engineering*, vol.31, 1986, p383-390

88. COPPAGE,J.E. and LONDON,A.L.; Heat transfer and flow friction characteristics of porous media; *Chemical Engineering Progress*, vol.52, no.2, 1956, p57-F - 63-F

89. TONG,L.S. and LONDON,A.L.; Heat transfer and flow friction characteristics of woven-screen and crossed-rod matrices; *Trans ASME*, vol.79, 1957, p1558-1570

90. MIKULIN,E.I. and SHEVICH,Yu.A.; Experimental study of heat transfer in meshed matrices; (translation): *J Engineering Physics*, 1972, p777-778

91. RAYLEIGH,Lord J.S.; On the influence of obstacles arranged in rectangular order upon the properties of a medium, art.200, 1892; *Scientific Papers*, vol.IV; Cambridge University Press, 1920

92. KELLER,H.B. and SACHS,D.; Calculations of the conductivity of a medium containing cylindrical inclusions; *J Applied Physics*, vol.35, 1964, p537

93. QVALE,E.B. and SMITH,J.L.; A simple correlation for the heat transfer characteristics of a family of matrices subjected to complex flow conditions; *Cryogenics*, vol.9, 1969, p62-63

94. VONK,G.;A compact heat exchanger of high thermal efficiency; *Philips Technical Review*, vol.29, 1968, p158-162

95. VORONIN,V.I., TREKOV,V.N. and VORONIN,A.V.; Using vacuum diffusion bonding to produce laminated perforated materials; *Welding Production*, no.10, 1984, p31-33

96. GIFFORD,W.E., ACHARYA,A. and ACKERMANN,R.A.; Compact cryogenic thermal regenerator performance; *Adv Cryo Eng*, vol.14, 1969, p353-360

97. BRUNNER,W.F. and BATZER,T.H.; Practical vacuum techniques; Reinhold Publishing Corporation, New York, 1965

98. HONIG,R.E.; Gas flow in the mass spectrometer; *Journal of Applied Physics*, vol.16, Nov. 1945, p646-654

99. NIER,A.O, ABBOTT,T.A., PICKARD,J.K., LELAND,W.T., TAYLOR,T.I., STEVENS,C.M., DUKEY,D.L. and GOERTZEL,G.; Recording mass spectrometer for process analysis; *Analytical Chemistry*, vol.20, no.3, 1948, p188-192

100. HALSTEAD,R.E. and NIER,A.O.; Gas flow through the mass spectrometer viscous leak; *The Review of Scientific Instruments*, vol.21, no.12, 1950, p1019-1021

101. VENKATARATHNAM,G.; Private correspondence, May 4th,5th,23rd, 1995

102. IUPAC, CHEMICAL DATA SERIES; from International Thermodynamic Tables of the Fluid State - 6, Nitrogen; Pergamon Press, Oxford, 1979

103. BARFORD,N.C.; Experimental measurements: precision, error and truth, 2nd ed.; John Wiley & Sons, Chichester, 1987

104. KISER,R.W.; Introduction to mass spectrometry and its applications, Prentice-Hall Inc., New Jersey, 1965

105. Typical RGA fingerprints; Residual gas analysers, Spectramass brochure; Spectramass Ltd., Radnor Park Industrial Estate, Back Lane, Congleton, Cheshire CW12 4XR, UK

106. VG Quadrupoles Publication no. AJW.PT639

107. REED,R.I.; Modern aspects of mass spectrometry, Plenum Press, New York, 1968, p35

108. GURSU,S., SHERIF,S.A., VEZIROGLU,T.N. and SHEFFIELD,J.W.; Analysis and optimization of thermal stratification and self-pressurization effects in liquid hydrogen storage systems - Part 1: Model development; *J. Energy Resources Technology*, vol.115,

Sept., 1993, p221-227

109. GURSU,S., SHERIF,S.A., VEZIROGLU,T.N. and SHEFFIELD,J.W.; Analysis and optimization of thermal stratification and self-pressurization effects in liquid hydrogen storage systems - Part 2: Model results and conclusions; *J. Energy Resources Technology*, vol.115, Sept., 1993, p228-231

110. AYDELOTT,J.C. and SPUCKLER,C.M.; Effect of size on normal gravity self-pressurization of spherical hydrogen tankage; *NASA Technical Note TN D-5196*, National Space and Aeronautics Administration, Washington, DC, 1969

111. ARNETT,R.W. and VOTH,R.O.; A computer program for the calculation of thermal stratification and self-pressurization in a liquid hydrogen tank; *NASA Contractor Report No. 2026*, National Aeronautics and Space Administration, Washington, DC., 1972

112. TATOM,J.W., BROWN,W.H., KNIGHT,L.H. and COXE,E.F.; Analysis of thermal stratification of liquid hydrogen in rocket propellant tanks; *Advances in Cryogenic Engineering*, vol.9, 1963, p265-272

113. ROTENBURG,Y.; Vibration enhanced boil-off rate from a cryogenic hydrogen tank; *Proc. 6th World Hydrogen Energy Conf.*, vol.1, 1986, p164-172

114. ROTENBURG,Y.; Numerical simulation of self pressurization in a small cryogenic tank; *Advances in Cryogenic Engineering*, vol.31, 1986, p963-971

115. STEWART,W.F.; Operating experience with a liquid hydrogen fuelled Buick and refuelling system; *Hydrogen Energy Progress IV*, vol.3, 1982, p1071-1093

Appendix A

This program was written for exhaustive search optimisation of MHE geometry within a user specified range of various geometric variables, for user specified increments. The program can also be used for calculating the performance of a single set of input variables. MHE performance is calculated in terms of total volume, number of plates required and the pressure drop. The program HXPerf.pas referred to in the comments was the original version used for calculating the performance for one input data set. This program requires a data file containing air properties at various temperatures, listed for the temperature range of interest. The properties in the data file are listed in rows; the temperature, followed by the property values at that temperature. The order of the listing in each row is: temperature, density, specific heat, viscosity, conductivity and Prandtl no.. The constant adataE in the program is defined as the number of data sets or rows. Any values required that fall between the data sets are calculated by linear interpolation. The program is in Turbo Pascal.

```
program HXPopt2;                          {Vikas Ahuja, January 1993}
                                          {This program is a modification of HXPerf.pas}
                                          {to optimise the MHE design by trying all the}
                                          {possible combinations of surface and overall}
                                          {geometry, within limits specified by the user,}
                                          {and record the best combinations which give}
                                          {minimum 'goodness factor', a weighted }
                                          {average of HX volume, number of plates and}
                                          {pressure drop.}

uses crt;                                 {Allows use of clrscr}

const
   adataE = 10;                           {Number of data elements in air property data}
   kCu = 386;                             {Thermal conductivity of screen material, W/m-K}
   ksp = 0.5;                             {Thermal conductivity of spacer material, W/m-K}
   epsilon = 1E-6;                        {Floating point error elimination}
   lowest = 10;                           {Number of lowest values to be recorded}

type
   airdata = array [1..adataE] of real;   {Array for handling air property data}

var
   dfile1          : text;                {File set up to take air properties data from}
                                          {\HUMIDAIR.TXT}
   rfile           : text;                {Result file}
   T               : airdata;             {Temperature, K}
   rho             : airdata;             {Density, kg/cu-m}
   Cp              : airdata;             {Specific heat, kJ/kg-K}
   mu              : airdata;             {Viscosity, Pa s X10-6}
   k               : airdata;             {Thermal conductivity, mW/m-K}
   Pr              : airdata;             {Prandtl number}
   outlist: array [1..lowest] of array [1..10] of real;
                                          {Output array of variables giving the lowest}
                                          {goodness factor, including results}
   Tbulk1          : real;                {Average of warm inlet and cold outlet temp., K}
```

```
    deltaT          : real;                 {Temperature increment to be used for analysis}
    Ntueff          : real;                 {Ntu, effective, for each increment}
    mh2             : real;                 {Mass flow rate of hydrogen, g/s}
    mair            : real;                 {Mass flow rate of air, kg/s}
    Hf              : real;                 {Fin height, m}
    Afr             : real;                 {Frontal area, sq-m}
    Acr             : real;                 {Spacer area for axial conduction, sq-m}
    spitch          : real;                 {Spacer pitch, for axial conduction coefficient}
    l               : real;                 {Plate thickness, m}
    ss              : real;                 {Perforation side for square perforation, m}
    p               : real;                 {Porosity}
    beta            : real;                 {Surface area per unit volume, sq-m/cu-m}
    xt              : real;                 {Transverse pitch}
    W               : real;                 {Channel width}
    lowl,highl,stepl,lowss,highss,stepss,lowsp,highsp,stepsp,lowW,
    highW,stepW,lowHf,highHf,stepHf,lowAfr,highAfr:real;
                                            {Iteration end and increment markers}
    number          : integer;              {User selected number of increments for analysis}
    again           : char;                 {Y/N for running another data set}
    uname           : string[6];            {User specified output file name}

procedure welcome;                          {Writes welcome address}

begin
  writeln('This program is a modification of HXPERF.PAS to optimise');
  writeln('MHE design by trying all the combinations of surface and');
  writeln('overall geometry specified by the user.');
  writeln('Only rectangular geometry is considered, and specified by');
  writeln('channel width and height.');
  writeln('Iteration end markers and increments are asked as LOW');
  writeln('HIGH STEP values, to be entered separated by a space.');
  writeln('The results are written to a user specified file.');
  writeln;
  writeln
end;

procedure datain1;                          {Reads in air property data from file to arrays}

var
   s:integer;

begin
   assign(dfile1,'\HUMIDAIR.TXT');
   reset(dfile1);
   for s:= 1 to adataE do
       readln(dfile1,T[s],rho[s],Cp[s],mu[s],k[s],Pr[s]);
   close(dfile1)
end;

procedure zero;                             {Assigns zero values to OUTLIST array}

var
   s,m:integer;

begin
   for s:= 1 to lowest do
       for m:= 1 to 10 do
           outlist[s,m]:=100
end;

procedure prelim;                           {Asks input values, does preliminary calculations}

var
   eff   : real;                            {Effectiveness, %}
   ThIn  : real;                            {Warm end inlet temp. (ambient), K}
   TcIn  : real;                            {Cold end inlet temp., K}
   TcO   : real;                            {Cold end outlet temp., K}
```

```
begin
   writeln('Please enter the data requested');
   writeln;
   write('Desired effectiveness, % = ');
   readln(eff);
   write('Ambient temperature, K = ');
   readln(ThIn);
   write('Cold end temperature, K = ');
   readln(TcIn);
   write('Number of temperature increments for calculation of air ');
   write('properties = ');
   readln(number);
   write('Mass flow rate of hydrogen, g/s = ');
   readln(mh2);
   mair:= mh2/1000*85.74;
   write('Plate thickness, mm, low high step ');
   readln(lowl,highl,stepl);
   write('Perforation side (square), mm, low high step ');
   readln(lowss,highss,stepss);
   write('Spacer pitch, low high step ');
   readln(lowsp,highsp,stepsp);
   write('Channel width, mm, low high step ');
   readln(lowW,highW,stepW);
   write('Channel hieght, mm, low high step ');
   readln(lowHf,highHf,stepHf);
   write('Frontal area limits, sq-mm, low high ');
   readln(lowAfr,highAfr);
   write('Enter a six letter name for the output file ');
   readln(uname);
   TcO:= eff/100*(ThIn-TcIn)+TcIn;
   Tbulk1:= (ThIn+TcO)/2;
   deltaT:= (TcO-TcIn)/number;
   Ntueff:= deltaT/(ThIn-TcO)
end;

procedure area(var Go,Re,rhoval,TotalA,n:real;  Tbulk,kax:real);

                                                {Interpolates air properties for temperature}
                                                {increments, calculates Go,Re,h,U,kax and hence}
                                                {the area required, for the necessary heat}
                                                {transfer and length increment for calculating}
                                                {the pressure drop}
var
   zeta          : real;                        {Multiplication factor for interpolation}
   Cpval         : real;                        {Specific heat, J/kg-K}
   kval          : real;                        {Thermal conductivity, W/m-K}
   Prval         : real;                        {Prandtl no.}
   muval         : real;                        {Viscosity, Pa-s}
   first, second, third, fourth, fifth : real;  {Intermediates for Nu}
   Nu            : real;                        {Nusselts no.}
   h             : real;                        {Convection heat transfer co-efficient, W/sq-m-K}
   U             : real;                        {Overall thermal conductance, W/sq-m-K}
   Ntufl         : real;                        {Intermediate factor for deltaA}
   plates        : real;                        {Intermediate factor for deltaA}
   ax            : real;                        {Intermediate factor for deltaA}
   po            : real;                        {Intermediate factor for deltaA}
   deltaA        : real;                        {Area increment for temperature increment, sq-m}
   delL          : real;                        {Same as totL in ITERATE}
   x             : integer;                     {Index for array manipulation}

begin
   x:=1;
   while NOT((Tbulk>=T[x]) AND (T[x+1]>Tbulk)) do
     x:=x+1;
   zeta:=(Tbulk-T[x])/(T[x+1]-T[x]);
   rhoval:=rho[x]+zeta*(rho[x+1]-rho[x]);
```

```
    Cpval:=(Cp[x]+zeta*(Cp[x+1]-Cp[x]))*1000;
    muval:=(mu[x]+zeta*(mu[x+1]-mu[x]))/1000000;
    kval:=(k[x]+zeta*(k[x+1]-k[x]))/1000;
    Go:= mair/(p*Afr);
    Re:= ss*Go/muval;
    first:= 7.32*l/ss;                          {ss, hydraulic diameter for the holes}
    second:= 0.146*Re/(1+0.012*exp(0.8*ln(Re*ss/l)));
    third:= 0.475*exp(0.476*ln(Re))/SQRT(p);
    fourth:= 0.0237*exp(0.72*ln(Re))*(1+SQRT(p))/SQRT(p);
    fifth:= (1-p)/p+2*l/ss;
    Nu:= (first+second+third+fourth)/fifth;
    h:= Nu*kval/ss;
    U:= h/2;
    Ntufl:= -2*U*beta*Afr*l/(mair*Cpval);
    plates:= (1+exp(Ntufl))/(1-exp(Ntufl));
    ax:= kax*Acr/(l*mair*Cpval);
    po:= 2*Go*p*Cpval*Hf*Hf/(3*kCu*l);
    deltaA:= Ntueff*beta*Afr*l*(plates+ax+po);
    TotalA:= TotalA+deltaA;
    delL:= deltaA/(beta*Afr);
    n:= delL/l
end;

procedure friction(var TotalP:real; Go,Re,rhoval,n:real);

                                            {Calculates pressure drop for the length}
                                            {increment calculated in AREA, by the method}
                                            {of Shevyakova and Orlov.}
var
    Cd2             : real;                 {Drag coefficient based on Sh&Or}
    TotP2           : real;                 {Incremental pressure drop, Pa}

begin
    Cd2:= SQR(1.707-p)/2;
    if Re <= 160 then
        Cd2:= 16.34*exp(-0.55*ln(Re))*Cd2;
    TotP2:= n*SQR(Go)/rhoval*Cd2;
    TotalP:= TotalP+TotP2
end;

procedure iterate;                          {Executes area and friction procedures,}
                                            {iterating for user defined temperature}
                                            {increments. Calculates incremental values and}
                                            {total area, no. of plates and total pressure}
                                            {drop. Writes the results to a user defined file.}
var
    dif             : array [1..lowest] of real;
                                            {Array for comparing results and placing in order}
    TotalA          : real;                 {Total surface area required, sq-m}
    TotalP          : real;                 {Total pressure drop, Pa}
    totL            : real;                 {Total length of HX assuming perfect stacking, m}
    TotalL          : real;                 {Total length, m}
    Volume          : real;                 {Total volume, cu-m}
    Goodf           : real;                 {Goodness factor}
    Tbulk           : real;                 {Bulk fluid temperature, K}
    Go              : real;                 {Flow stream mass velocity, average, kg/s-sq-m}
    Re              : real;                 {Reynolds no.}
    rhoval          : real;                 {Density, kg/cu-m}
    n               : real;                 {Number of plates required}
    s               : real;                 {Spacer thickness, mm}
    kax             : real;                 {Thermal conductivity, axial direction, W/m-K}
    i               : integer;              {Variable for number of iterations}
    z,m             : integer;              {Variables to put an initial 1.5*l value to ss}
    r,index,t,c,d   : integer;              {Variables for array manipulation, to record}
    minimum         : real;                 {only the lowest LOWEST values}

begin
```

```
l:=lowl*1E-3;
repeat
 ss:=1.5*l;
 If lowss*1E-3>ss then
   begin
    m:=0;
    ss:=lowss*1E-3
   end
 else
   m:=TRUNC((ss-lowss*1E-3)/(stepss*1E-3));
 z:=1;
 repeat
  xt:=1+(l+0.2E-3)/ss;                    {minimum gap is thickness+0.2mm}
  p:= 1/SQR(xt);
  beta:= 2/l-2/SQR(xt)*(1/l-2/ss);
  spitch:=lowsp;
  repeat
   s:= (spitch-1)*l;
   kax:= (s+l)/(l/kCu+s/ksp);
   W:=lowW*1E-3;
   repeat
    Hf:=lowHf*1E-3;
    repeat
      Afr:= W*Hf;
      If (Afr>=lowAfr*1E-6)  and (Afr<=highAfr*1E-6)  then
      begin
       Acr:= (W+6E-3)*4.5E-3+Hf*6E-3;      {3mm edges and separator}
       TotalA:= 0;
       TotalP:= 0;
       for i:= 1 to number do
         begin
            Tbulk:= Tbulk1+deltaT/2-deltaT*i;
            area(Go,Re,rhoval,TotalA,n,Tbulk,kax);
            friction(TotalP,Go,Re,rhoval,n);
         end;
       totL:= TotalA/(beta*Afr);
       TotalL:= totL*spitch;
       n:= TRUNC(totL/l)+1;
       Volume:=(Afr+Acr)*TotalL;
       Goodf:=Volume*1E3+n/1E3+TotalP/1E4;
       If Goodf<outlist[lowest,10]  then
       begin
          for r:= 1 to lowest do
             dif[r]:= Goodf-outlist[r,10];
          minimum:= dif[1];
          index:= 1;
          for t:= lowest downto 2 do
             If dif[t]>=0 then
                If dif[t]<minimum  then
                   begin
                      minimum:= dif[t];
                      index:= t
                   end;
          If dif[1]<=0 then
             index:=0;
          for c:= lowest downto (index+2) do
             for d:= 1 to 10 do
                outlist[c,d]:=outlist[c-1,d];
          outlist[index+1,1]:=l;
          outlist[index+1,2]:=ss;
          outlist[index+1,3]:=xt;
          outlist[index+1,4]:=spitch;
          outlist[index+1,5]:=W;
          outlist[index+1,6]:=Hf;
          outlist[index+1,7]:=Volume;
          outlist[index+1,8]:=n;
          outlist[index+1,9]:=TotalP;
```

```
                outlist[index+1,10]:=Goodf
            end;
           end;
           Hf:=Hf+stepHf*1E-3
         until Hf>highHf*1E-3;
         W:=W+stepW*1E-3
        until W>highW*1E-3;
        spitch:=spitch+stepsp
       until spitch>highsp;
       ss:=(m+z)*stepss*1E-3+lowss*1E-3;
       z:=z+1;
      until ss>highss*1E-3+epsilon;
      l:=l+stepl*1E-3
    until l>highl*1E-3+epsilon;
    writeln;
    write('Would you like to run another data set ? Y/N  ');
    readln(again);
    writeln
end;

procedure out;                                  {Writes LOWEST arrays to output file}

var
   s,m:integer;

begin
    assign(rfile,'\'+uname+'.TXT');
    rewrite(rfile);
    for s:= 1 to lowest do
        begin
            write(rfile,outlist[s,1]*1E3:3:1,'  ');
            write(rfile,outlist[s,2]*1E3:3:1,'  ');
            write(rfile,outlist[s,3]:5:3,'  ');
            write(rfile,outlist[s,4]:3:1,'  ');
            write(rfile,outlist[s,5]*1E3:3:0,'  ');
            write(rfile,outlist[s,6]*1E3:3:0,'  ');
            write(rfile,outlist[s,7]*1E3:5:3,'  ');
            write(rfile,outlist[s,8]:4:0,'  ');
            write(rfile,outlist[s,9]:5:0,'  ');
            writeln(rfile,outlist[s,10]:5:3)
        end;
    close(rfile)
end;

begin                   {------MAIN PROGRAM-------}
    clrscr;
    welcome;
    datain1;
    again:='y';
    while again='y' do
    begin
        zero;
        prelim;
        writeln;
        writeln('**************  PROGRAM RUNNING ****************');
        iterate;
        out
    end
end.
```

Appendix B

The data acquisition was done using a Universal Pulse Processor I/O board (UPP) interfaced with a PCLD-889 multiplexer and programmable gain amplifier (mux). The UPP board reads inputs between 0 - +5V, whereas the mux board output range is between -10 - +10V. A purpose built amplifier and comparator were used to ensure that all inputs to the UPP board were within it's range, and a marker was set to indicate whether the original input was +ve or -ve. This program was written for monitoring and control of the experimental apparatus used. It records various temperatures, pressures and flowmeter outputs. It uses the UPP board programmable digital outputs to control the mux board and the solenoid actuated spool valve used for cross-over valve actuation. It uses the UPPL.lib library that accompanies the UPP board, and the TC025.lib from Quinn-Curtis; Real time graphics and measurement/control tools for Borland/Turbo C; IPC-TC-025; release 3.0. The program is in Turbo C.

```
/*************************************************************************/
/* File:   RUNRIG5.C       Cross over valve timing setting added                 */
/* Authors:                Ahuja,V                                               */
/* Date:  22-2-1996        MPX5050DP pressure transducer reading added           */
/*                         MUX & AMP calibrated 24-8-95                          */
/*                         Includes keyboard controlled cross over valve         */
/* Version:        5.0     operation                                             */
/*************************************************************************/

#define DELAY           10
#include <stdio.h>      /* Include the standard header files                     */
#include <stdlib.h>
#include <dos.h>        /* delay() etc.                                          */
#include <math.h>       /* pow(),fabs()                                          */
#include <upp.h>
#include <conio.h>      /* clrscr(),window(),textcolor(),etc                     */
#include <time.h>       /* clock()                                               */
#include <rttcref.h>    /* tclinearize(), ensure TCV2T0.TXT and RTSTDHDR.H are present. These */
                        /* are from Quin-Curtis; Real-time graphics and measurement/control tools for */
                        /* Borland/Turbo C, IPC-TC-025 release 3.0.              */

float GetAD(int line)                                   /* Return a/d value to program */
{
        int                     count;
        long int  data=0;

        for(count=0;count<10;count++)                   /* Sample data x times */
        {
                UPPStartAD(Card.a2,STARTAD|line);       /* Start a/d conversion */
                delay(DELAY);
                while(UPPIntStatAD(Card.a2));           /* Wait until conversion finished*/
                delay(DELAY);
                data+=UPPReadAD(Card.a2,line);
                delay(DELAY);
        }
        return((float)data/10);                         /* Take average for x samples */
}/* GetAD() */

void screen()
{
        textbackground(7);
        window(1,24,80,25);
        clrscr();
```

```
        gotoxy(3,1);
        textcolor(4);
        cprintf("Q");
        textcolor(0);
        cprintf("-Quit");
        gotoxy(11,1);
        textcolor(4);
        cprintf("F");
        textcolor(0);
        cprintf("-start writing to File");
        gotoxy(36,1);
        textcolor(4);
        cprintf("H/L");
        textcolor(0);
        cprintf("-flowmeter selection High/Low");
        gotoxy(70,1);
        textcolor(4);
        cprintf("P");
        textcolor(0);
        cprintf("-Pause");
        gotoxy(3,2);
        textcolor(4);
        cprintf("C");
        textcolor(0);
        cprintf("-rotate Cross over valve");
        gotoxy(31,2);
        textcolor(4);
        cprintf("T");
        textcolor(0);
        cprintf("-set CR valve auto Timing");
        gotoxy(60,2);
        textcolor(4);
        cprintf("O");
        textcolor(0);
        cprintf("-CR valve auto Off");

        textbackground(1);
        textcolor(15);
        window(1,2,20,23);
        clrscr();
        gotoxy(1,3);
        cprintf("Ambient temp\n\rCO2MHE in\n\rCO2MHE out\n\rBYPASS out\n\r\
LN2-HX in\n\rLN2-HX out\n\rCIavg\n\rActuator\n\r\
Radiation shield #1\n\rRadiation lid #2\n\rBYPASS in\n\rPORT1 in\n\r\
PORT3 in\n\rZero\n\rPORT1 out\n\rFlowmeter\n\rPORT3 out");

        window(61,2,80,23);
        clrscr();
        window(36,2,60,23);
        clrscr();
        gotoxy(1,3);
        cprintf("Volume flow, l/min\n\rEff CO2MHE, cold hot\n\r\
Eff H2OMHE, cold hot\n\rEff overall, LN2 based\n\rPress diff, kPa\n\r\
Time/split time, s");
        window(21,2,35,23);
        clrscr();
}

short int polarity(float polarityd)
{
 if(polarityd>512)
        return(-1);
 else
        return(1);
}
```

```
void main()
{
        char tmprofile[12],Y,reply,flowr='h';
        int theres_a_file=0,write_to_file=0,tc=KTC,err,count1,no,massflowknown,
        crossovervalve=0,Xvalvetimeset=0;
        float tempd,zero,CJCd,CJCv,GAIN=477.5,polarityd,timeelapsed=0,volflowd,
        volflowv,volflow,volflowtemp,CO2MHEin,CO2MHEout,BYPASSout,BYPASSin,
        PORT1in,PORT1out,PORT3in,PORT3out,CIavg,Cp=1.042e3,hfg,rho,
        effectivenessh,effectivenessc,effLN2,massflowhx,ambpressure,
        within10,presscorrect,laptime=0,oldtimeelapsed=0,UPPadjust=1.0036,
        volflowhx,Thin,Thout,Tcin,Tcout,channelthree,pressuredifkPa,
        Xvalvetime=0,Xvalvelaptime=0;

        realtype tempv,CJCtemp,temp;
        clock_t start,lap;
        FILE *fp;
        Card.a2=0x232;
        UPPContactEnable(0x232,0);
        UPPPortDir(0x232,1,0xff);
        UPPPortDir(0x232,2,0xff);
        UPPDataDir(0x232,0xffff);

        clrscr();
        cprintf("Do you require an output file? y/n ");
        Y=getche();
        if(Y=='y')
                {
                cprintf("\n\rEnter  filename : Name.dat ");
                gets(tmprofile);
                fp=fopen(tmprofile,"wt");                       /* Opens output file                */
                }
        cprintf("\n\rEnter  volume flow rate in hx (lpm), or 'u' if unknown: ");
        massflowknown=cscanf("%f",&volflowhx);
        if(!massflowknown) getch();
        cprintf("\n\rPlease  enter ambient pressure (mbar): ");
        cscanf("%f",&ambpressure);
        getch();
        clrscr();

        within10=(ambpressure-1013.25)/1013.25;
        if(fabs(within10)<0.1)  presscorrect=1-within10*0.07/100;
        /* Second order polyfit for hfg of N2, versus pressure                                   */
        hfg=(1.03684167e4*pow(ambpressure/1e4,2)-0.52494021e4*ambpressure/1e4\
        +0.59897709e4)/28.013*1e3;

        textbackground(7);
        window(1,1,80,1);
        clrscr();
        textcolor(0);
        if(!massflowknown) cprintf("  Volume flow rate: unknown   Ambient\
 pressure: %4.0f",ambpressure);
        else cprintf("Volume  flow rate: %3.0f   Ambient pressure: %4.0f",\
volflowhx,ambpressure);
        if(Y=='y') cprintf("  Data file: %12s",tmprofile);

        UPPWritePort(0x232,2,crossovervalve);                   /* Check X-valve is in position 0*/
        screen();
        start=clock();
do                                                              /* Loop until q hit on keyboard     */
{
        do                                                      /* Loop until f,p,h,l,c  or q hit   */
        {
                if(theres_a_file && laptime>=60) write_to_file=1;
                window(21,2,35,23);
                gotoxy(1,3);

                CJCd            =GetAD(8);
```

```
CJCv            =CJCd*UPPadjust*5/1024;
CJCtemp         =CJCv*1000/24.4;
cprintf("CJC   %4.1f\n\r",CJCtemp);

/* Selects mux channel and gain and gets inputs from ADC.                    */
/* Refer to PCLD-889 manual                                                  */
/* Gain settings 50=64,100=80,200=96,1000=112.                               */
/* Channel settings 0=0,1=1..                                                */
/* Therefore ..1,80 means Port1 gain 100 channel 0, ..1,81 means             */
/* gain 100 channel 1 etc.                                                   */
/* Inverter/amp/comparator has gain=0.5 therefore GAIN variable is set as ½*/

for(count1=112;count1<128;count1++)
{
        UPPWritePort(0x232,1,count1);
        delay(DELAY);
        tempd           =GetAD(9);
        polarityd =GetAD(0);
        /* Convert digital input to voltage and set polarity                 */
        zero    =polarity(polarityd)*tempd*UPPadjust*5/1024;
        /* Convert read voltage to TC input microV                           */
        tempv   =(zero*1e6/GAIN);
        temp    =tclinearize(tempv,tc,CJCtemp,&err);
        no      =count1-112+1;
        switch(no)
        {
         case 1: CO2MHEin=temp; break;
         case 2: CO2MHEout=temp; break;
        /* case 3: BYPASSout=temp; break;*/
         case 6: CIavg=temp; break;
         case 10: BYPASSin=temp; break;
         case 11: PORT1in=temp; break;
         case 12: PORT3in=temp; break;
         case 14: PORT1out=temp; break;
         case 15: volflowtemp=temp; break;
         case 16: PORT3out=temp; break;
        }
        cprintf("TC %2i %6.1f\n\r",no,temp);
        if(write_to_file) fprintf(fp,"%6.1f ",temp);
} /* end for */

window(61,2,80,23);
gotoxy(1,3);

if(flowr=='l')
{
        /* Volume flow rate reading using mass airflow sensor AWM5101VN     */
        volflowd=GetAD(2);
        volflowv=volflowd*UPPadjust*5/1024;
        volflow=(volflowv-1)*5/4;
        if(volflow>5)
        {
         cprintf("Above scale\n\r");
         if(write_to_file) fprintf(fp,"0 ");
        }
        else
        {
         clreol();
         cprintf("%6.3f\n\r",volflow);
         if(write_to_file) fprintf(fp,"%6.3f ",volflow);
        }
}

if(flowr=='h')
{
        /* Volume flow rate reading, including temperature and pressure      */
        /* correction (1115 - 912 mbar), for N2, using Flo-sensor            */
```

```
                volflowd=GetAD(1);
                volflowv=volflowd*UPPadjust*5/1024;
                volflowv=volflowv-((volflowtemp-25)*0.2/100*volflowv);
                volflowv=presscorrect*volflowv;
                volflow =1.01*(volflowv/5*20);
                if(volflow<4)
                {
                 cprintf("Below  scale\n\r");
                 if(write_to_file)  fprintf(fp,"0  ");
                }
                else
                {
                 clreol();
                 cprintf("%6.3f\n\r",volflow);
                 if(write_to_file)  fprintf(fp,"%6.3f  ",volflow);
                }
}

                /* Effectiveness calculation                                    */
                /* effectivenessc=(Tcout-Tcin)/(Thin-Tcin);                     */
                /* effectivenessh=(Thin-Thout)/(Thin-Tcin);                     */
                if(!crossovervalve)
                {
                        Thin=PORT3in;
                        Thout=PORT3out;
                        Tcin=PORT1out;
                        Tcout=PORT1in;
                }
                else
                {
                        Thin=PORT1in;
                        Thout=PORT1out;
                        Tcin=PORT3out;
                        Tcout=PORT3in;
                }

                if(CO2MHEin-CIavg!=0)
                {
                        /* For the CO2 HX                                       */
                        effectivenessc=(CO2MHEout-CIavg)/(CO2MHEin-CIavg);
                        effectivenessh=(CO2MHEin-BYPASSin)/(CO2MHEin-CIavg);
                        cprintf("%4.2f   %4.2f\n\r",effectivenessc,effectivenessh);
                        if(write_to_file)
                         fprintf(fp,"%4.2f  %4.2f ",effectivenessc,effectivenessh);
                }
                else
                {
                        cprintf("0   0\n\r");
                        if(write_to_file)  fprintf(fp,"0  0 ");
                }

                if(Thin-Tcin!=0)
                {
                        /* For the water HX, Thin etc. have been set depending on the   */
                        /* cross-over valve position.                                   */
                        effectivenessc=(Tcout-Tcin)/(Thin-Tcin);
                        effectivenessh=(Thin-Thout)/(Thin-Tcin);
                        cprintf("%4.2f   %4.2f\n\r",effectivenessc,effectivenessh);
                        if(write_to_file)
                         fprintf(fp,"%4.2f  %4.2f ",effectivenessc,effectivenessh);
                }
                else
                {
                        cprintf("0   0\n\r");
                        if(write_to_file)  fprintf(fp,"0  0 ");
                }
```

```
                    if(!massflowknown)
                    {
                     cprintf("Unknown\n\r");
                     if(write_to_file)  fprintf(fp,"0  ");
                    }
                    else
                    {
                     if(Thin-CIavg!=0)
                     {
                            /* N2 in hx mass flow calculation including rotameter correction for outlet */
                            /* temperature and ambient pressure.                                        */
                            /* See test no. 7__ data sheet                                              */
                            massflowhx=volflowhx/1000/60/296.8/18.285*\
                            pow(ambpressure*100/(273.15+Tcout),1.5);

                            rho=ambpressure*100/296.8/(volflowtemp+273);
                            effLN2=1-(volflow*1e-3/60*rho*hfg/(massflowhx*Cp*\
                            (Thin-CIavg)));

                            /* Note: effLN2 will be calculated regardless of the flowmeters being  */
                            /* switched for the appropriate flow rate.                             */
                            cprintf("%4.2f\n\r",effLN2);
                            if(write_to_file)  fprintf(fp,"%4.2f  ",effLN2);
                     }
                     else
                     {
                            cprintf("0\n\r");
                            if(write_to_file)  fprintf(fp,"0  ");
                     }
                    }

            /* Pressure differential measurement using MPX5050DP transducer                        */
            channelthree=GetAD(3);
            channelthree=UPPadjust*channelthree*5/1024;
            pressuredifkPa=(channelthree-0.50)/80e-3;
            cprintf("%4.2f\n\r",pressuredifkPa);
            if(write_to_file)  fprintf(fp,"%4.2f  ",pressuredifkPa);

            /* Time measurement                                                                    */
            lap =    clock();
            oldtimeelapsed=timeelapsed;
            timeelapsed=(lap-start)/CLK_TCK;
            laptime+=timeelapsed-oldtimeelapsed;
            if(write_to_file)
            {
                    fprintf(fp,"%6.1f\n",timeelapsed);
                    laptime=0;
                    write_to_file=0;
            }
            cprintf("%5.1f  %3.1f",timeelapsed,laptime);

            Xvalvelaptime+=timeelapsed-oldtimeelapsed;
            if(Xvalvetimeset && Xvalvelaptime>=Xvalvetime)
            {
                    if(crossovervalve) crossovervalve=0;
                    else crossovervalve=1;
                    UPPWritePort(0x232,2,crossovervalve);
                    gotoxy(1,20);
                    cprintf("Cross over valve\n\rposition = %1i",crossovervalve);
                    Xvalvelaptime=0;
            }
}
while(!kbhit());
reply=getch();
if(reply=='f' && Y=='y')
{
 theres_a_file=1;
```

```
            gotoxy(1,14);
            textcolor(RED|BLINK);
            cprintf("Writing  to\n\r%12s",tmprofile);
            textcolor(15);
           }
           if(reply=='p')
           {
            do
            {
                    sleep(5);
            }
            while(!kbhit());
            reply=getch();
           }
           if(reply=='h'|| reply=='l') flowr=reply;
           if(reply=='c')
           {
            if(crossovervalve) crossovervalve=0;
            else crossovervalve=1;
            UPPWritePort(0x232,2,crossovervalve);
            gotoxy(1,20);
            cprintf("Cross over valve\n\rposition = %1i",crossovervalve);
           }
           if(reply=='t')
           {
            gotoxy(1,17);
            cprintf("Cross over valve\n\rtiming (s): ");
            cscanf("%f",&Xvalvetime);
            getch();
            Xvalvetimeset=1;
           }
           if(reply=='o') Xvalvetimeset=0;
 }
 while(reply!='q');
 if(theres_a_file) fclose(fp);
}
```

Appendix C

This program, in Turbo C, was written to interface with, and download data from the mass spectrometer using the RS232 port. It writes code used by software resident in the mass spectrometer to the RS232 to specify channel and gain settings. The code for driving the mass spectrometer software is presented in chapter ten of it's manual (*Instruction manual for dataquad, version V3, Dataquad DAQ200/DXS*).

```
/*********************************************************************/
/* File:          massspec.c                                         */
/* Author:        Vikas Ahuja                                        */
/* Date:          14/2/96                                            */
/* Version:       1.00                                               */
/*********************************************************************/

#include <stdio.h>                      /* Include the standard header files   */
#include <stdlib.h>
#include <string.h>
#include <ctype.h>
#include <time.h>
#include <dos.h>
#include <conio.h>
#include <async2.h>

char scale_reading[7],*readm_eno,reply,number_only[4];
int *er,count,count1,count2;

void main(void)
{
        char massspecreading[12];
        int write_to_file=0,theres_a_file=0,timeelapsed;
        FILE *fp;
        clock_t start,lap;

        clrscr();
        cprintf("Do you require an output file? y/n ");
        reply=getche();
        if(reply=='y')
        {
         cprintf("\n\rEnter  filename : Name.dat : ");
         gets(massspecreading);
         fp=fopen(massspecreading,"wt");
         write_to_file=1;
        }

        clrscr();
        window(1,23,80,25);
        gotoxy(15,2);
        cprintf("Program  for writing MS data to file:");
        if(write_to_file)  cprintf(" %s",massspecreading);
        gotoxy(10,3);
        cprintf("Press  Q to quit, P to pause, F to start writing  to file");
        window(1,1,80,3);
        cprintf("  Time  H2O  Ar   CO2\r\n   (s)  18   40   44");
        window(1,4,80,22);

        opencom(1,1200,0,2,8,er);
        sethandshakemode(1,0);

        start=clock();
        do
```

```
{
 do
 {
        lap=clock();
        timeelapsed=(lap-start)/CLK_TCK;
        cprintf("%6i   ",timeelapsed);
        if(theres_a_file)  fprintf(fp,"%6i  ",timeelapsed);
        for(count=1;count<4;count++)
        {
         switch(count)
         {
                case 1: readm_eno="#21\r\n";  break;
                case 2: readm_eno="#22\r\n";  break;
                case 3: readm_eno="#23\r\n";
         }
         writecom(1,readm_eno,er);
         readlncom(1,scale_reading,er);
         count1=0;
         count2=0;
         while(count1<4)
         {
                if(isdigit(scale_reading[count1]))
                        number_only[count2++]=scale_reading[count1];
                count1++;
         }
         cprintf("%s   ",number_only);
         if(theres_a_file)  fprintf(fp,"%s  ",number_only);
        }
        cprintf("\r\n");
        if(theres_a_file)  fprintf(fp,"\r");
        delay(24800);
 }
 while(!kbhit());
 reply=getch();
 if(reply=='p')
        { do sleep(5); while(!kbhit);  getch();}
 if(reply=='f' && write_to_file)  theres_a_file=1;
}
while(reply!='q');
if(theres_a_file)  fclose(fp);
closecom(1);
}
```

Appendix D

Self-pressurisation and venting effects in liquid hydrogen tanks: an investigation, using the homogeneous and surface evaporation models

Three models have been used previously for calculating the rate of pressure increase from self-pressurisation in a cryogenic container. These are a homogeneous model, a surface evaporation model, and a thermal stratification model. The first two are isothermal models, based on the assumption that no temperature gradient exists in the vapour and liquid regions. The homogeneous model assumes that the temperature of the entire tank is uniform at all times, whereas the surface evaporation model assumes that all the heat entering the vessel is used to vaporise the liquid cryogen. The thermal stratification model is based on the assumption that the heat leak is too small to cause nucleate boiling and that the heat is absorbed by liquid in proximity of the walls setting up convection currents which carry the warmed liquid to the surface where surface evaporation occurs. The homogeneous model typically gives lower rates of pressure rise than those measured because in the real case only part of the liquid is heated. The surface evaporation model typically gives rates of pressure rise greater than those measured because in the real case not all the heat is used for vaporisation. All three methods have been reviewed by Gursu et al.[108,109].

Aydelott and Spuckler[110] reiterate that a majority of the work available on measuring and modelling self-pressurisation in stored liquid hydrogen is based on large vertical cylinders with heating, only on the side walls. The thermal stratification model developed by Arnett and Voth[111] uses natural convection theory for vertical plates to predict heat and mass transfer. Tatom et al.[112] found that bottom heating caused more heat from the side walls to be transferred to the bulk liquid and reduced the extent of thermal stratification. Vibration considerably enhances boil-off. An increase of up to 12 times is reported by Rotenburg[113]. It is interesting that at low levels of vibration excitation, the pressure rise is actually lower. This is thought to be due to the energy being absorbed in causing a mixing of the fluid and preventing thermal stratification. The same result is obtained by stirring[30], which is reported to reduce the boil-off rate by up to a factor of three. Most of the liquid hydrogen tanks built and used in automobiles in the recent past have been horizontal cylinders with hemispherical ends, and are small in size. Convection currents in these tanks may have effects similar to stirring. The application of the thermal stratification model, in particular, considering the development of a boundary layer along the vertical tank walls, is difficult for small vehicular tanks.

Rotenburg[114] developed a numerical model based on the homogeneous model for self-pressurisation in small cryogenic tanks. Experimental correlation was done against the tank used by Stewart[115]. His results predicted the rate of pressure rise, 1.3 times lower than measured for nearly empty tanks, and 1.6 times lower for nearly full tanks. Aydelott and Spuckler[110] show that heat flux per unit volume may be used as a scaling parameter.

In order to understand the effects of venting on cryogenic storage, the homogeneous and surface evaporation models used for self-pressurisation, were extended into the venting process. From the steady flow energy equation, for mass leaving the

control volume,

$$m_2 = \frac{Q - m_i(u_f - u_i)}{h_2 - u_f} \tag{D.1}$$

where
Q = heat added, kJ
m = mass, kg
h = specific enthalpy, kJ/kg
u = specific internal energy, kJ/kg

and subscripts
i = initial
f = final
2 = exiting control volume

For intermittent venting, ie. for defined vent cracking and re-seal pressures, it has been assumed that the venting process is instantaneous and that for the duration of venting, the system is adiabatic. All the heat addition occurs while the system pressure is rebuilding after venting. The system is assumed homogeneous at all times. Alternatively, if the venting is continuous at the operating pressure of the tank, then the heat leak, Q, must be included in the equation. In this case the system is seen as homogeneous until the pressure at which the vent opens is reached. Following this all the heat added is consumed by liquid vaporisation. In either case since u_f is a function of m_2 the equation becomes

$$m_2 = m_i - \frac{Q + m_i(u_i - h_2) + tvol\dfrac{u_l - u_g}{v_g - v_l}}{u_l - h_2 + v_l\dfrac{u_l - u_g}{v_g - v_l}} \tag{D.2}$$

where
tvol = tank volume, m^3
v = specific volume, m^3/kg

and subscripts
l = liquid
g = gas

It is assumed that change in gas velocity in the vent valve can be neglected in the above equations.

Two programs were written to calculate rates of pressure rise based on the homogeneous and surface evaporation models. The results for pressure rise calculated using the homogeneous model match those of Rotenburg[114]. The results of this analysis, shown in Figure D.1, indicate that the time to empty is lower for the surface evaporation case, as expected. This time to empty decreases with increasing vent pressure because the latent heat of vaporisation decreases with increasing pressure. For the homogeneous case time to empty is maximum between 0.2 and 0.4 MPa. This is because the difference between specific enthalpy and internal energy is maximum in this pressure range, and this difference represents the net lowering of internal energy of the system due to venting. This implies that this pressure range is theoretically the best for venting pressure.

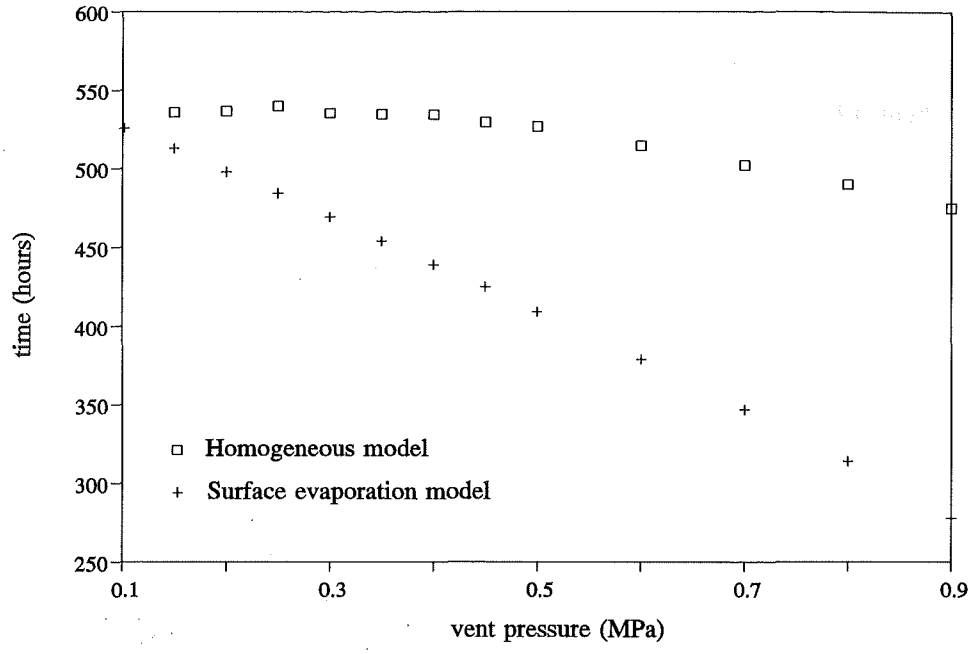

Figure D.1 Time to empty for a vented cryogenic tank (50% liquid fill, 1W heat leak). Difference between cracking and re-seal pressure for the intermittent venting (homogeneous) case was taken as 0.034 MPa (5 psi).